LEACHING OF BORNITE

by

F.J.G. UGARTE-ALVAREZ,
Ing. Civil de Minas (U. de Chile)

A thesis submitted for the degree of Doctor of Philosophy of the University of London

August, 1971

ABSTRACT

Bornite (Cu_5FeS_4), was synthesized from the elements. Particulate synthetic bornite was leached in acidified ferric sulphate solution at temperatures ranging from 15° to 90° C.

Bornite dissolved in two stages; in the first the bornite easily lost copper by diffusion and transformed, via a nonstoichiometric bornite, to a solid phase with composition Cu_3FeS_4. In the second stage, the solid phase with composition Cu_3FeS_4 was converted directly to elemental sulphur.

The apparent activation energy for the first stage of the leaching process was determined.

The mechanisms and rate controlling steps of the two stages of dissolution are given.

The solid phases were studied by x-ray diffraction, electron probe microanalysis, reflectivity dispersion measurements and microscopic examination.

CONTENTS

INTRODUCTION

Bornite (Cu_5FeS_4) is a very common and widespread mineral, which occurs in many copper deposits as an important copper ore.

Recent technological developments, such as solvent extraction and bacterial leaching, have made possible the economic treatment of large tonnages of low grade sulphides ores by heap leaching and electrowinning[1]. The copper sulphide minerals require the presence of an oxidant for their dissolution. The most important oxidant in commercial operation is ferric sulphate, which is formed during the process of heap leaching.

The reaction of acidic ferric sulphate solutions with bornite is therefore of practical interest for both bacterial and heap leaching. The kinetics and mechanism of this reaction have been studied in the present work, which forms part of a comprehensive investigation on the leaching of copper sulphides being carried out in the Hydrometallurgy Group, Metallurgy Department, Royal School of Mines, under the supervision of Dr. A.R. Burkin.

Because of the importance of the solid-state transformations during leaching[2] a considerable part of the present work deals with the study of these transformations.

In order to avoid the strong influence that impurities might have on the dissolution process, a synthetic bornite was used.

Special emphasis has been given to the comparison between the leaching of this synthetic bornite and the alteration by oxidation of the natural occurring mineral.

In the present investigation, the activation energy has been expressed in units of kilocalories for comparison with other work. (1 kcal = 4.1868 kJ).

SECTION 1

LITERATURE SURVEY

1.1 Previous Work on the Leaching of Bornite

J.D. Sullivan[3] was the first to study the leaching of Bornite. He worked with natural crushed minerals as nearly pure as could be obtained, and he used ferric sulphate solutions in most of the runs.

The experimental procedure involved placing 10 gr samples in 5 pint bottles containing 500 cc of the desired leaching solution, on revolving rolls in a room having thermostatically controlled temperatures. The mouths of the bottles were left unstoppered and samples were taken during the test by siphoning off 400 cc of solution and adding other 400 cc of fresh solution in order to keep constant the concentration of leaching reagents. The copper analyses were done on samples taken from the 400 cc of removed solution.

The principal parameters considered by Sullivan were: 1) The effect of particle size of the mineral on the rate of dissolution; 2) the effect of the concentration of ferric ion in the leaching solution;

3) the effect of the concentration of sulphuric acid in the leaching solution, the ferric ion content remaining constant; 4) the effect of temperature; and 5) the effect of air and water alone on bornite.

Fig. 1 shows the effect of temperature on the rate of dissolution of -100 +200 mesh bornite, when leached with a solution containing 1 % of iron as ferric sulphate plus 0.5 % of sulphuric acid.

The conclusions of Sullivan's work can be summarized as follows.

a) The rate of dissolution of bornite was virtually independent of the strength of ferric sulphate if enough reagent was present.

b) The rate of dissolution was independent of the acid strength of the solution if the ferric ion concentration remained constant.

c) Particle size did not affect the dissolution rate and it was shown, for example, that although there is a great difference in surface per unit weight for -10 +200 mesh particles, their rates of dissolution are practically identical (fig. 2). The -200 mesh material dissolved at only a slightly faster rate than the larger sizes. The larger pieces did not crumble in leaching but retained practically their original forms. The shell was composed of

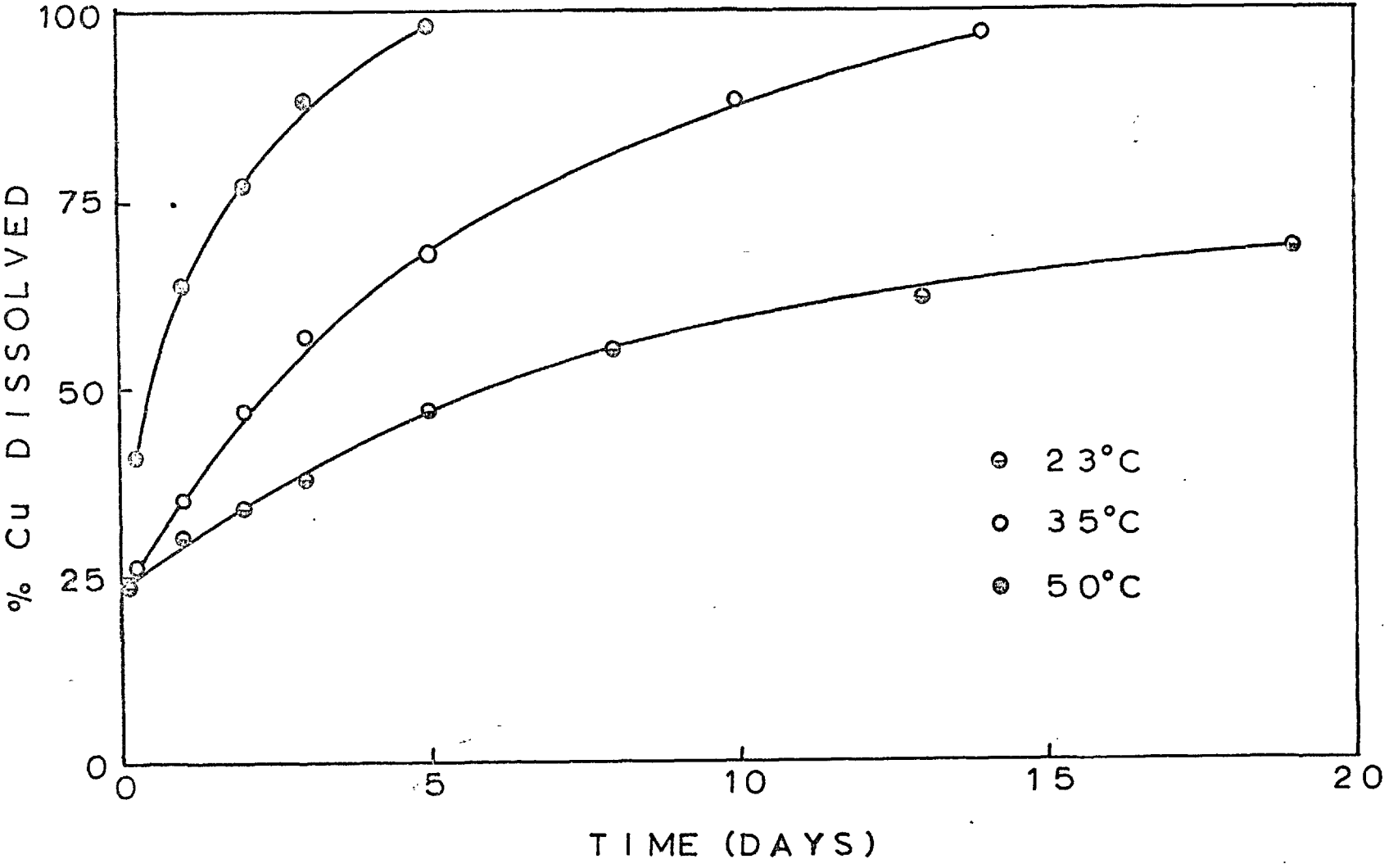

FIG.1 Effect of temperature on the rate of leaching -100 +200 mesh bornite J.D. Sullivan[3].

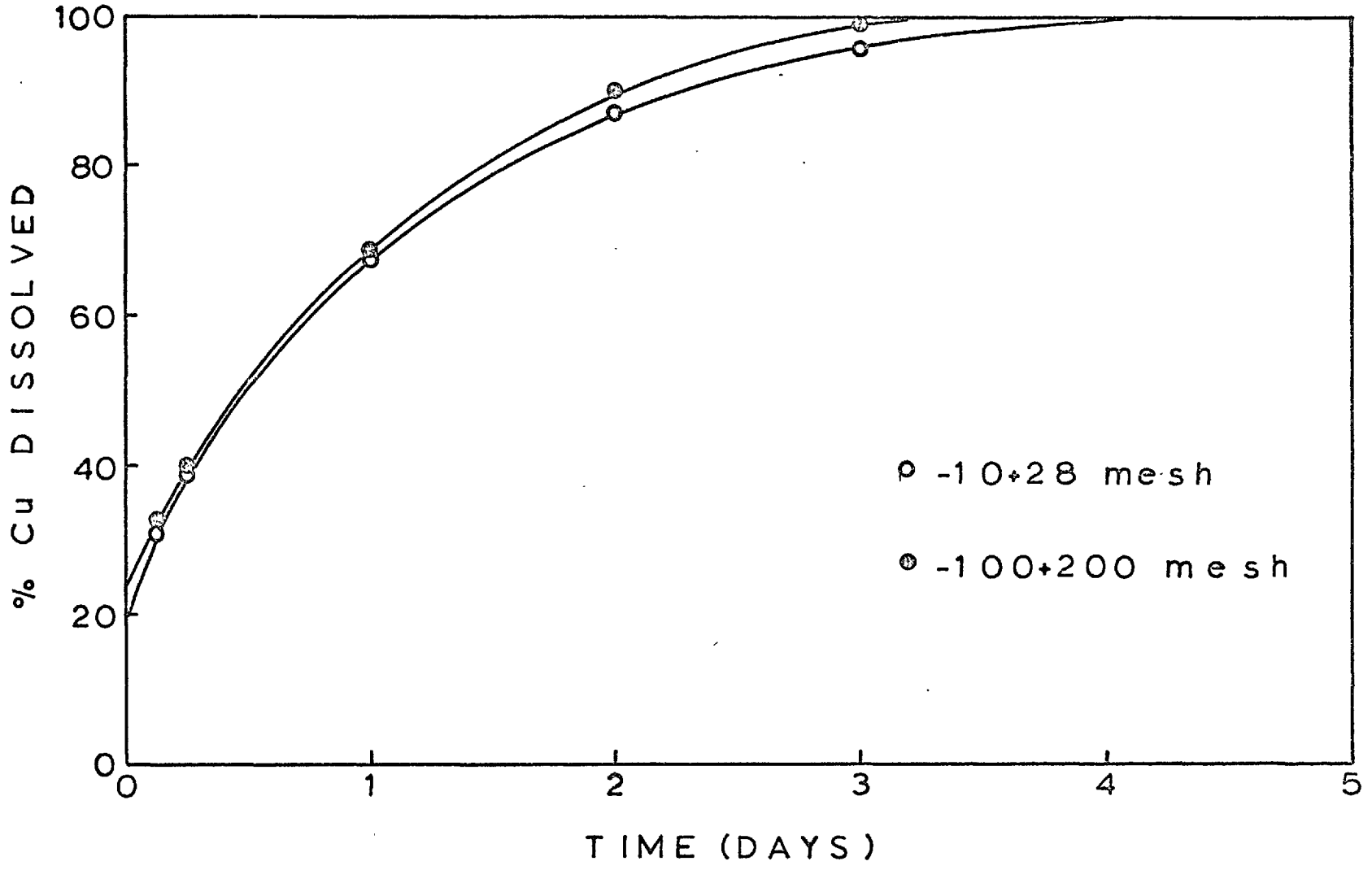

FIG. 2 Effect of particle size on the rate of leaching bornite J.D. Sullivan[3].

sulphur and insoluble material.

d) Sulphuric acid plus air attacked bornite more slowly than ferric sulphate solutions.

e) The rate of dissolution was markedly affected by temperature.

Sullivan noticed that during the early part of the tests, the copper was dissolved whereas the iron and sulphur were not attacked. However, as the test progressed the iron and sulphur were both attacked appreciably.

Finally, Sullivan discussed the mechanism of dissolution of bornite in ferric sulphate solutions.

He suggested that Bornite (Cu_5FeS_4), can be written as $2Cu_2S.CuS.FeS$ and that Chalcocite (Cu_2S) is dissolved in ferric sulphate solutions in two steps.

$$Cu_2S + Fe_2(SO_4)_3 = CuSO_4 + 2FeSO_4 + CuS \quad 1)$$

$$CuS + Fe_2(SO_4)_3 = CuSO_4 + 2FeSO_4 + S \quad 2)$$

The second reaction also expresses the dissolution of covellite in ferric sulphate.

Sullivan also suggested that the reaction in which FeS dissolves in ferric sulphate probably can be written as:

$$FeS + Fe_2(SO_4)_3 = 3FeSO_4 + S \quad 3)$$

From these three reactions we can derive an overall reaction for the dissolution of bornite as:

$$Cu_5FeS_4 + 6Fe_2(SO_4)_3 = 5CuSO_4 + 13FeSO_4 + 4S \quad 4)$$

Stender and Saltovskiy[4] studied the solubility of bornite in acidified ferric sulphate solutions. However, their work is not discussed here because they used a very impure bornite sample whose "degree of purity" amounted to 33%.

Uchida et al.[5] studied the leaching of bornite in acidified ferric sulphate solutions using different Japanese copper sulphides ores.

Bornite was concentrated from a bornite-rich ore. The chemical analysis showed that the composition was very close to Cu_5FeS_4 and x-ray diffraction gave the bornite lines only.

This bornite was leached in a 0.01 N sulphuric acid, 24 mg/cc ferric iron solution at 30°C. After one hour 25% of the copper had dissolved.

Uchida et al. also studied the effect of particle size, concentration of ferric iron and concentration of sulphuric acid on the dissolution of the ores. The results are similar to those of Sullivan. They found that concentrations of ferric iron larger than 0.5 g/l does not improves the rate of leaching.

No mechanism of leaching was proposed.

Kopylov and Orlov[6] studied the kinetics of bornite dissolution in acidified ferric sulphate solutions using polished specimens of natural bornite,

checked by chemical analysis and x-ray diffraction. The purity of the bornite was shown to be 97%.

The samples were suspended in a flask thermostatically controlled and agitated with a variable speed, three blade propeller mixer. The copper in the solution samples was determined with a polarograph. In almost all of the experiments a solution containing 10 g/l sulphuric acid and 18 g/l Fe^{+++} in the form of ferric sulphate was used as the solvent.

Kopylov and Orlov studied the influence of the concentration of ferric iron, the influence of stirring speed and the influence of the temperature in the rate of dissolution of bornite.

According to Kopylov and Orlov an increase of Fe^{+++}(as ferric sulphate) concentration from 9 to 35 g/l increased the rate of bornite dissolution.

They also found that an increase in mixer speed from 200 to 1000 rpm increased only slightly the rate of copper dissolution.

Finally it was shown that the factor which most greatly affected bornite dissolution, was the temperature. Kopylov and Orlov determined the activation energy for the dissolution of bornite. The average value given was 5.5 ± 1.4 kcal per mole and it was pointed out that such a low value indicates

a process controlled by diffusion.

An important result from their work was the finding of the formation of a new solid phase after the first few minutes of dissolution. From the x-ray diffraction analysis they concluded that the new solid phase was chalcopyrite, since the interplanar distances established for the crystal lattice coincided quite closely with the tabulated data for chalcopyrite.

Using this discovery as a basis the authors discussed the mechanism of the dissolution of bornite writting the formula as $2Cu_2S.CuFeS_2$ instead of $2Cu_2S.CuS.FeS$ as given by Sullivan. They explained the fact that bornite is less rapidly dissolved than chalcocite in ferric sulphate solutions, by saying that one copper atom of the bornite is bound in the form of the poorly soluble chalcopyrite.

Dutrizac et al.[7] studied the kinetics of dissolution of bornite in acidified ferric sulphate solutions using sintered discs of synthetic bornite.

The bornite was prepared by reaction-sintering pellets of CuS, FeS and Cu_2S in vacuum-sealed Pyrex ampoules. The three simple sulphides were ground to -150 mesh, mixed and then pressed into pellets at 80,000 psi. The pellets were vacuum-sealed in Pyrex ampoules, and sintered for three days. The final

pellets had the characteristic reddish colour associated with bornite, which gradually turns blue on standing in air. X-ray diffraction analysis confirmed that the material was tetragonal bornite. Microscopic examination indicated small white oolites. which constituted less than 1% of the volume. The polished bornite discs were cemented to lucite rods in such a way that only the polished face was exposed to the leaching solution.

The method used for the leaching consisted of rotating the disc at a given speed in an acidified ferric sulphate solution and periodically sampling and analyzing for the amount of dissolved copper, with a Technicon Autoanalyzer.

They found that when a partially leached pellet of bornite was broken in half it showed three distinct layers. One was the residual, unreacted bornite, and adjacent to this one there was a material whose x-ray diffraction pattern was similar to that of bornite, but with slightly different lattice spacings. The lattice spacings gradually decreased with increasing distance from the normal bornite. Finally, there was a yellow layer, which x-ray diffraction showed to be a mixture of chalcopyrite and sulphur. All these phases appeared only in tests made at temperatures above 40° C.

At temperatures below 40° C it was possible to convert the entire pellet to nonstoichiometric bornite without the appearence of any additional phases. Once the pellet had been converted to nonstoichiometric bornite the reaction virtually stopped.

Electron microprobe analyses made across the pellets, indicated that the S/Fe ratio remained fixed at 4 across both the bornite and the nonstoichiometric bornite and that the Cu/S and Cu/Fe ratios dropped steadily.

Using these results as a basis Dutrizac et al. proposed the following mechanism for the dissolution of bornite in acidified ferric sulphate solutions.

At temperatures above 40° C:-

$$Cu_5FeS_4 + xFe_2(SO_4)_3 = Cu_{5-x}FeS_4 + xCuSO_4 + 2xFeSO_4 \quad 5)$$

$$Cu_{5-x}FeS_4 + (4-x)Fe_2(SO_4)_3 = CuFeS_2 + (4-x)CuSO_4 + (8-2x)FeSO_4 + 2S \quad 6)$$

$$CuFeS_2 + 2Fe_2(SO_4)_3 = CuSO_4 + 5FeSO_4 + 2S \quad 7)$$

They explained the fact that sulphur appeared only in tests made for relatively long periods by saying that reactions 5) and 6) are very much faster than 7) and that the chalcopyrite formed was sulphur-rich.

At temperatures below 25° C the only reaction

observed was:

$$Cu_5FeS_4 + xFe_2(SO_4)_3 = Cu_{5-x}FeS_4 + xCuSO_4 + 2xFeSO_4 \qquad 8)$$

From the tests at low temperature they estimated the value of x in reaction 8) from the amount of copper dissolved. They found values of x as large as 1.2 which represents 25% of the copper dissolved. Iron and sulphur were not dissolved during the formation of the nonstoichiometric bornite.

At higher temperatures the nonstoichiometric bornite was attacked according to reaction 6). This reaction requires that sulphur be produced in great quantity, but a discrepancy in the amount formed was found. This was explained by the formation of sulphur-rich chalcopyrite and the oxidation of some sulphur to sulphate, which was not detected because of the high background of sulphate ion. Reaction 6) also predicts a Fe^{++}/Cu ratio of 2 but higher values were found.

Dutrizac et al. also studied the effect of ferric ion concentrations on the dissolution rate. This is shown in fig. 3. This figure shows that the rate depends directly on the ferric ion concentration for ferric ion strengths less than about 0.06 M, but that it is insensitive to higher ferric

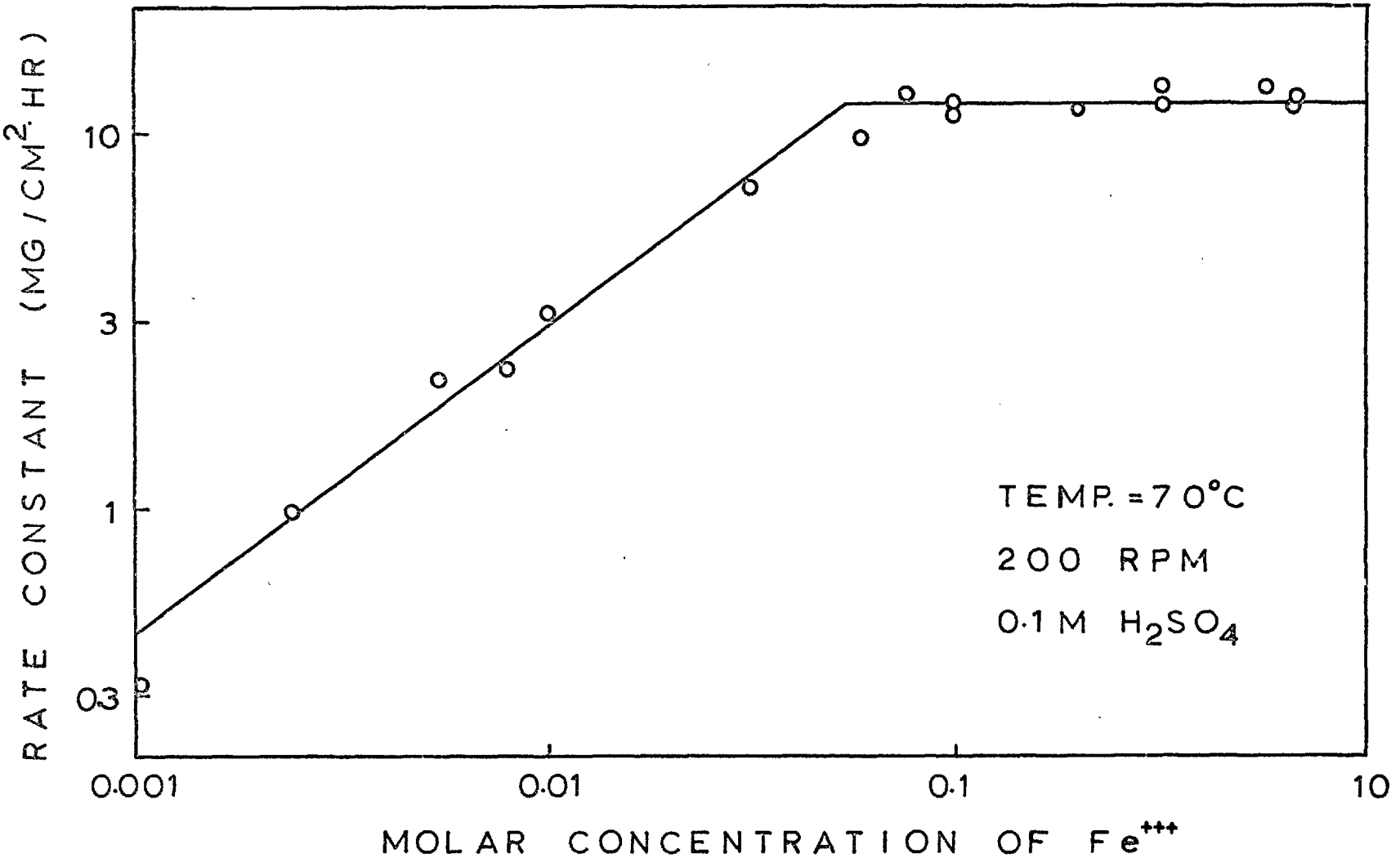

FIG. 3 Effect of ferric ion concentration on the rate of leaching bornite Dutrizac et al.[7].

concentrations.

It was found at different temperatures that acid (0.1 M H_2SO_4) alone did not attack the synthetic bornite. The effect of sulphuric acid concentration on the rate of bornite dissolution was negligible.

Activation energy as determined by their work showed an average value of 5.7 ± 1.3 kcal per mole. The experiments made with natural specimens of bornite showed that the natural bornite dissolves like the synthetic material and at approximately the same rate.

1.2 Crystal Structures

1.2.1 Structure of Bornite

De Jong[8] was the first to attempt the determination of the crystal structure of bornite, using natural specimens. He reported a structure with a cubic cell in which a = 10.910 ± 0.005 kX. (1 kX = 1.00202 A). However, this structure did not account for the observed intensities.

Lundqvist and Westgren[9] studied the structure of synthetic materials using the powder method which gave bornite a cubic cell with a = 10.94 kX. This structure, with spacial group Fd3m (O_h^7), consisted of a cubic close-packing of sulphur atoms, with the metal atoms in the interstices. They proposed some possible distributions of the metallic atoms, but none of this could be confirmed by means of the intensities of the reflections.

Tunnell and Adams[10] examined crystals of bornite from Carn Brea Mine, Illogan, Cornwall and they proposed a cubic unit cell with a = 32.8 A. They proposed a structure giving reasonable intensities for all strong and medium reflections, but a great number of weak reflections remained unaccounted for. The very same specimen was reexamined in a polished

section and by x-ray precession photographs by Morimoto, Greig and Tunnell[11] and it was found to consist of three phases.

Frueh[12] produced x-ray, thermal and electrical evidence indicating that bornite can exist in both a low and a high-temperature form and considered the structural differences between them to be of order-disorder.

Kullerud and Roseboom[13] confirmed the existence of two forms of bornite and gave the inversion temperature as about 190° C, for bornite coexisting with digenite along the Cu_9S_5-Cu_5FeS_4 join.

Kullerud, Donnay and Donnay[14] reported two forms of bornite, one cubic with a=21.94 ± 0.06 A, (diffraction aspect P***), and the other with primitive orthorhombic lattice, in which pseudotetragonal dimensions a=b=21.90 ± 0.06 A, c=50.95 ± 0.03 A.

Morimoto and Kullerud[15] studied the polymorphism in bornite and confirmed the existence of two stable forms and one transitional metastable form. The high-temperature form which is stable above 228 ± 5°C changes to a transitional metastable form on cooling below 228 ± 5° C. The high temperature form is cubic with a=5.50 ± 0.01 A, Z=1 (diffraction aspect F***). The transitional metastable form is also cubic with a=10.94 A, Z=8, diffraction aspect Fd**. In the low

temperature form (belonging to the space group $P\bar{4}2,c$) a=10.94, c=21.88 A.

The different cell dimensions and symmetries found in specimens of natural bornite, such as those of Frueh and Kullerud, Donnay and Donnay, were explained by twinning of the low-temperature form.

Morimoto[16] discussed the transitions between the polymorphs from the structural point of view and determined the structures of the high temperature form and of the metastable form.

According to Morimoto, the crystal structure of the high temperature form is essentially the antifluorite structure, only slightly more complicated (fig. 4). The sulphur atoms occupying the nodes of the cubic face-centered lattice with a=5.50 A, are cubically close-packed. Each tetrahedron of sulphur atoms, on the average, contains 3/4 of a metal atom. This fractional atom is itself statistically distributed over 24 equivalent sites inside the sulphur tetrahedron. In the whole cell, six metal atoms are statistically distributed over 24 x 8 = 192 sites.

The metastable form is transitional between the high-temperature form and the low-temperature form.

The metastable form shows two characteristics: a) the existence of a cubic sub-cell with a=5.47 A

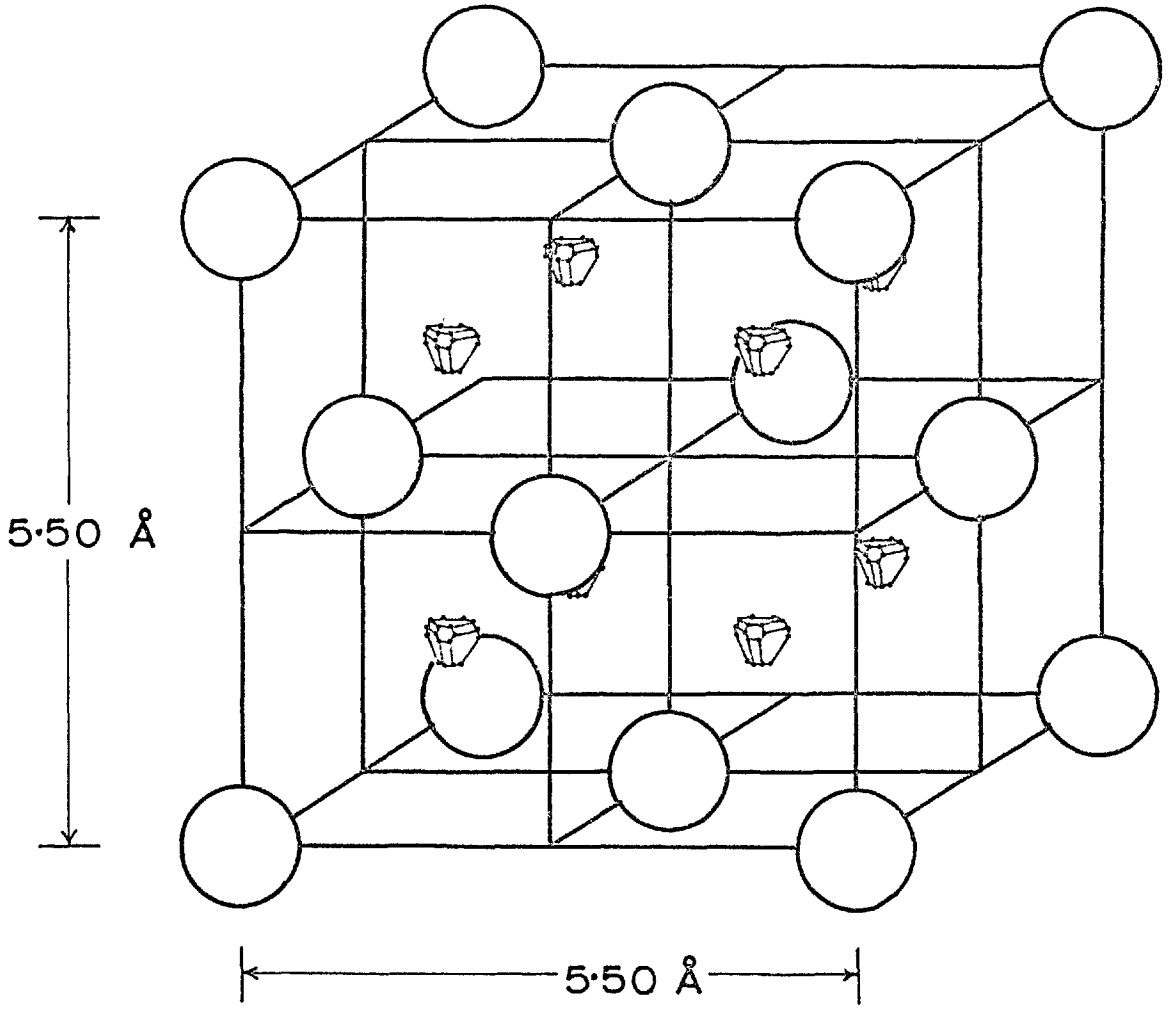

FIG. 4 STRUCTURE OF THE HIGH-TEMPERATURE FORM OF BORNITE

MORIMOTO [16]

and b) the fact that only reflections with indices (4m ± 1, 4n ± 1, 1) can appear (this forms a special extinction rule).

Attempts to find a single-crystal structure that would account for the observed cubic reflections were unsuccessful. The nature of the pseudocrystal became apparent to Morimoto, because the twinning hypothesis proposed by Donnay, Donnay and Kullerud[18] was found to apply also in the case of metastable bornite.

According to Morimoto the cubic arrangement of the metastable form is a result of the twinning of a large number of small domains in eight different orientations. All the domains that have the same orientation constitute one crystal, even if they are not singly connected. Each such crystal has rhombohedral symmetry with a_{rh} = 6.70 A and $\alpha = 33^{\circ}32'$. These eight crystal are in twin relations.

The structure of the rhombohedral form can be derived from that of the high-temperature form by considering the latter along the body diagonal (111) of the cubic cell (fig. 5). All the sulphur atoms remain in place, retaining the cubic close packing. Of the four partial metal atoms in sulphur tetrahedra in the high temperature form, two do not change at all. One tetrahedron becomes vacant and the metal 3/4 atom which occupied it in the high-temperature

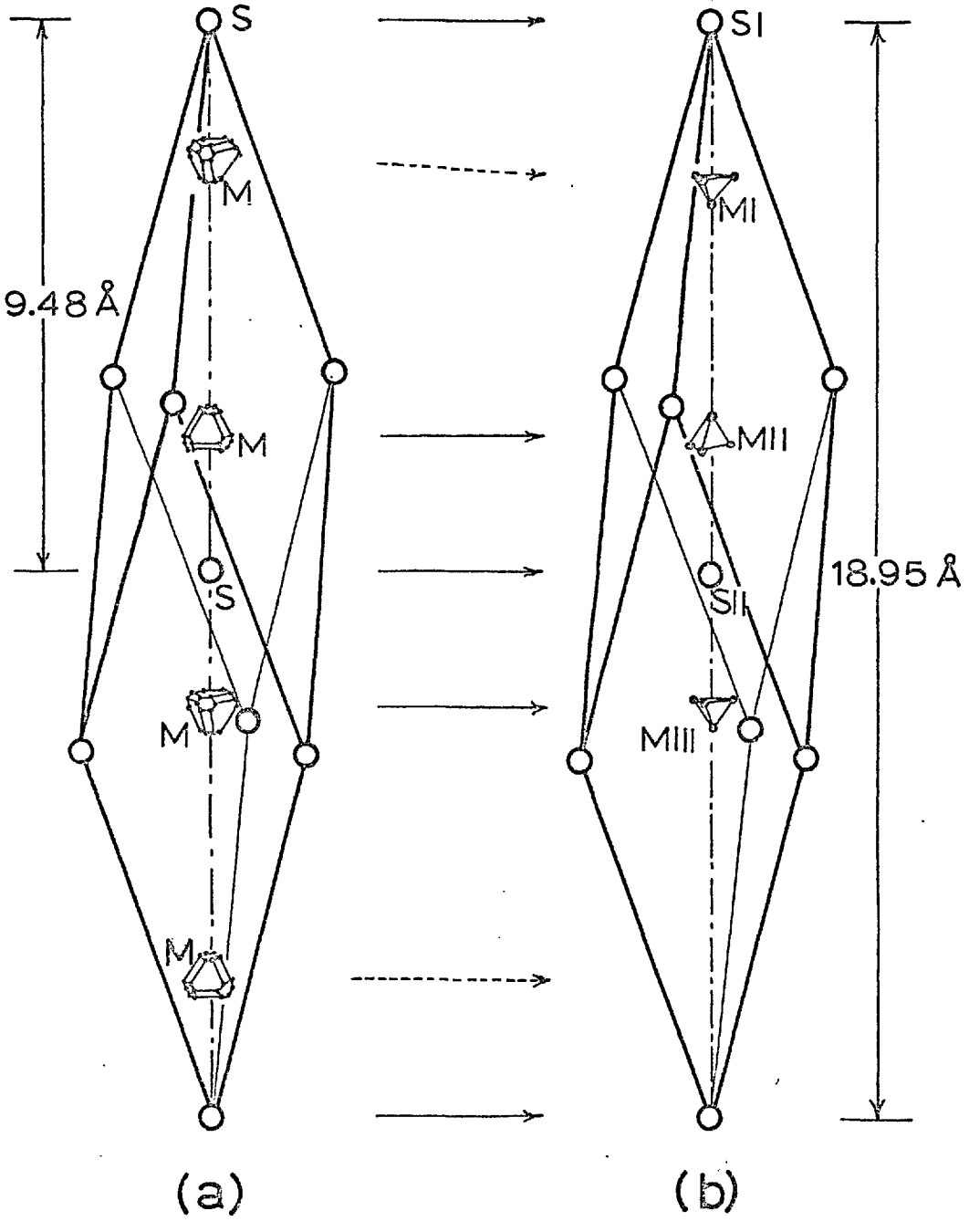

FIG. 5

DERIVATION OF THE STRUCTURE OF THE METASTABLE FORM (b)

FROM THAT OF THE HIGH-TEMPERATURE FORM (a)

MORIMOTO [16].

form is redistributed among the other three sites. The corresponding three sulphur tetrahedra now contain one full metal atom each. To compensate for the vacant tetrahedron, the last metal M_I moves slightly inside its tetrahedron. The statistical distribution of 3/4 of the metal atom among 24 possible sites inside each sulphur tetrahedron changes to the statistical distribution of one metal atom among four possible sites (fig. 6).

This structure can be described as a layer structure parallel to (0001). There are two kinds of sulphur layers, S_I and S_{II}, and three kinds of metal layers, M_I, M_{II}, and M_{III}. The S_I layers are sandwiched between the M_{II} and M_{III} layer, while the S_{II} layers only have the M_I layers on one side.

The x-ray data of the low-temperature form gives tetragonal symmetry with cell dimensions a = 10.94 A and c = 21.88 A. Strong and medium reflections generally have similar intensities in the metastable and low temperature forms, indicating that the two crystal structures have a common basic structure. The reflections of the low- temperature form, however, do not obey the special extinction rule.

There are two differents ways to explain the fact that the special extinction rule does not apply

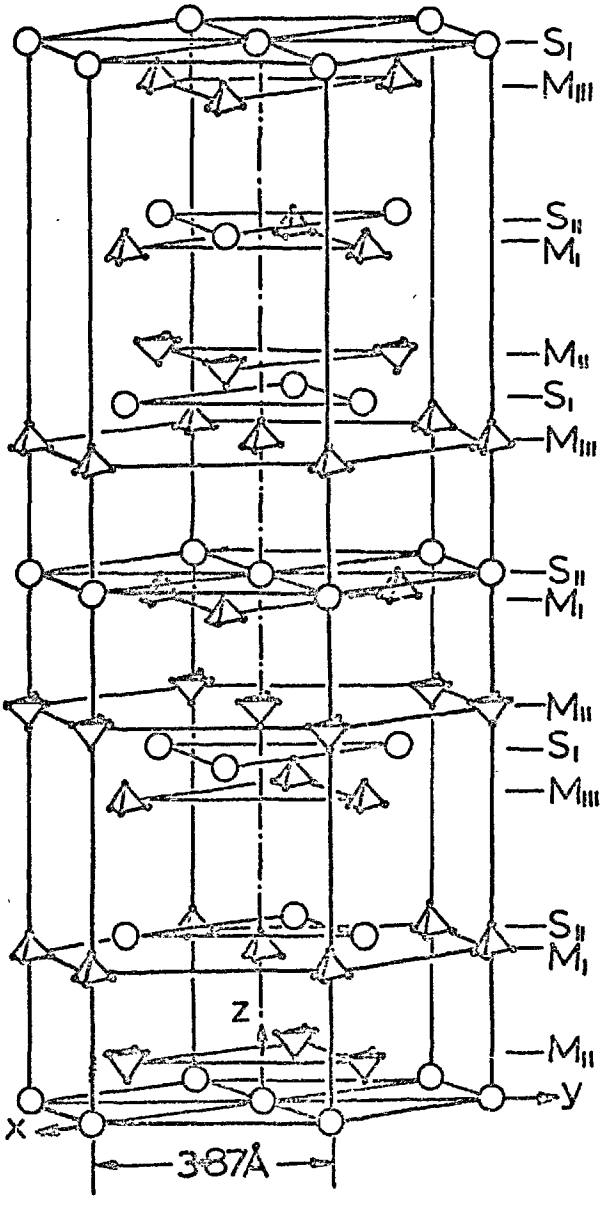

FIG. 6

STRUCTURE OF THE RHOMBOHEDRAL FORM OF BORNITE

MORIMOTO [16]

in the low-temperature form: a) the disappearance of the twinning as the crystal symmetry changes from rhombohedral to tetragonal; or b) the lowering of the cystal symmetry from rhombohedral to monoclinic, as the twin symmetry changes from cubic to tetragonal. In the absence of any morphological or optical evidence in favor of twinning, the latter hypothesis could be justified only by the structure determination.

According to Morimoto it seems certain that metal atoms statistically distributed in the metastable form, would preferentially choose one of the sites in each position on transition (although the structure of the low-temperature form was not actually determined). This ordering of metals atoms would be accompanied by slight adjustments of the surrounding atoms. The stoichiometric chemical formula confirmed for most natural bornite specimens, suggests that the Fe atoms are ordered in the low-temperature form.

Fig. 7 shows the structural relationship between the three polymorphs, all of which are represented as layer structures parallel to $(111)_{rh}$. The structures of single crystals (domain orientations) are shown for the metastable and low-temperature forms.

All three structures are built on the basis of the cubic close-packing of the sulphur atoms. The

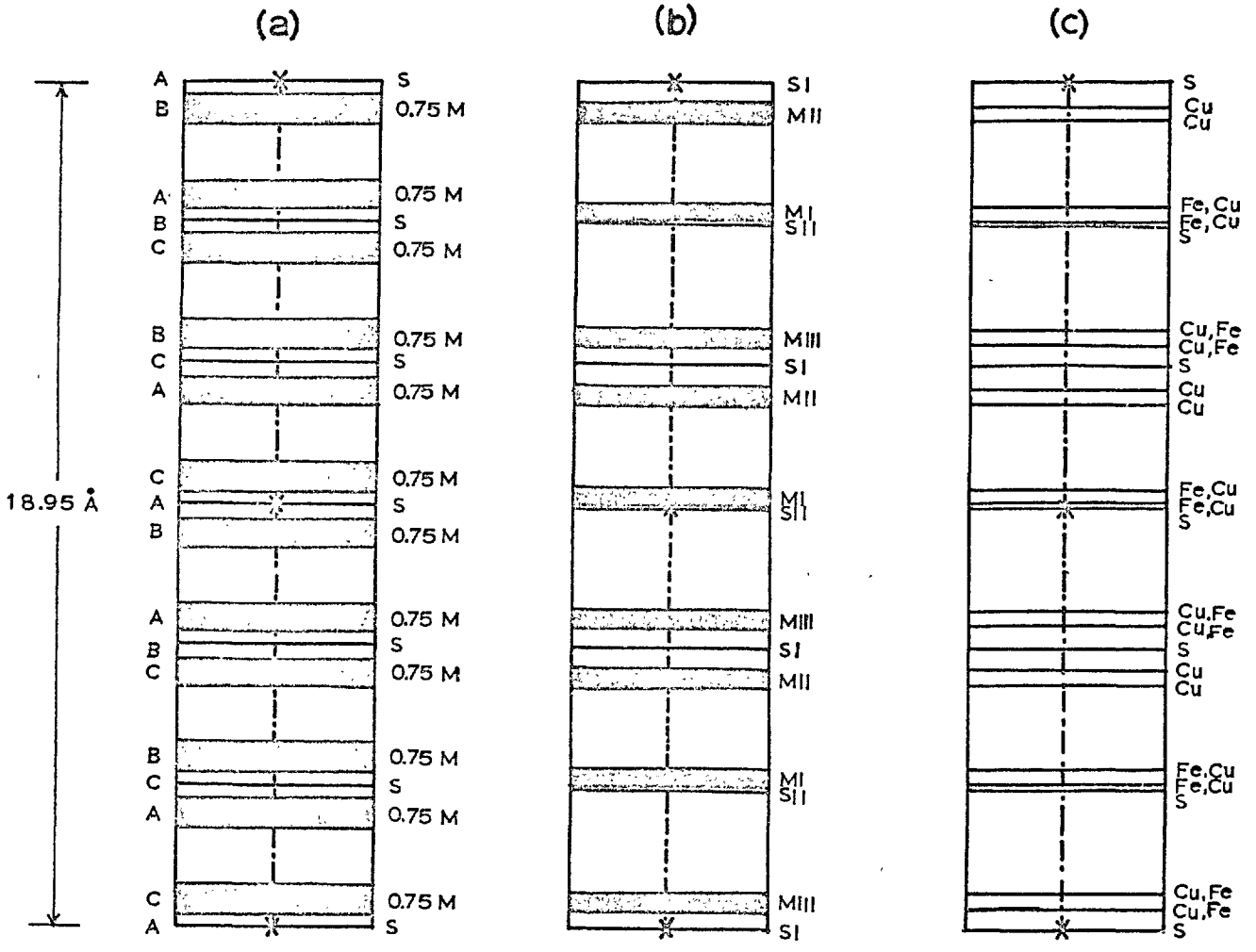

FIG. 7 LAYER STRUCTURES OF THE THREE POLYMORPHS OF BORNITE. MORIMOTO[17]

statistically distributed metal atoms are represented as bands in the high-temperature and metastable forms. The M_I layers move closer to the sulphur layers to compensate for the vacant layers in the metastable and low-temperature forms. The distance between each M_I layer and the adjacent sulphur layer becomes shorter, which suggest the possibility that the Fe atoms concentrate in the M_I layers.

In a paper on the bonding properties of sulphur in bornite P.G. Manning[19] studied the structure of the low-temperature form.

His study was based on the structure of the metastable rhombohedral form of bornite determined by Morimoto, using the average positions of the metals.

The sulphur atoms in the rhombohedral form are seemingly 5 and 7-coordinate (S_{II} and S_I) (fig. 8). If some of the S_I-M bonds are of the "purely" ionic or van der Waals type, the effective coordination number of the S_I atoms is less than seven.

In discussing the bonding properties of S in bornite, Manning considered the following possibilities:

i) Some of the M-S_I bonds are ionic (non-coordinate).

ii) The S_I coordination number is a manifestation of covalent-ionic resonance.

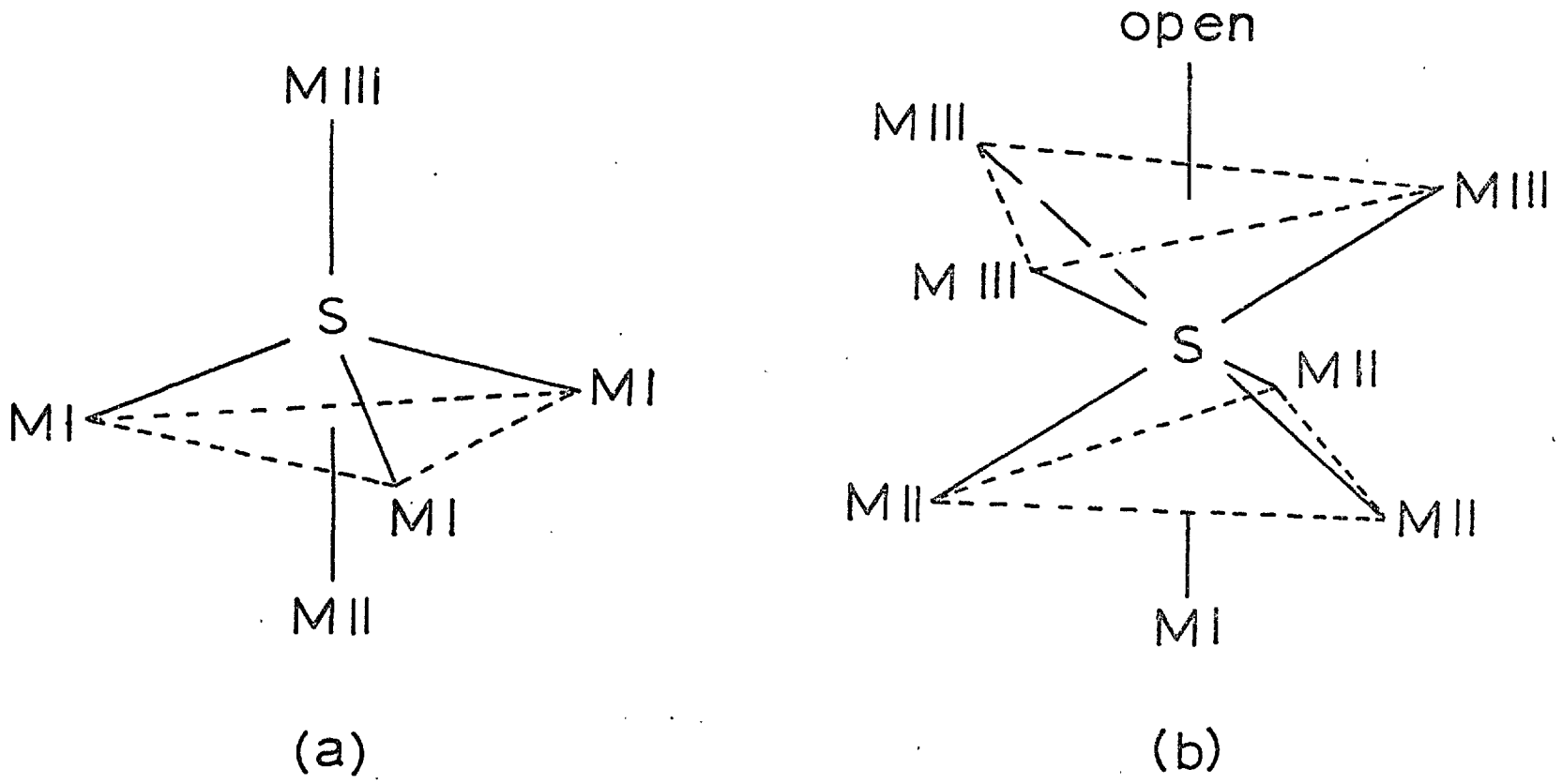

FIG. 8 S ENVIRONMENTS IN BORNITE. (a) "5-COORDINATE" SII, (b) "7-COORDINATE" SI

MANNING [19]

iii) The S_I atoms are 7-coordinated, implying the ready availability of the 3d orbitals for bonding.

i) This scheme, was an attempt to explain the S bonding in terms of 3s and 3p hybridization i.e. 3 or 4-coordinated S atoms. Manning considered that a 6-coordinated S atom does not seem worthwhile, as energetically the system would be little different from that of a 7-coordinated S (from the point of view of the availability of the d-orbitals for bonding). Also, for a 5-coordinated S_I (two non-coordinated bonds), he said that it is difficult to choose two bonds that are in any way exceptional; and such a scheme would seem artifitial. This leaves two possibilities, either the S_I atoms are 3-coordinated with four non-coordinated bonds or the S_I atoms are 4-coordinated with 3 non-coordinated bonds. He suggested that the later is energetically the more favourable scheme, and, moreover , that it is not possible to choose uniquely three coordinate bonds that correspond to any simple 3- coordinate structure. He concluded that it is apparent that scheme i) demands a 4-coordinated (tetrahedral) S atom.

These thoughts transcribe into practice well, because the M_I-S_I and the three S_I-M_{III} bonds are oriented tetrahedrally. According to Morimoto the

M atoms lie at the apices of small tetrahedra and the M_I-S_I-M_{III} angles range between 100° and 113°, with an average value of 110°. These angles are close to the classical tetrahedral angle of 109° 28' and Manning said that it seems reasonable to suppose that the S_I are bonded tetrahedrally to an M_I and three M_{III} atoms. The small displacement of the metal atoms from the centres of the S tetrahedra could be due to the admixing of e.g. sp^2 hybrid orbitals, or the balancing of electrostatic forces over many cell distances. However, the small displacement would seem to be of secondary importance in an understanding of the basic structure of the crystal.

According to the scheme i) given by Manning, the M_{II} atoms are bound by electrostatic forces.

The "5 coordinate" S_{II} atoms are also tetrahedrally coordinated (to one M_{III} and three M_I atoms). The theory of Manning can account for the high coordination number of both the S_I and S_{II} atoms and proposes tetrahedral coordination for S_I and S_{II}.

Manning indicated that the bornite structure can be likened qualitatively to a sphalerite-type skeleton containing layers of ionically bound interstitial atoms. Taking the sphalerite-bornite analogy one step further, he said that the "interstitial"

ionic M_{II} atoms in bornite would seem to be Cu (I) because the preferred coordination of Cu (I) is tetrahedral. The remaining Fe and Cu atoms are therefore, distributed among the M_I and M_{III} sites.

Manning proposed to write the bornite structure as:

$$(Cu_3FeS_4)^{2-} 2Cu^+$$

Electrical measurements have shown that bornite has the properties of a semiconductor. Therefore, according to Manning the electrons of the "interstitial" Cu^+ must partake in the tetrahedral coordination of the sphalerite-type skeleton. The electronic configuration of the free S atom is $3s^2 3p^4$, so that two additional electrons can make up the four tetrahedrally oriented electron pairs. He said that the sphalerite-type skeleton of bornite is therefore one of Cu (I) and Fe (III).

Summarizing, for Manning scheme i) has a number of attractive features. These are:

a) The S_I and S_{II} atoms are 4-coordinate.

b) A single theory can explain the coordination properties of S_I and S_{II}.

c) The bornite-sphalerite analogy seems reasonable, especially in view of the detection of interstitial cations in sphalerite and the correlation of tetrahedral structures with d^5 and d^{10} cations.

Scheme ii) led Manning to the same conclusion as scheme i), that the M_{II} are bound ionically.

Scheme iii) also led to the conclusion that the M_{II} atoms are bound ionically, but a 7-coordinate S atom would be a $s^1 p^3 d^3$ hybrid which is unlikely energetically. Manning concluded that a 7-coordinate scheme does not have the atractive features of scheme i).

As final conclusion he said that an analysis of the bonding properties of the S atoms in bornite had shown that bornite has a sphalerite-type structure that contains layers of ionically-bound interstitial atoms, Cu (I). This scheme has the advantage in that the S atoms are tetrahedrally coordinated, which agrees with the contention of Craig & Magnusson [20] that the S 3d orbitals are unavailable for chemical bonding. The Cu atoms are Cu (I) and the Fe atoms are Fe (III).

Further support for the hypothetical structure of the low temperature form of bornite is given by the following:

Mossbauer measurements [21] have shown that Fe is present as Fe (III) in bornite.

Magnetic measurements [22] suggest that Cu is present as Cu (I).

The ordering of iron atoms in the low temperature

form of bornite have been demostrated by Allais and Curien[23]

Manning[24,25] has proved that interstitial sites in sphalerite are stable with respect to metal occupation. He also showed[19] that ZnS structures are often observed for sulphides of d^5 and d^{10} cations: ZnS (d^{10} cation), CdS (d^{10}), red MnS (d^5)[26] and chalcopyrite (d^5 and d^{10})[27]

G. Allais[28] found that in the metastable form of bornite the arrangement of the unoccupied sites has cubic symmetry, and that only the displacement of the metal atoms in the tetrahedral cavities requires a lower symmetry: thus the fundamental cell has no apparent distortion.

Using the studies of Morimoto and Manning as a basis, a ball model (figs. 9 and 10) of the low temperature structure of bornite was built. The ionically bound copper layers, parallel to $(111)_{rh}$, are shown in brown balls (fig. 10). Abstraction of the ionically bound copper atoms results in the formation of a chalcopyrite-like unit cell, with formula unit Cu_3FeS_4.

If four (0 ½ 3/4) iron atoms of the chalcopyrite structure (fig. 14) are replaced by copper atoms the structure of Cu_3FeS_4 (fig. 11) is obtained.

FIG. 9 Hypothetical crystal structure of the low temperature form of bornite. The Cu_3FeS_4 sphalerite-type skeleton is formed by sulphur atoms(yellow), iron atoms (blue) and copper atoms (orange). The interstitial, ionically bound copper atoms are shown in brown.

FIG. 10 Hypothetical structure of bornite showing atomic layers parallel to $(111)_{rh}$. (White unions should be ignored).

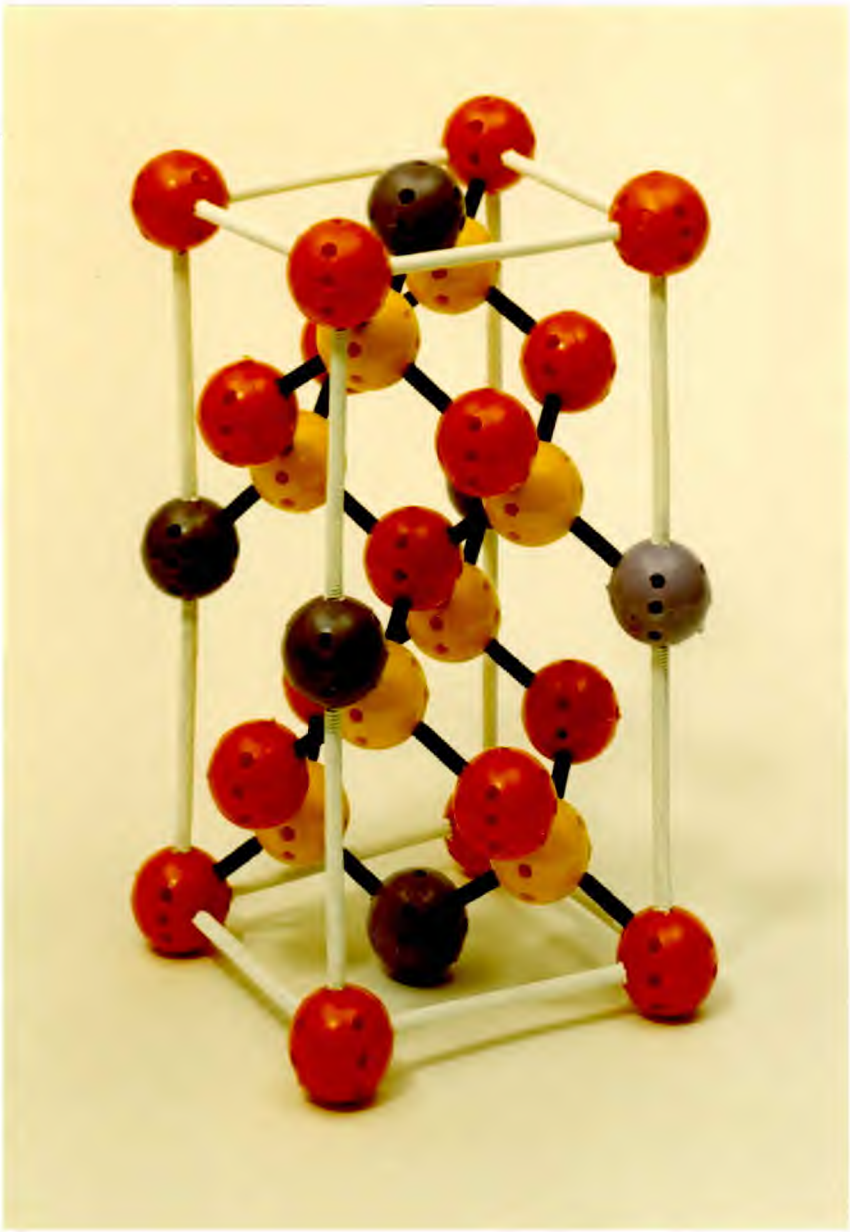

FIG. 11 Crystal structure of Cu_3FeS_4 resulting from the removal of the ionically bound copper atoms from the structure of bornite.

1.2.2 Structure of Chalcopyrite.

The arrangement that prevails in chalcopyrite, $CuFeS_2$, is essentially a superlattice on that of zinc blende. Though a shorter cell was earlier described for this crystal[29], its unit cell is an elongated tetragonal prism containing four molecules.

Its dimensions are[30]:

a = 5.24 A , c = 10.30 A.

Atoms are in special positions of Vd^{12} ($I\bar{4}2d$):

Cu: (4a) 0 0 0; 0 1/2 1/4; B.C.

Fe: (4b) 0 0 1/2; 0 1/2 3/4; B.C.

S : (8d) u 1/4 1/8; $\bar{u}$ 3/4 1/8; 3/4 u 7/8;
1/4 $\bar{u}$ 7/8; B.C.

with u = ca. 1/4.

As is evident from fig. 12 the doubled c compared to the a axis is an expression of the way atoms alternate with one another in the metallic planes normal to this axis. Metallic atoms are surrounded here, as in ZnS, by tetrahedra of sulphur atoms, while each sulphur in turn has a tetrahedron of metallic atoms as closest neighbours, two of which are copper and two iron. The significant interatomic distances are: Fe-S = 2.20 A, Cu-S = 2.32 A, S-S = 3.56 A.

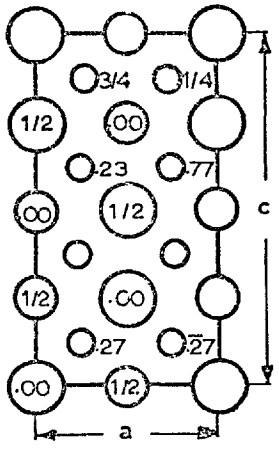

FIG.12 A projection of the tetragonal structure of chalcopyrite, $CuFeS_2$, upon an a-face. Copper, iron and sulphur atoms are represented by circles of decreasing size. Wyckoff[26]

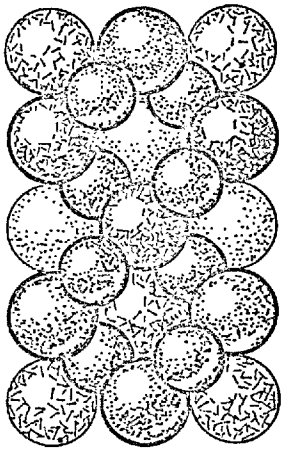

FIG.13 A packing drawing of the CuFeS structure inwhich the atoms have been given their neutral radii. The line-shaded spheres are the copper atoms. Wyckoff[26]

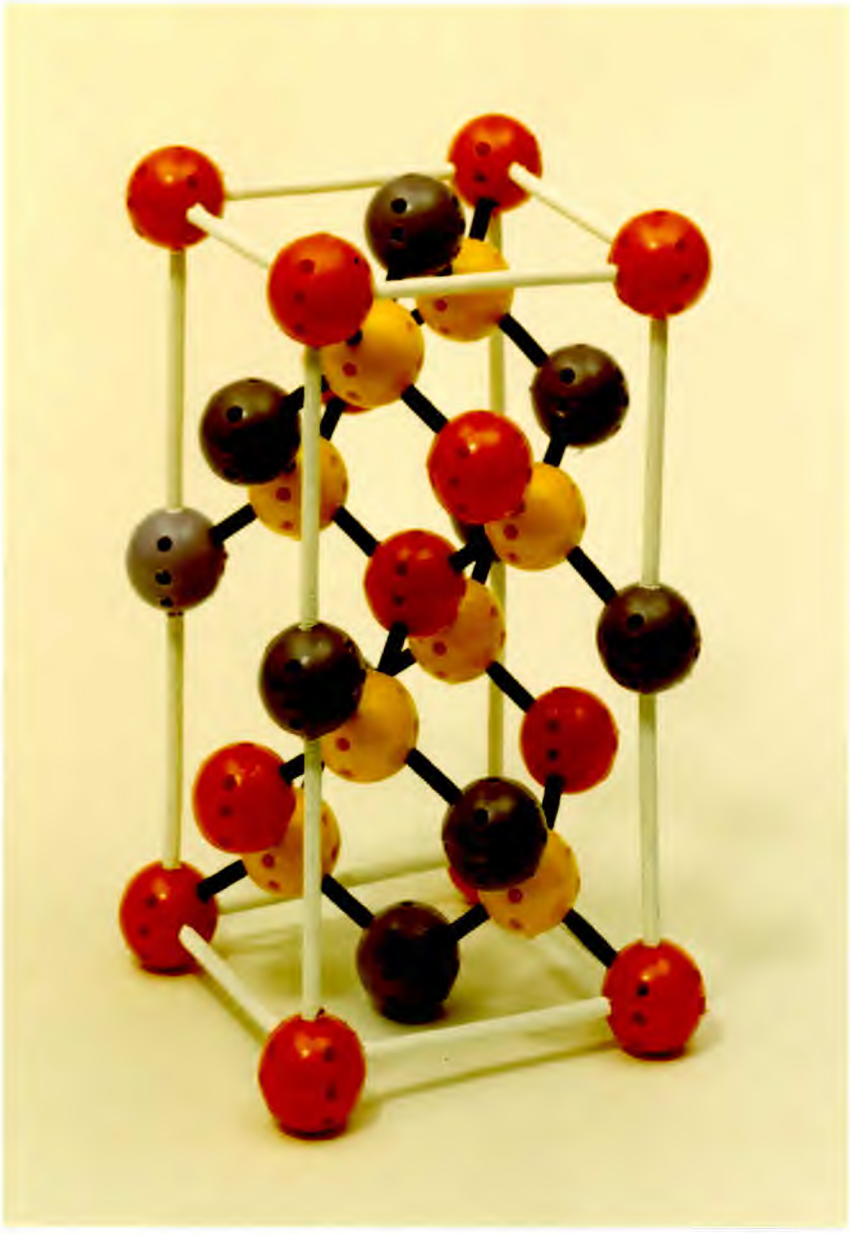

FIG. 14 Crystal structure of chalcopyrite. The edges of the unit cell are shown in white. Copper atoms are shown in orange, iron atoms in blue and sulphur atoms in yellow.

Structure of Orthorhombic Sulphur.

The unit cell of ordinary orthorhombic sulphur, S, is a very large one containing 128 atoms and having

a = 10.467 A, b = 12.870 A, c = 24.493 A (25^{o} C)

The space group is V_h^{24} (Fddd) with all of these atoms in general positions which, placing the origin in a center of symmetry, have the coordinates:

(32h) ± (xyz; x,1/4-y, 1/4-z; 1/4-x, y,1/4-z; 1/4-x,1/4-y,z); F.C.

A recent detailed study[31] confirms the original determination and results in parameters, which though more accurate are not greatly different from those established many years ago. The structure is an assemblage of 16 S_8 molecules per cell(fig. 15) Each molecule is a closed puckered ring of sulphur atoms in which the S-S separation is 2.048 A and the S-S-S angle is ca. 107^{o} 54'. The nearest approach of the sulphur atoms of adjacent molecules is 3.69 A.

Parameters of the atoms in orthorhombic sulphur:

Atom	x	y	z
S (1)	0.8554	0.9526	0.9516
S (2)	0.7844	0.0301	0.0763
S (3)	0.7069	0.9795	0.0040
S (4)	0.7862	0.9073	0.1290

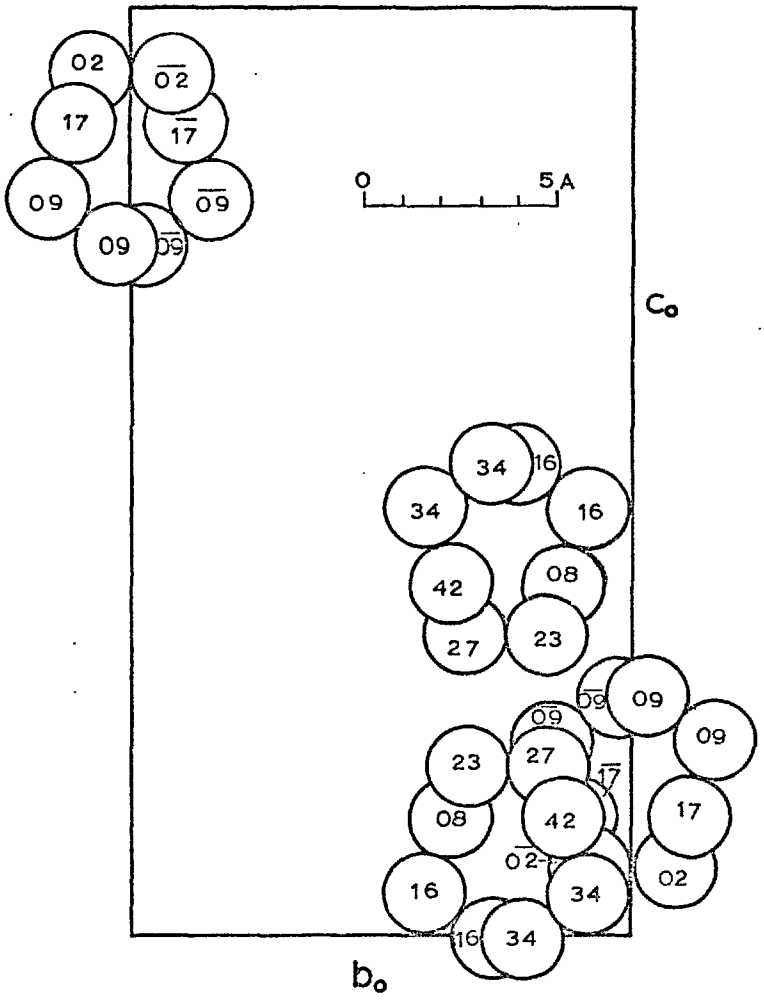

FIG.15 A projection along the a_o axis of the orthorhombic unit of rhombic sulphur, showing four of its 16 molecules. Origin in lower right. Wyckoff [26]

1.3 Idaite

Frenzel[32,33], studying natural bornite in the process of decomposition, observed that it was converted into a mineral he could not analyse, because of the small amount present in his sample. He thought the optical properties and structure were similar to a synthetic compound prepared by Merwin and Lombard[34] and more recently synthesized by Roseboom[35] and Yund and Kullerud[36]. By deduction Frenzel gave this new mineral the formula Cu_5FeS_6 and he called it Idaite. Frenzel described idaite as a supergene sulphide which is formed, characteristically, by the alteration of bornite by oxidation. Ramdohr[37] who had observed idaite from hundreds of localities, pointed out that in each instance the idaite is apparently the first oxidation product of bornite. This mineral has been recognized in association with bornite, at Yauricocha, Perú (Kobe[38]), in various deposits in Argentina (Brodtkorb[39]), from deposits in Japan (Takeuchi and Nambu[40]), at Litija, Yugoslavia (Grafenauer[41]), at Baincauroum, France (Picot[42]), at Sommerkahl, Germany (von Gehlen[43]), at Kormerud, Norway (Kraisse[44]), at Trattenbach, Austria (Tufar[45]) and at Copiapó, Chile (Sillitoe and Clark[46]).

Electron probe microanalyses (Levy[47] and Sillitoe and Clark[46]), of naturally-occurring,

supergene idaite have shown that idaite has the composition Cu_3FeS_4 (fig. 16). Levy has pointed out that the powder data given by Frenzel bears close resemblance to the tetragonal pattern of stannite and mawsonite (sphalerite structure) and that idaite, with formula Cu_3FeS_4, represents the tin-free end-member of the $Cu_{2+x}Sn_{1-x}FeS_4$ solid solution series. The other member (end-member) is the stannite Cu_2SnFeS_4. Between these there are brown stannite and orange bornite or mawsonite.

Levy also demonstrated that natural idaite, yields spectral reflectivity dispersion curves (fig. 17) differing markedly from of the original Cu_5FeS_6 synthesized by Merwin and Lombard and studied in more details by Yund[48], who gave it the general formula $Cu_{5.5x}Fe_xS_{6.5x}$ and dimensions a = 3.77 A, c = 11.18 A.

Similar measurements were done by Sillitoe and Clark in the Reichert microphotometer of the Geology Department (Royal School of Mines). This confirmed Levy's observations and supported the difference in crystal structure between idaite and Cu_5FeS_4.

Frenzel and Ottemann[49] have, on the other hand, presented microprobe data for a hypogene,

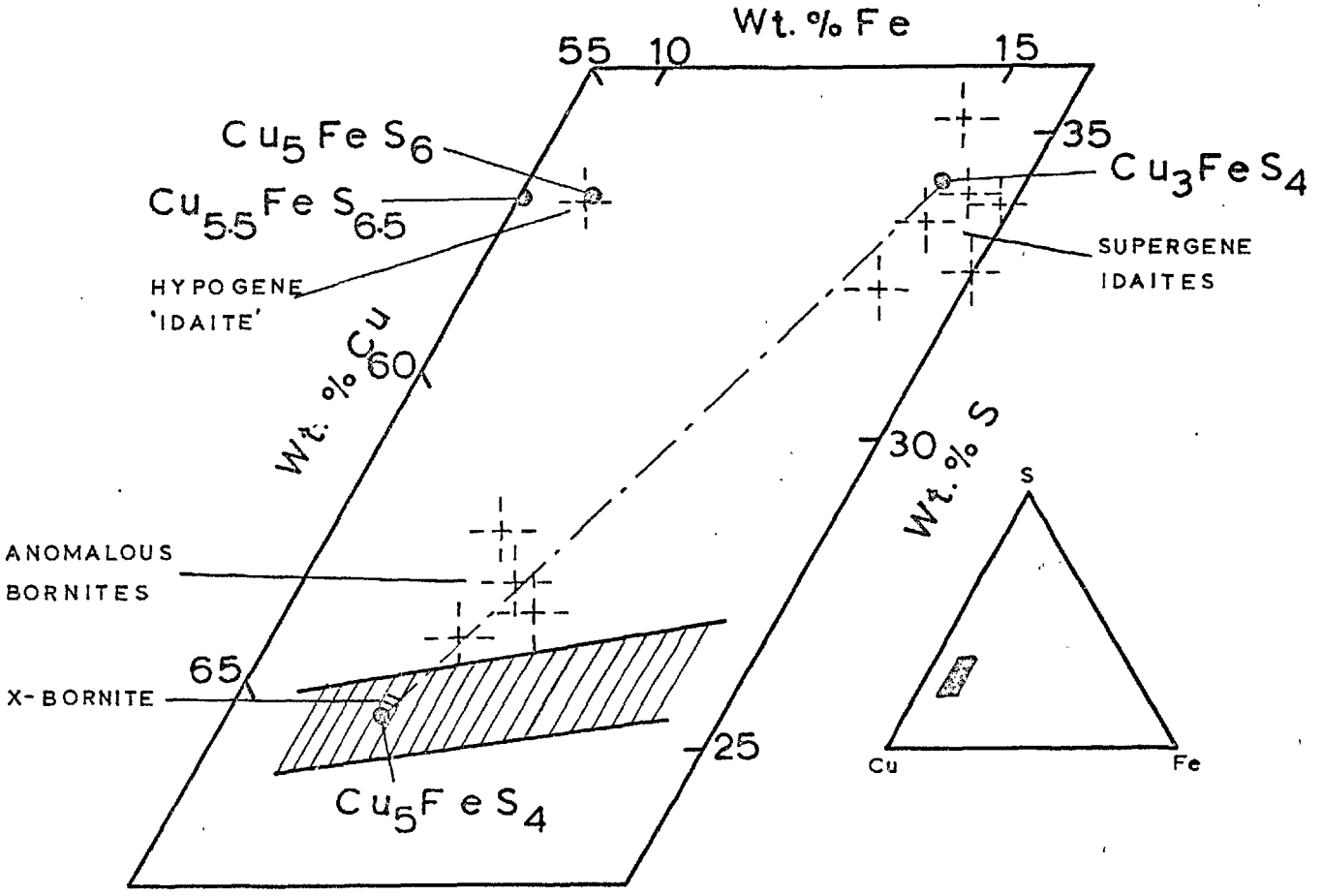

FIG. 16 Compositional relations in part of the system Cu-Fe-S. Sillitoe and Clark[46]

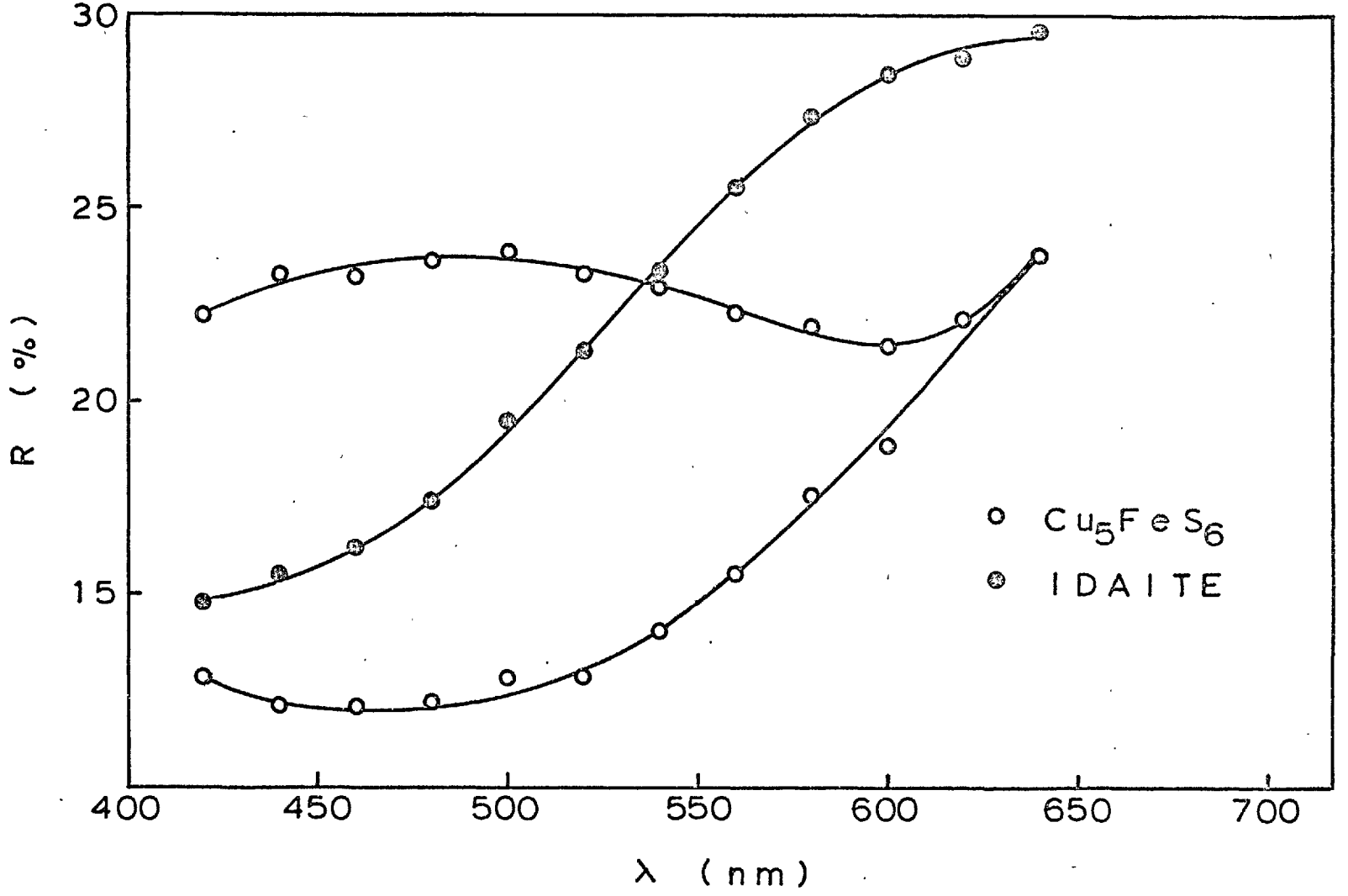

FIG. 17 Reflectivity dispersion profiles.. Levy[47]

idaite-like mineral from Nukundamu, Fiji, indicating a composition close to Cu_5FeS_6. Hexagonal cell parameters of a = 3.78 ± 0.001 A and c = 11.18 ± 0.003 A were determined for this sulphide, clearly allying it to the synthetic $Cu_{5.5x}Fe_xS_{6.5x}$ phase.

A second occurrence of a mineral with a composition close to Cu_5FeS_6, and clearly comparable to that synthesized by Yund and Kullerud[36] and earlier workers, was reported in Aucanquilcha , Chile (Clark[50]).

In order to avoid confusion, Sillitoe and Clark have recommended that the name Idaite be retained for the probably tetragonal natural sulphide, as originally described by Frenzel, in zones of supergene oxidation, with the implication that the more-rich phase reported by Frenzel and Ottemann is in fact a new mineral.

Phase Relations in the System Cu-Fe-S.

The phase relations in this ternary system have been studied in great detail from 1100° C to 25° C. The first major contribution to the study of the system Cu-Fe-S was that of Merwin and Lombard [34]. They presented a diagram of the phase relations at variable temperature but under sulphur vapour pressure of 455 mm.

Investigations of liquidus relations in this system were undertaken by Schlegel and Schuller [51], by Jensen [52,53], by Greig, Jensen and Merwin [54], by Kullerud [55], Yund and Kullerud [36], Barton and Skinner [56] and Kullerud, Yund and Moh [57].

Although the phase relations in this system have received so much attention, it still remains one of the most confusing systems and many important questions remain unanswered.

The tie lines between the stable phases at 700° C are shown in fig. 18 and those at 25° C in fig. 19 . The first figure was taken from Yund and Kullerud and the second from Barton and Skinner. In the latter the dotted line corresponds to the controversial stable join between chalcocite and pyrite proposed by Yund and Kullerud and Barton and Skinner. Idaite in this diagram of phase

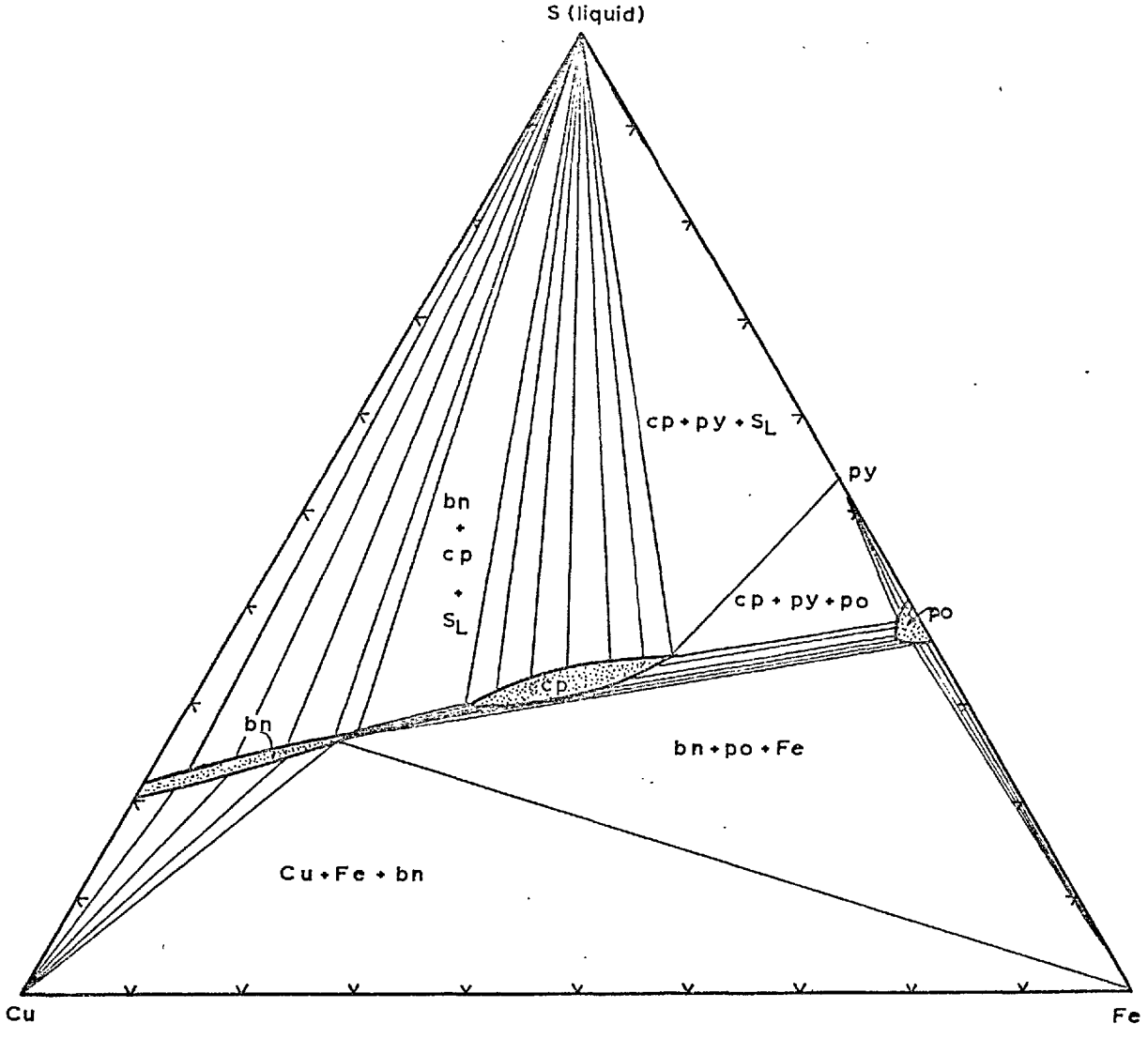

FIG. 18 Phase relations in the Cu-Fe-S system at 700°C [36]

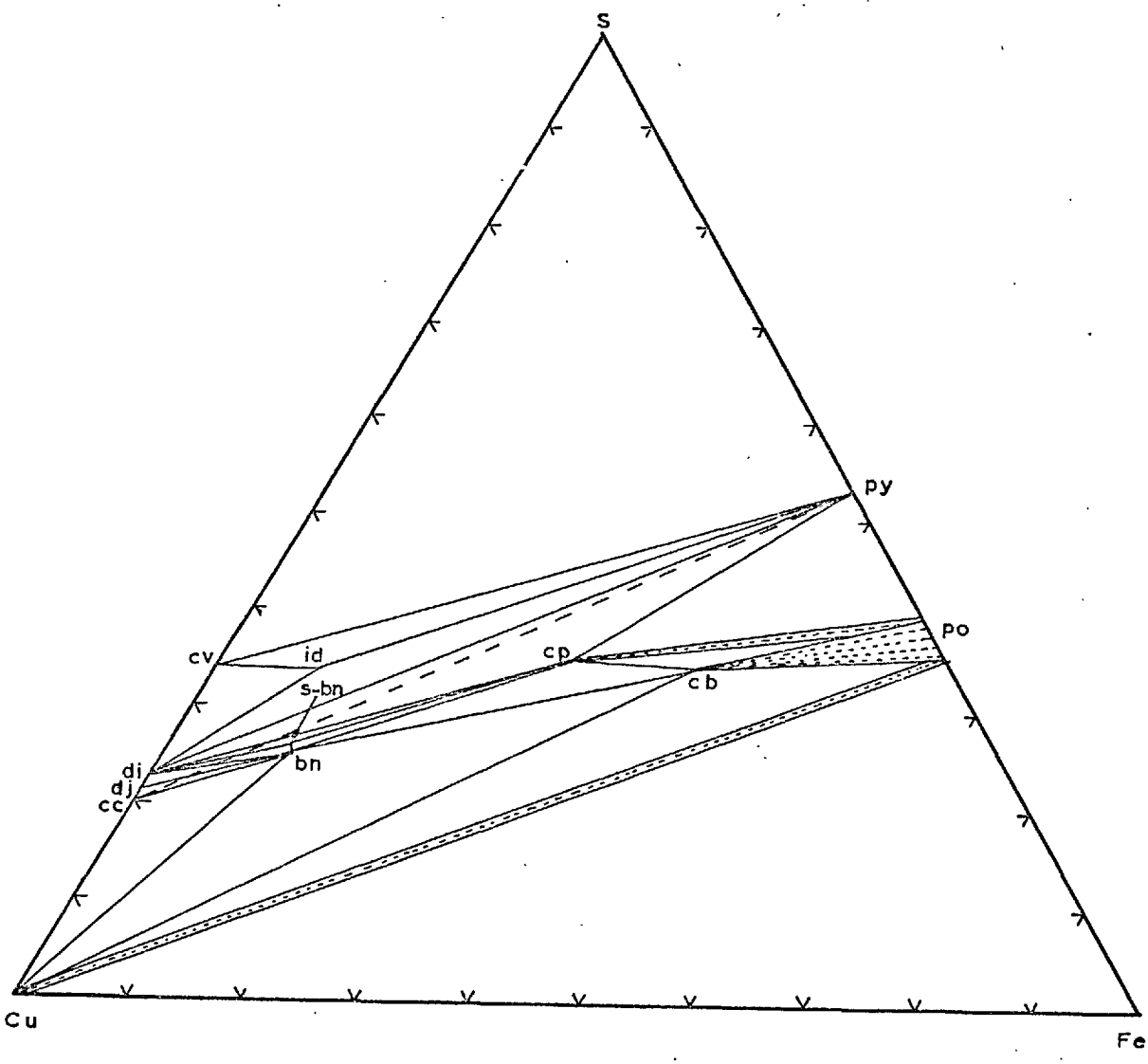

FIG. 19 Phase relations in the Cu-Fe-S system at 25°C (56)

relations is given the composition Cu_5FeS_6.

The main features of the Cu-Fe-S phase relations can be described in terms of the three principal solid-solutions series (fig. 18).

The abbreviations used in fig. 18 are listed in table 1.

The first solid-solution series is the pyrrhotite field which is of relatively little importance mineralogically.

The second solid-solution field is that extending from a composition of $CuFe_2S_3$ (cubanite) to a composition with a Cu/Fe atomic ratio of almost 2/1. This solid-solution field has a sphalerite-type structure, is called the chalcopyrite solid-solution field, and occurs only at high temperatures (above 550°C). At lower temperatures the field separates into two roots, a chalcopyrite root with compounds having a sphalerite-like structure, and a cubanite root with compounds having a wurtzite-like structure.

The third solid-solution field is the large single-phase area including, above 290°C, chalcocite (Cu_2S), digenite ($Cu_{1.8}S$) and bornite (Cu_5FeS_4) and is designated as bornite solid-solution field.

Extensive solid solution of chalcopyrite ($CuFeS_2$) in bornite (Cu_5FeS_4) extends the bornite solid-solution field at about 700° C, to

TABLE 1

Phases in the Cu-Fe-S system

Phase	Abbreviation	Composition
Chalcocite	cc	Cu_2S
Djurlite	dj	$Cu_{1.96}S$
Dijenite	di	$Cu_{1.8}S$
Covellite	cv	CuS
Pyrrhotite	po	FeS
Pyrite	py	FeS_2
Bornite	bn	Cu_5FeS_4
Sulphur-rich bornite	s-bn	-
Idaite	id	Cu_5FeS_6 *
Chalcopyrite	cp	$CuFeS_2$
Cubanite	cb	$CuFe_2S_3$

* In the present work Idaite is taken to have the composition Cu_3FeS_4.

give a Cu/Fe ratio of less than 3.

All three solid-solution fields have marked variations in their metal/sulphur ratios and copper/ion ratios.

In ore deposits, with the possible exception of those of pyrrhotite, none of the solid-solution fields are quenched, because they reequilibrate by exsolution and internal reactions to yield compositions consistent with much lower temperatures. This is consistent with the highly cation-disordered structures in which the energy barriers are so small between the ordered and the disordered forms, that the disordered states cannot be quenched.

In fig. 16 is shown a portion of the system Cu-Fe-S, taken from Sillitoe and Clark[46] to which some natural idaites compositions taken from Levy[47] were added.

This figure shows the lack of correspondence of the anomalous bornite (nonstoichiometric bornites) and the supergene idaite with known synthetic phases.

One line joining normal bornite (Cu_5FeS_4) to the composition Cu_3FeS_4 has also been drawn in this figure. This join has been drawn because it is important in the study of the solid-phase transformations during the leaching of bornite

as performed in the present work.

This line suggests a phase equilibria between bornite, nonstoichiometric bornite and idaite thus prohibiting the existence of tie-lines connecting digenite and pyrite and chalcocite and pyrite.

All the compositions shown in fig. 16 have been determined by electron probe microanalyses.

SECTION 2

EXPERIMENTAL PROCEDURE

2.1 Synthesis of Bornite (Cu_5FeS_4).

Bornite was synthesized by holding mixtures of pure copper, iron and sulphur (of required stoiehiometric amounts) at 900° C for 10 days. The technique employed involved the use of two-compartment silica tubes of the same form as those used by King [58]. This tube, containing synthesized bornite is shown in fig.20, it is possible to see the large size of the crystals formed.

The reason for the two compartments is to avoid contact of the melted sulphur with the copper and iron at the beginning of the synthesis which would cause uncontrollably fast reaction.

The apparatus used in the synthesis of bornite consisted basically of a horizontal electric furnace, specially designed to reach 1100° C, with a zone of constant temperature at least the same lenght as the silica tube used. A temperature profile was constructed to find the width of the zone of constant temperature. The temperature was controlled by an Ether , transitrol, electronic controller which

FIG.20 Silica vessel used for the synthesis of bornite.

allowed temperatures with a variation of only ± 2° C. The input of the furnace was controlled with a Variac autotransformer. An ammeter was connected to the circuit.

The temperature in the silica tube was accurately measured with a 13% Pt-Pt/Rh thermocouple placed inside the furnace and in contact with the silica tube. The potentiometer used was a Croydon, type 4, connected to the thermocouple with compensating wire.

This apparatus was also used for the reduction of iron sponge with hydrogen.

The purity of the elements used as starting materials is given in section 2.10.

Iron sponge was reduced by passing a current of H_2 over an alumina boat filled with the iron sponge, at a temperature of 500° C.

From the weight of two rods of pure copper, the stoichiometric amounts of sulphur and iron needed to form bornite (Cu_5FeS_4) were calculated.

The necessary amount of sulphur was weighed on an analytical balance and then transfered to the smaller compartment of the silica tube. The tube was held horizontally and the two copper rods were introduced in the larger compartment. Then the necessary amount of reduced iron powder was

weighed on the analytical balance and then poured into the larger compartment with the help of a magnet and a special funnel.

Immediately after the introduction of the starting materials an oil diffusion pump was connected to the open end of the tube and the system was evacuated. With the pump still working the tube was sealed with an oxygen torch.

The sealed silica tube was placed in the horizontal electric furnace.

Because of the initially high pressure due to the pure sulphur vapour pressure[15,59], the tube was heated to 600° C until all the free sulphur had been consumed. Fig. 21, shows the vapour pressure curve for sulphur. This curve was taken from Kullerud and Yoder[59]. It was constructed from the measured sulphur vapour pressures in the range 100-550°C[60] and the extrapolation of J.R. West[61] to the observed critical temperature of 1,040° ± 5° C[62] and an averaged critical pressure of 118 ± 31 bars based on various approximation methods. A very recent study by E.H. Baker[63] has confirmed the values from fig. 21 for the range of interest but gives higher pressures above 800° C. The mean deviation between the calculated values using the expression

$$\log P \text{ atm} = 6.00282 - 3584.42/T - 2.23934 \times 10^{-3} T + 1.14662 \times 10^{-6} T^2$$

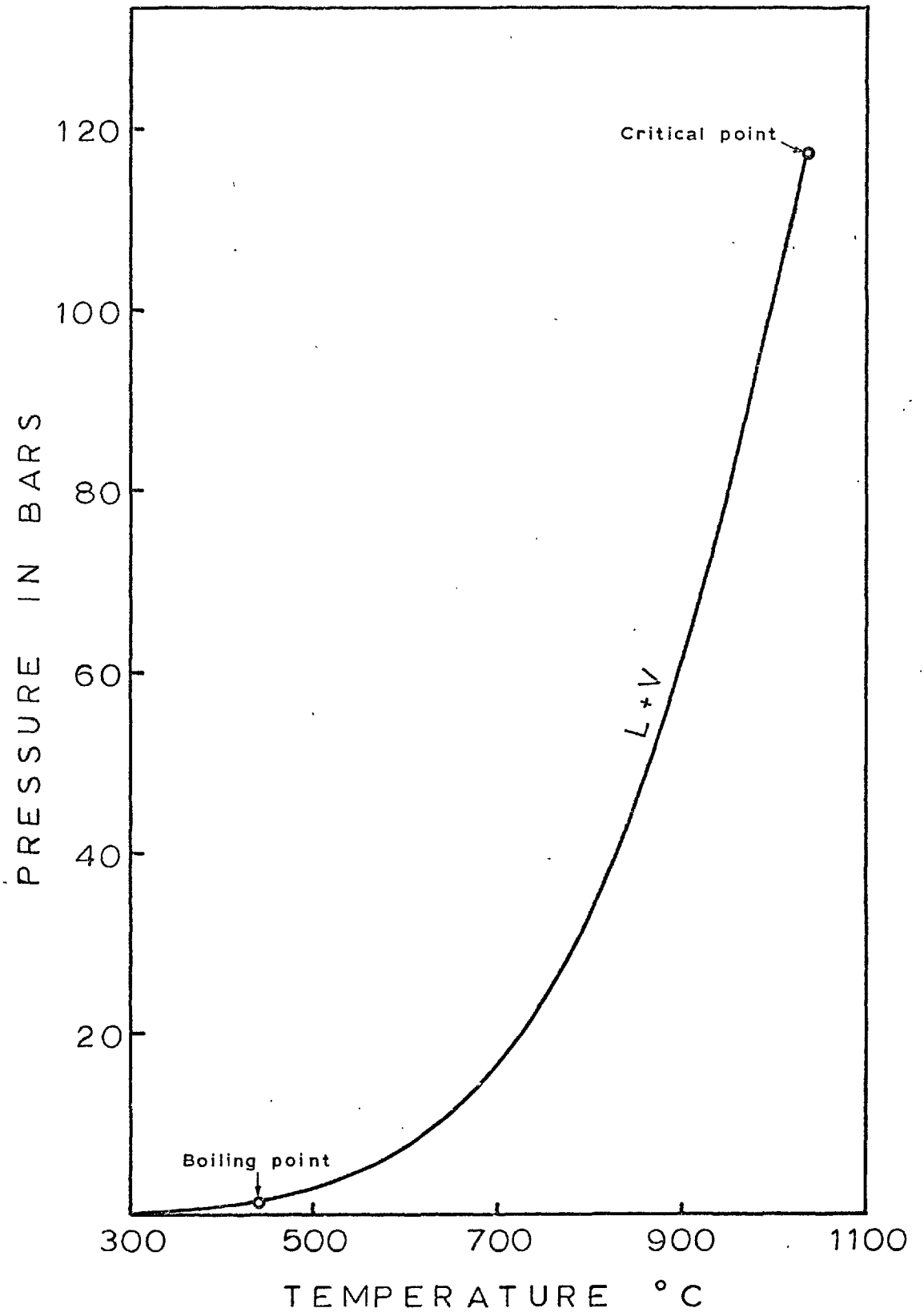

FIG. 21 Liquid-vapour curve for pure sulphur. Kullerud and Yoder[59]

and observed values for 55 measurements in this work was 1.2 per cent. The critical pressure was found to be 205.0 atm.

Thus, if the furnace temperature is 750° C the pressure inside the tube could be 25 atm which can cause an explosion. When the free sulphur is consumed by reaction with the metals, the vapour pressure decreases gradually. Merwin and Lombard give a pressure of 400 mm Hg at 750° C for the dissociation pressure of bornite, and even at 1000° C this pressure is very low[64]; the loss of sulphur and of metals to the vapour is therefore, negligible.

When all the liquid sulphur was seen to have disappeared, the temperature was increased to 900° C and maintained at this value for ten days.

After the ten days of synthesis the temperature was lowered slowly (0.5° C/min) to 700° C, maintained at this temperature for about 10 hours, then cooled down again to 200° C, maintained at this level for a further 6 hours and finally cooled down slowly to room temperature.

The ten days of heating allowed the complete homogenization and crystallization of the synthetic bornite.

The mechanism of the synthesis seems to be as follows:

The reaction starts when the sulphur distills onto the metals and begins the formation of the sulphides. This formation continues with homogenization occurring as copper and iron diffuse through these sulphides to the gas-solid interface. This mechanism was confirmed by the inspection of the final product, where the two holes left in place of the two initial copper rods are easily seen.

When the tube was taken out of the furnace after the synthesis, it was possible to see, through the transparent wall of the unopened silica tube, that the crystals of bornite had the brassy or tombac colour ascribed by mineralogists to a fresh fracture of bornite.

On opening the tube in air, the colour changed immediately through brownish purple to the iridescent blue of the natural bornite.

When this synthetic bornite is crushed in air the brassy colour again appears on the fresh fractures.

The x-ray diffraction pattern of the synthetic bornite had only the lines of tetragonal bornite fig. 52a. The interplanar spacings and intensities of the lines agree perfectly with the data of the A.S.T.M. file (table 41, Appendix 3).

Under the polarizing microscope polished sections of the synthetic bornite showed a pinkish colour immediately after polishing. This colour changed to

purple and bluish violet by oxidation. Under polarized light the synthetic bornite showed a very slight anisotropism.

All these characteristics agree perfectly with the optical properties of natural bornite.

Electron probe microanalysis showed uniformity in composition.

However, in some small zones of the synthetic bornite it was possible to see minute intergrowths of another phase. Due to the small size of these intergrowths they can only be seen under high magnification (fig. 36). From the optical characteristics of these intergrowths they are presumed to be chalcocite[65,66,67].

These small zones were not used in the leaching experiments.

The synthetic bornite was stored in closed containers to avoid excessive oxidation and only the necessary amount for leaching, usually one gram, was crushed.

2.2 Single Crystal Preparation.

Several attempts were made to prepare single crystals from the polycrystalline bornite in the apparatus shown in fig. 22, using a modified Bridgman method. Basically, the method consisted of filling the capillary hole at the bottom of the silica container with crushed bornite. The silica tube was stoppered with a silica glass rod to avoid losses of sulphur and it was then placed in a platinum crucible hanging by a 0.008" Pt/20% Rh wire from the lowering device at the top of the furnace.

The crucible with the bornite was lowered at 2½" per hour and maintained for about one hour in the hotest zone (1100° C)(fig. 23) to ensure melting. It was then lowered at a rate which gave a cooling of 100° C per inch.

All experiments made at pressures from 1 atm to 55 atm of N_2 resulted in the formation of polycrystalline bornite.

One interesting observation was that the loss of sulphur was very small even at pressures of about 6 atm of N_2. The only noticeable loss was measured in the experiment performed at 1 atm in which the loss of sulphur amounted to 0.2%.

The melting point determined during these runs, from the heating curve, agreed very well with those determined by Kullerud[68]. Bornite starts to melt at 1030°C and shows complete melting at 1060°C.

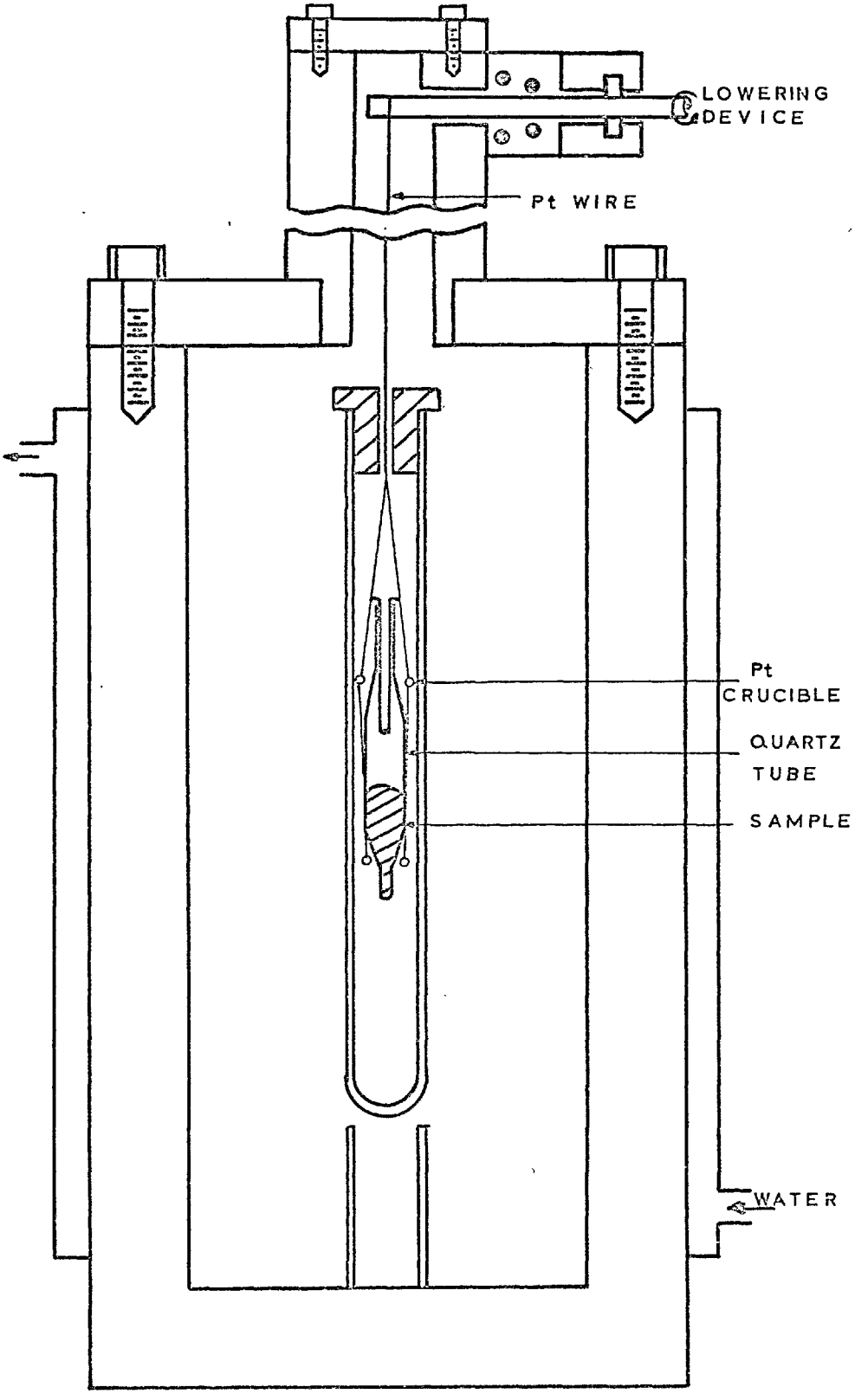

FIG. 22 High-pressure furnace

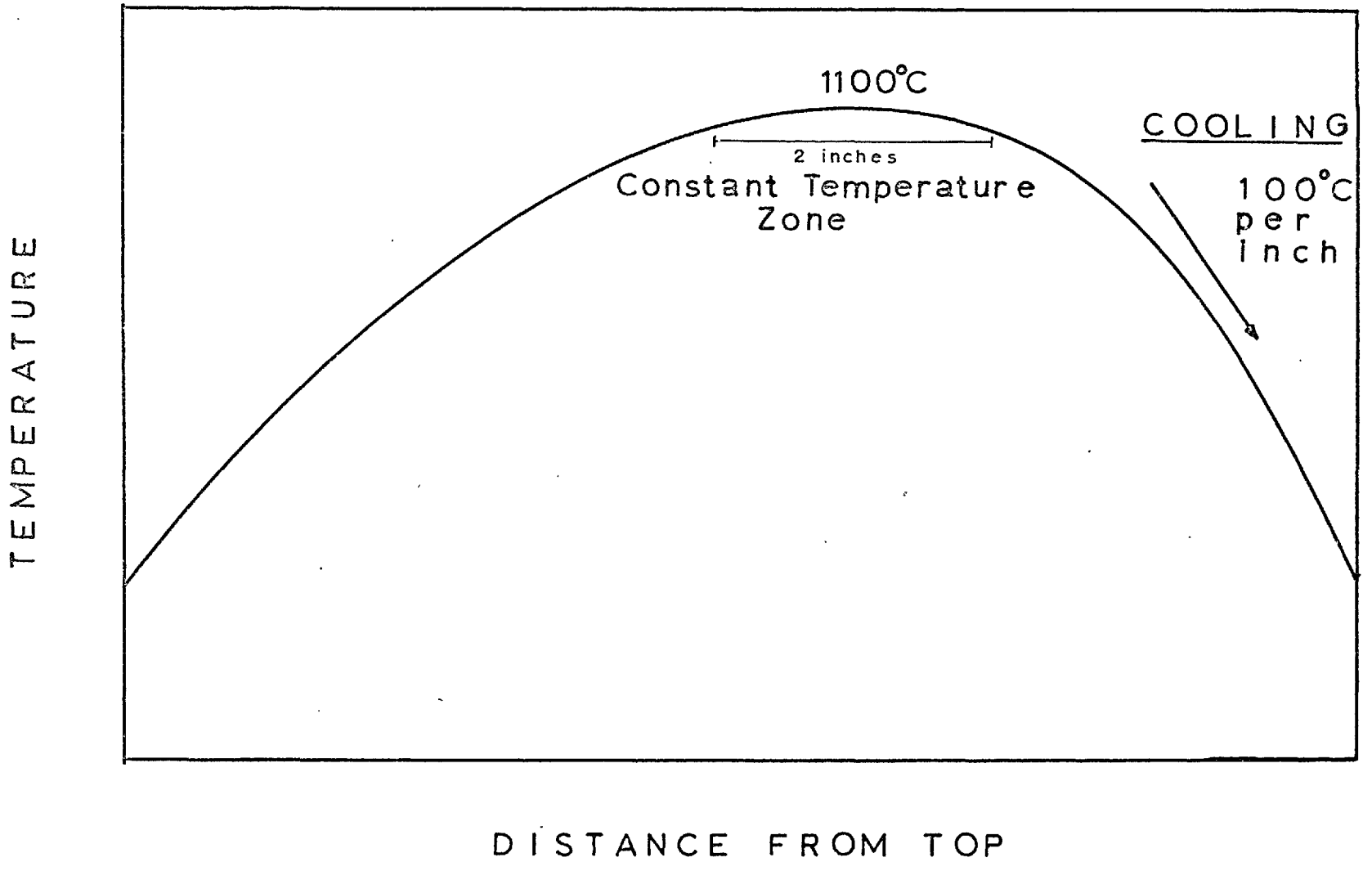

FIG. 23 Schematic temperature-profile of the high-pressure furnace.

2.3 Leaching Apparatus and Experimental Procedure.

The synthetic bornite was always leached in a particulate form. To produce particles of the required size, a small portion (1-2 grams) of the synthetic lump of bornite was chosen. This portion was crushed in an agate mortar and screened in 4" diameter nylon test-sieves to the required mesh size. This process was usually carried out only minutes before starting a run of leaching, to avoid oxidation of the crushed bornite.

About one gram of this particulate, synthetic bornite was placed in a dry and clean container and accurately weighed on an analytical balance.

The apparatus used in the leaching consisted of a Quickfit wide neck reaction vessel of 250 cc volume, joined to to a 5 necks lid by a metallic clip (fig. 24). The central neck held a mercury seal and the shaft of the glass stirrer. The stirrer was a simple two blade propeller mixer which was tested in a special run.

The thinner neck was used to hold a baffle employed to produce a turbulent regime during the leaching.

The thermometer was placed on the opposite side to the baffle, thus providing at the same

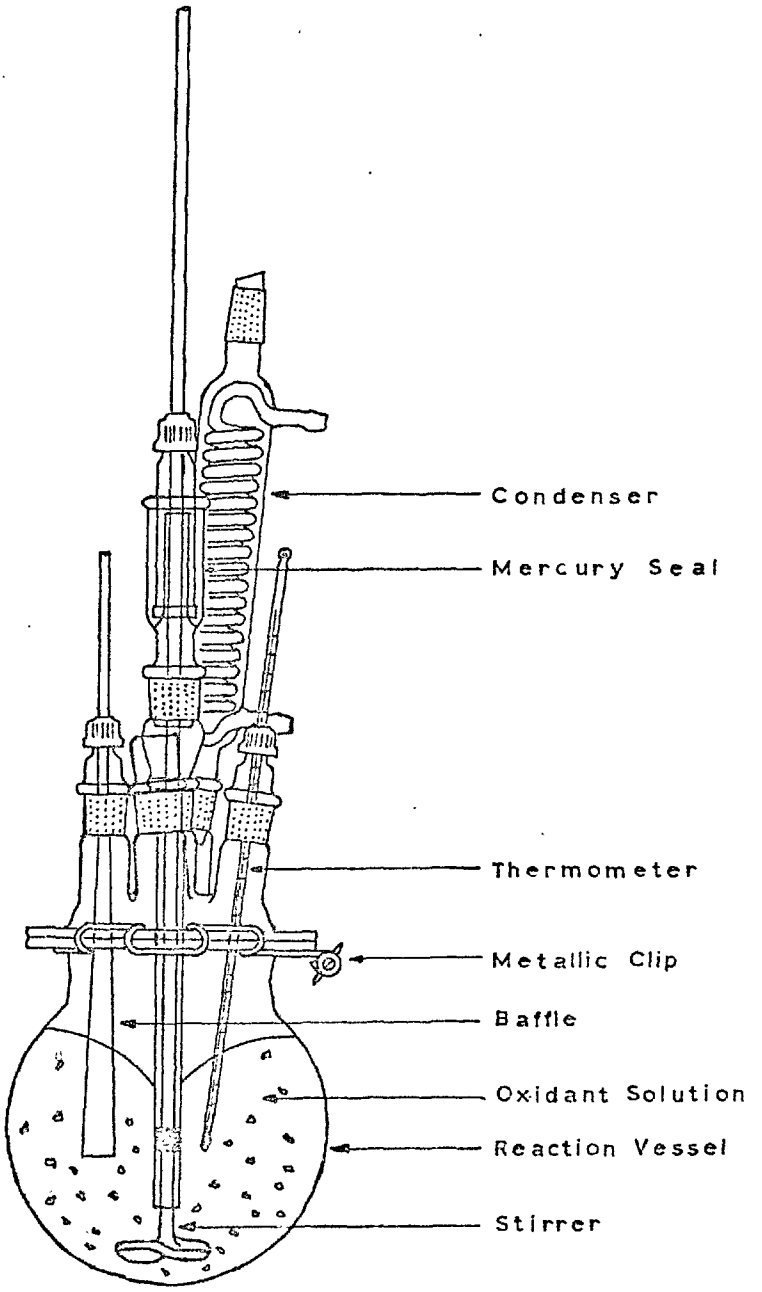

FIG. 24 Leaching apparatus

time a symmetric baffling of the solution. In one of the remaining necks a condenser was fitted in order to reduce losses by evaporation in the runs carried out at high temperatures. The neck used for sampling was the opposite to the condenser.

The whole system described above was immersed in an oil bath to the level of the vessel-lid joint.

The oil bath used was a 27 cm wide by 52 cm long TECAM CTB-2 constant temperature bath. Some specifications of this bath are:

Heater size TE-4	2000 watts.
Temperature range	-20° C $+200^{\circ}$ C
Temperature sensitivity	$\pm$ 0.05° C

The stirrer was connected by a rubber joint to a RTZ motor of variable speed.

For some runs at low temperature it was necessary to use a cooling device which consisted of a lead coil connected to the mains water tap and immersed in the oil bath.

The stirred leaching reaction vessel took two hours to come to thermal equilibrium with the oil bath.

The leaching procedure was as follow:

The leaching solution, usually 250 cc of ferric sulphate solution of the appropiate concentration , was prepared by dissolving the

necessary amount of previously weighed ferric sulphate powder in dilute sulphuric acid of the required strength.

With the leaching solution at the required temperature the synthetic bornite was poured into the reaction vessel.

Aliquots of leach liquor were extracted from the reaction vessel every 3, 5 or 15 minutes during the early part of the runs and every 30 minutes or 1 hour subsequently. The aliquots were extracted with 1 cc pipettes and diluted, with dilute sulphuric acid, to the volume required for the analysis, using polythene stoppered volumetric flasks.

At the end of the leaching run the reaction vessel was taken out of the oil bath and the contents filtered through Whatman filter paper N^{o} 542, to separate the solid residue from the leaching solution. The latter was stored and the solid residue washed several times with water and acetone and then dried in a hot air oven at 70^{o} C for 24 hours.

2.4 Analysis of the Leach Solution.

Initially a colorimetric method of analysis was used. These analyses were performed in a UVISPEK Hilger UV and visible spectrofotometer.

The copper was analysed using sodium diethyldithiocarbamate[69], this reagent, if added to a slightly acidic or ammoniacal solution of copper (II) in low concentration, produces a brown colloidal suspension of the cupric dithiocarbamate, but it is far better to extract the coloured copper complex, which is soluble in chloroform and other organic solvents.

The interference of iron was prevented by complexing with disodium ethylenediaminetetraacetate (E.D.T.A.). Chloroform was used for the extraction of the copper complex because chloroform solutions are more stable (for at least 30 minutes in bright daylight and several hours in difuse daylight) and disolve more of the copper carbamate than carbon tetrachloride.

The procedure used was as follow: 5 cc of ammonium citrate and 10 cc of sodium ethylenediaminetetra-acetate were added to the sample solution and followed by concentrated ammonia until a pH-meter showed about pH 8.5. The solution was diluted to

about 50 cc and transferred to a separating funnel. 5 cc of sodium diethyldithiocarbamate solution and 10 cc of chloroform were added and the funnel was shaken vigorously for 1-2 minutes. The chloroform extract was removed and placed in a 25 cc volumetric flask. 5 cc of chloroform were added to the remaining solution in the funnel and the chloroform extract again removed. This step was repeated once more. The combined extracts were diluted to 25 cc with chloroform . The absorbance was measured at 435 nm.

However, because atomic absorption analyses gave the same accuracy and it is a far faster and easier method, all the analyses of copper and iron from leach solutions were made in the atomic absorption spectrophotometer.

The apparatus used was a single beam Perkin Elmer 290 B atomic absorption spectrophotometer joined to a Honeywell Electronik 194 recorder.

Standard solutions for copper and iron were prepared from 1000 ppm analar stock solutions using diluted sulphuric acid of the same strength as that used for the leaching.

Before the analyses, a calibration curve using the standards was always drawn. Fig. 25 shows a typical calibration curve using deflection vs. ppm.

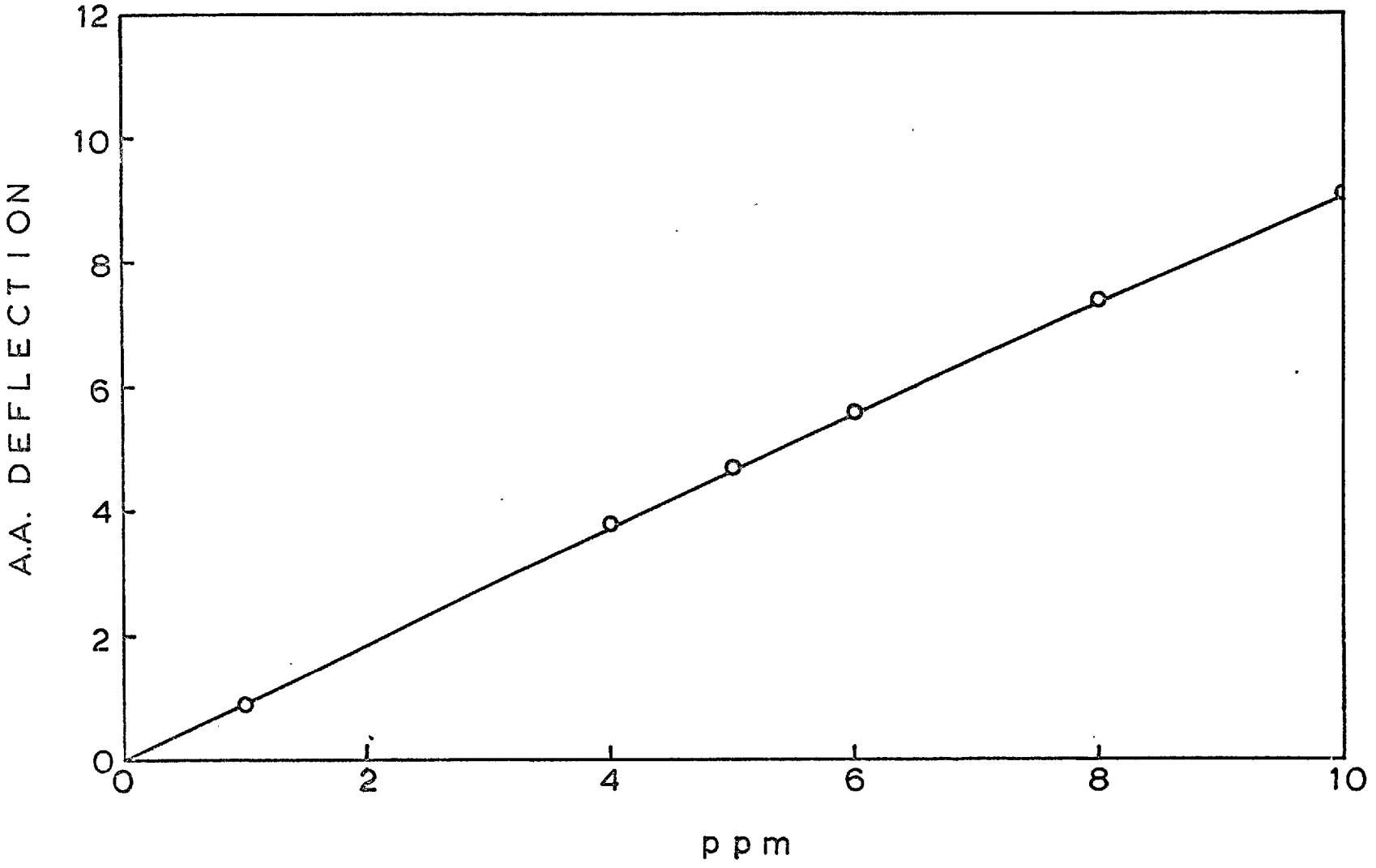

FIG. 25 Typical calibration curve for atomic absorption analyses

Most of the analyses were made using a multielement lamp and a 2" burner. The wavelengh position used for copper was 2483 A and for iron 3247 A. The slit for spectral width was 2 A for Cu and Fe [70].

The initial and final pH readings of the leach solutions were made using a "Dynacap" pH meter equipped with Pye Ingold type 401 combined glass and reference electrodes.

2.5 X-ray Diffraction.

X-ray diffraction was used to check the purity of the synthetic bornite and to analyze the residues of the leaching.

A Philips generator of 1 KW, type 1009 with filament current stabilizer to 1% was used.

The camera used was a Debye-Scherrer camera of 114.83 mm diameter.

The dried sample was crushed in an agate mortar and sieved to obtain a -320 mesh powder. This powder was put into a 0.2 mm glass capillary tube and this tube was then placed in the Debye-Scherrer camera.

The camera was loaded with Ilford Industrial G film.

In most of the x-ray analyses a Cu target was used , but in some, Co radiation was used instead.

The operating conditions of the Cu target were, usually, 40 KV and 20 mA with a Ni filter. The usual time of exposure for these operating conditions was 3 hours for the high intensity windows and 16 hours for the others.

After the necessary development, the films were measured using a film measuring ruler

(Hilger & Watts) with 1 vernier div. = 0.05 mm.

Calculation of the d spacings and other cell parameters were performed using tables and a electronic desk calculator.

Intensities of reflections were estimated by visual comparison.

Some x-ray diffraction analyses of the synthetic bornite were performed in a Philips diffractometer using a 2 KW, ultra stable, high voltage Philips generator. Type PW 1310. The tube current and high voltage are stabilized to within 0.03 % for main fluctuations of ± 10 %. This gives a very high reproducibility of results.

Cu radiation, a Ni filter and an internal quartz standard were used.

Several speeds of scanning and diameters of slits were tried until the best combination was found.

2.6 Microscopic Analysis.

The microscopic observations and photomicrography of polished samples were performed in a Reichert Universal Camera Microscope MeF. This is an inverted instrument fitted with a camera-back and a Reichert Remiphot exposuremeter. This works with transmited or reflected, normal or polarized light and is suitable for working from macro to oil immersion objetives.

The samples were mounted in Seemar or Araldite resins, then ground, first on emery paper and then on 8 micron and 1 micron diamond impregnated cloth laps, using an automatic Streuers Polisher.

Photomicrographs were taken on standard 5x4 plates and then printed.

The colour photomicrographs with polarized light were taken on 35 mm High Speed Kodachrome film for slides and then printed.

2.7 Electron Probe Microanalysis.

A Cambridge Microscan X-ray Analyser was used in the microanalyses of the different samples.

Fig.26 shows a schematic representation of the electron microprobe.

Some of the more important specifications of the apparatus used are given below:

Probe diameter : 1μ

Scanning area : Up to $\frac{1}{2}$ mm square.

Magnification : 250x to 3000x.

Resolution (electron image) : Usually better than 1μ .

Resolution (x-ray image) : Approximately 1μ .

Range of elements : 12-92 (Magnesium to Uranium).

Accuracy for quantitative analysis: Usually ± 1.0 % or better.

A built-in low power optical microscope is used to assist in accurately locating the field of interest on the specimen.

The x-ray spectrometer is a compact semi-focusing vacuum type equipped with 4 curved analysis crystals (3 lithium fluoride and 1 P.E.T. (penta-erythritol) which can be rotated to cover the entire Bragg angle range from 10^{o} to 65^{o}. For quantitative analysis the appropiate crystals are in turn

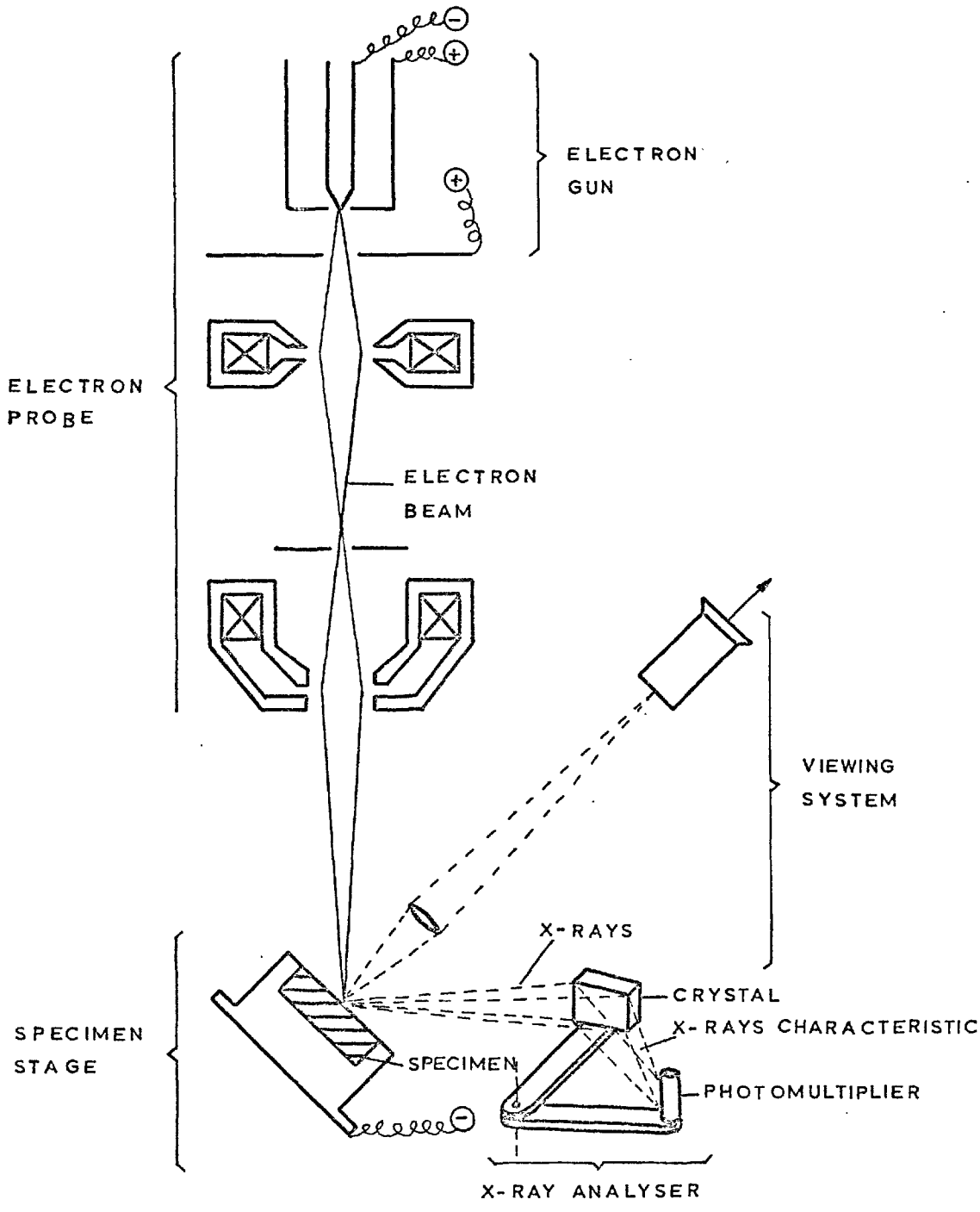

FIG. 26 Schematic representation of the electron microprobe[71]

rotated through the Bragg angles of the selected elements. The intensity of these reflected x-rays is measured by photomultiplier tubes and a pulse counter. These intensities are then compared with similar reflections produced from pure standards.

Specimens for the Microscan were prepared in exactly the same form as for a normal microscopic examination (section 2.6). The surface of the sample must be electrically conducting and non-conductors are vacuum-sputtered with carbon or aluminium.

Measurements were made at a number of fixed spots, chosen at random over the surface of an homogenous specimen.

The standards used were pure elements in the case of copper and iron, and in the case of sulphur pyrite was used. Corrections were applied to account for the following effects[72]:

1) Absorption: due to the fact that the standard and the specimen absorb the emitted radiation by different amounts.

2) Overvoltage: as the effective range of the incident electrons varies with the critical excitation energy of the x-ray lines being generated.

3) Atomic Number effect : because of the differences in the percentage of electrons backscattered

by the standard and the specimen, and the difference in electron retardation and x-ray production efficiency due to the difference in atomic number.

4) Characteristic Fluorescence: to allow for the production of radiation of one wavelength produced by characteristic radiation of another wavelength.

5) Background Fluorescence:since additional radiation at any particular wavelength may be excited by the continous background radiation.

An α correction procedure was applied using a formula of the type:

$$Cx = \frac{\%\ El\ (\ 1 + \alpha_1 C_1 + \alpha_2 C_2 + \ldots)_{SP}}{(\ 1 + \alpha_A C_A + \alpha_B C_B + \ldots)_{STD}}$$

% El : uncorrected % of element concerned

Cx : corrected % of element concerned

C_i : concentration of the other elements i in the phase concerned.

α_i : appropriate α_i values taken from a table specially prepared by T. Kelly[73].

(Subscripts 1,2, etc. refer to the phase analysed A,B, etc. refer to the standards).

This method is suitable for use with a desk calculator and is essentially a repetitive process.

2.8 Reflectivity Measurements.

A Reichert Reflex Spectral Microphotometer attached to a Reichert Zetopan microscope was used (fig. 27).

The instrument is composed essentially of a dialectric strip monochromator, ranging from 400 to 700 nm, together with a photomultiplier circuit of high stabilization specifications with dark current compensation. An ingenous mirror diaphragm optical system, of variable aperture, enables areas as small as 1μ to be measured at half-height bandwidths of 2-5 nm. This instrument, which is in normal use in the Royal School of Mines, combines simplicity of operation with consistent precision and linear response(74).

The standard chosen for the comparison of reflective power was pyrite, and the calibration made by D. Vaugham in December 1967 was used.

The deflections in the recording instrument of the sample and the standard were measured several times for each specimen. After taking the average of the readings the reflectivity was calculated by the simple formula:

$$R\ \% = \frac{\text{Deflection value of unknown}}{\text{Deflection value of standard}} \times k$$

when k = calibrated reflectivity of standard.

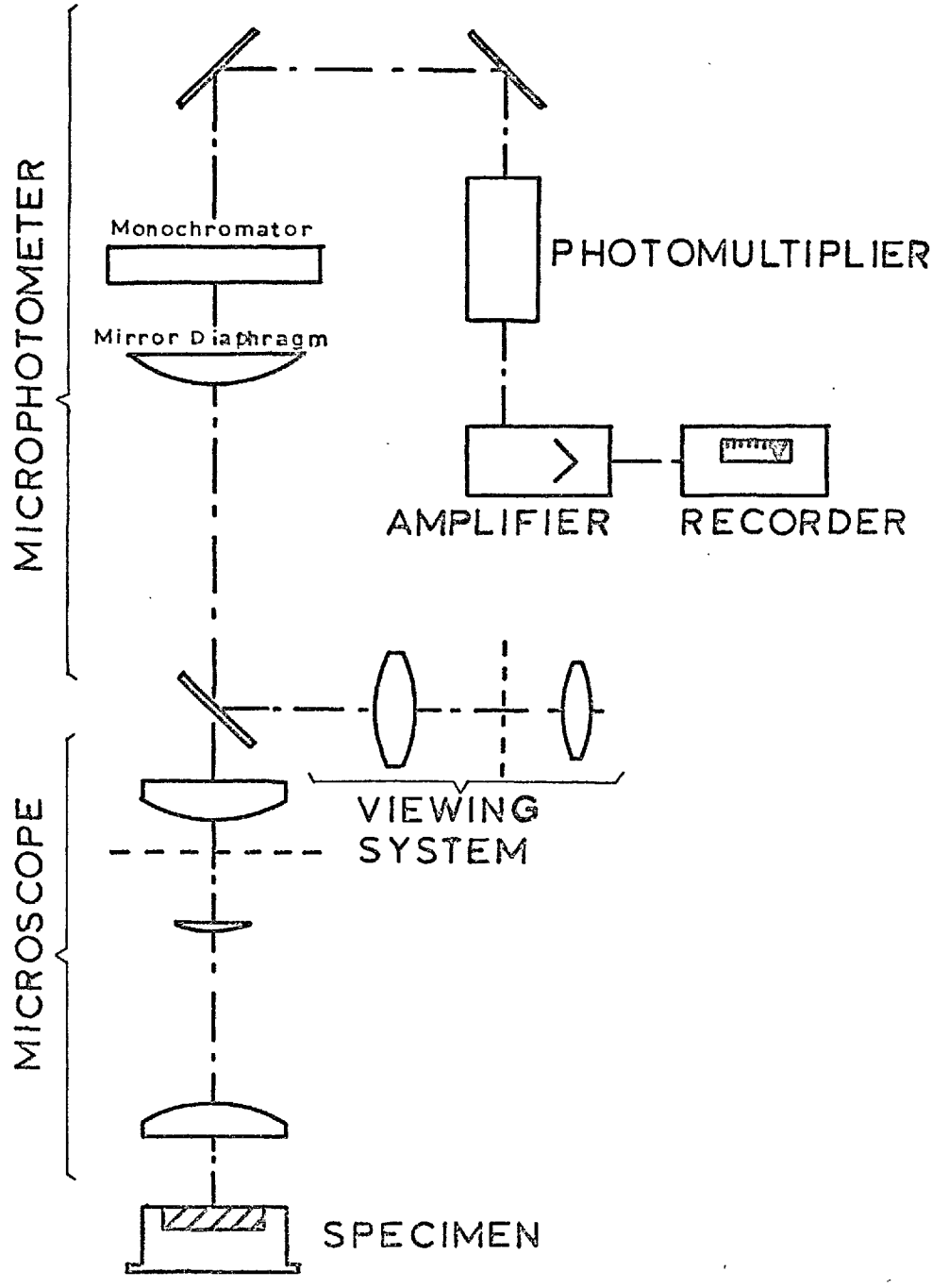

FIG. 27 Schematic representation of the microphotometer[74]

2.9 Density Measurements.

A pycnometer and a micro balance were used for the density measurements. The pycnometer was chosen because the material to measure the density was in powder form[75].

The following steps were followed in the density determinations: First, the powder was washed in absolute alcohol A.R. and dried in a hot air oven to a constant weight. The weighing was accurately performed on a micro balance. The empty pycnometer was also dried in the hot air oven and weighed on the micro balance.

The pycnometer was filled with distilled water. In order to eliminate air bubbles included among the mineral particles the bottle was suspended in a beaker filled with water and maintained at 50^{o} C. A rubber pipe conected the neck of the bottle to a vacuum system and in this way all the entraped air was removed and all the particles were collected at the bottom of the bottle.

Because a temperature control is essential, in order to avoid any variation in the volume of water, the bottle was suspended in a 1 liter beaker filled with distilled water. This beaker

was immersed in an oil bath with a constant temperature of 25° C. When the system reached an equilibrium the bottle was filled and the stopper replaced. Special care was taken to ensure that the water reached the top of the capillary tube. The small excess was wiped off with a soft tissue and the bottle was taken to the balance room to be weighed on the micro balance.

After taking the powder out, the pycnometer was again filled with water in the same manner as described above, using the oil bath at exactly the same temperature as before (25° C).

Finally, the pycnometer filled with distilled water was weighed on the micro balance.

The density was determined using the formula:

$$D = \frac{M - A}{(P + M - A - S) \times V_t}$$

Where

M = Weight of the pycnometer containing solid

A = Weight of the empty pycnometer

P = Weight of the pycnometer filled with distilled water

S = Weight of the pycnometer filled with solid and distilled water

V_t = Correction factor to relate the volumes of water at 25° C and at 4° C.

2.10 Purity of Materials.

a) Copper Rod (5 mm diameter by 15 cm long)

Spectrographically pure rods (Johnson Matthey).

Spectrographic examination:

Element	Estimate of quantity present
Silver	5 ppm
Lead	3 ppm
Nickel	1 ppm
Silicon	1 ppm
Bismuth	each less than 1 ppm
Cadmium	
Iron	
Magnesium	

b) Sulphur (powder)

Spectrographically pure sulphur (Johnson Matthey).

Spectrographic examination:

Element	Estimate of quantity present
Aluminium	0.5 ppm
Sodium	0.2 ppm
Zinc	0.2 ppm
Barium	0.1 ppm
Nickel	0.1 ppm
Copper	0.05 ppm

Titanium		0.05 ppm
Magnesium		0.03 ppm
Manganese		0.03 ppm
Silver		0.03 ppm
Boron		0.01 ppm
Calcium		
Iron	each less than	1 ppm
Silicon		

c) Iron (sponge)

Spectrographically pure iron (Johnson Matthey).

Spectrographic examination:

Element	Estimate of quantity present
Silicon	3 ppm
Magnesium	2 ppm
Manganese	2 ppm
Nickel	2 ppm
Copper each less than	1 ppm
Silver	

d) Sulphuric acid (H_2SO_4)

G.P.R. 1.84 gr wt. per cc.

Typical analysis:

Non volatile matter 0.015 % max.

Chloride 0.004 % max.

Nitrate 0.0005 % max.

Heavy metals 0.0025 % max.

e) Ferric sulphate ($Fe_2(SO_4)_3 \cdot 9H_2O$

G.P.R. (powder) Low in nitrate.

Typical analysis:

Chloride 0.04 % max.

Ferrous iron 0.028 % max.

Nitrate 0.003 % max.

$Fe_2(SO_4)_3 \cdot 9H_2O$ 97 % minimun.

f) Copper Standard Solution.

Reagent for atomic absorption spectrophotometry (Hopkin & Williams).

1000 ppm w/v of Cu in 0.1 N $HClO_4$

Metal content is within 0.5 % of the nominal value.

g) Iron Standard Solution.

Reagent for atomic absorption spectrophotometry (Hopkin & Williams).

1000 ppm w/v of Fe in 0.1 N $HClO_4$

Metal content is within 0.5 % of the nominal value.

SECTION 3

RESULTS AND DISCUSSION

3.1 Kinetic Rate-Curves of the Leaching of Bornite. Effect of the Leach Variables on the Rate of Reaction.

Bornite was leached, under different conditions, using the apparatus and technique described in section 2.3.

From the kinetic curve shown in fig. 28 it is possible to see the general characteristics of the dissolution of bornite. The principal feature shown by the curve is the existence of two clear distinct stages in the leaching reaction. The first stage, in which about 40 % of the copper was dissolved in only 30 minutes, occurred very fast. The second stage occurred much more slowly.

The conditions of leaching listed in fig. 28 are the best it was possible to obtain. Under these conditions, 96 % of the copper originally present in the synthetic bornite was dissolved.

The influence of the following factors on the leaching of bornite were studied:

1) Temperature.

2) Particle size.

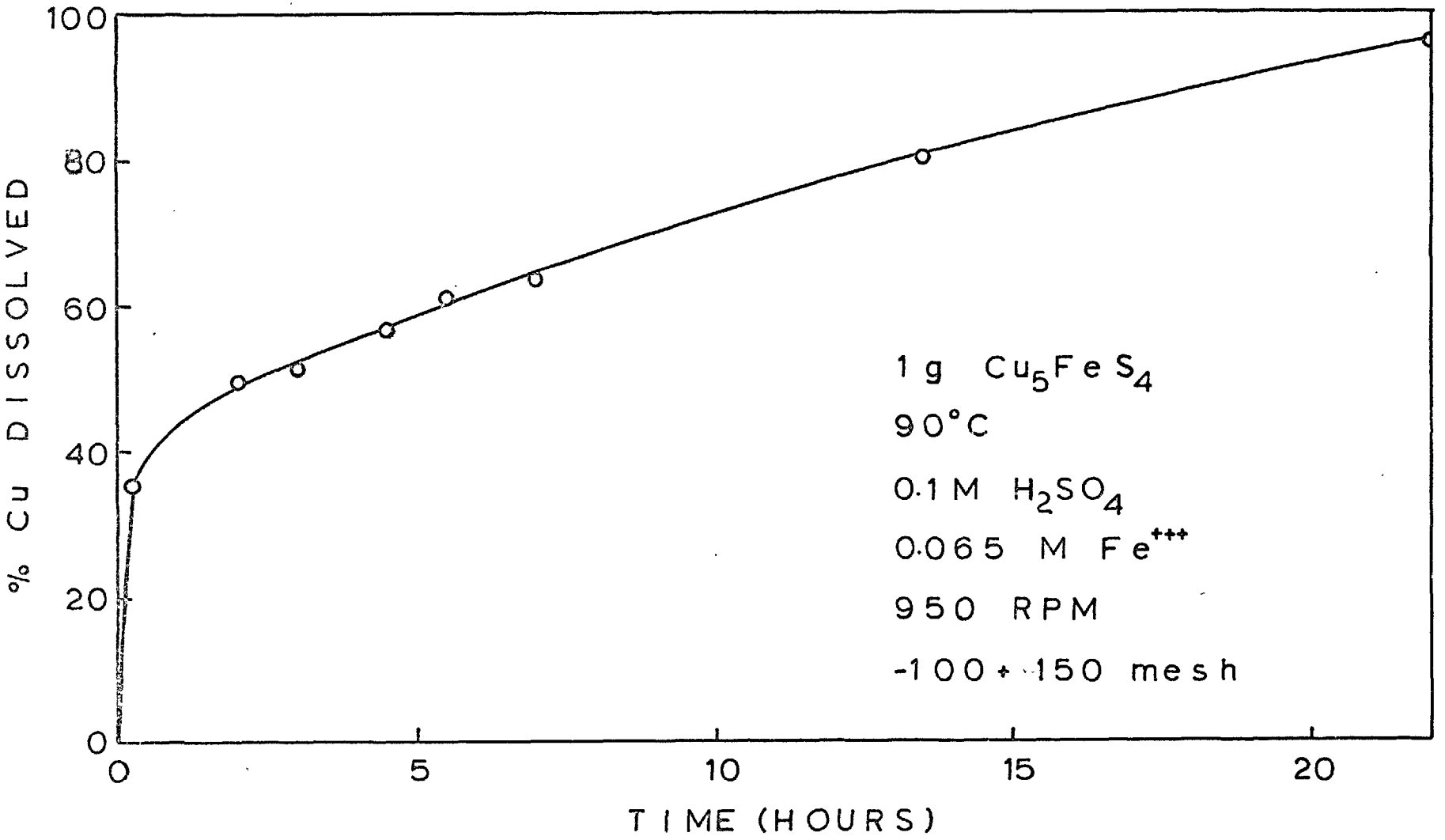

FIG. 28 General characteristics of the dissolution of bornite

3) Stirring speed.

4) Fe^{+++} concentration.

5) H_2SO_4 concentration.

6) Sample weight.

3.1.1 Temperature.

Figure 29 shows the effect of temperature on the rate of dissolution of bornite.

From fig. 29 it is possible to see that, in the runs made at 40° C and below, the reaction began to stop when about 27 % of the copper was dissolved. Table 8 (Appendix 1) shows that, in a run made at 30° C for 72 hours, only 37 % of the copper was dissolved.

At higher temperatures the reaction proceeded further, and at 70° C, 80° C, and 90° C the shape of the curve produced was the same as that shown in fig. 28. This curve was characterised by a first stage of fast dissolution of copper (lasting till about 40 % of the copper was dissolved), and a second stage of slow dissolution which was sensitive to temperature.

At temperatures below 40° C it is possible to separate the first part of the reaction into two sections: One section extending to the point when about 27 % of the copper is dissolved (showing a

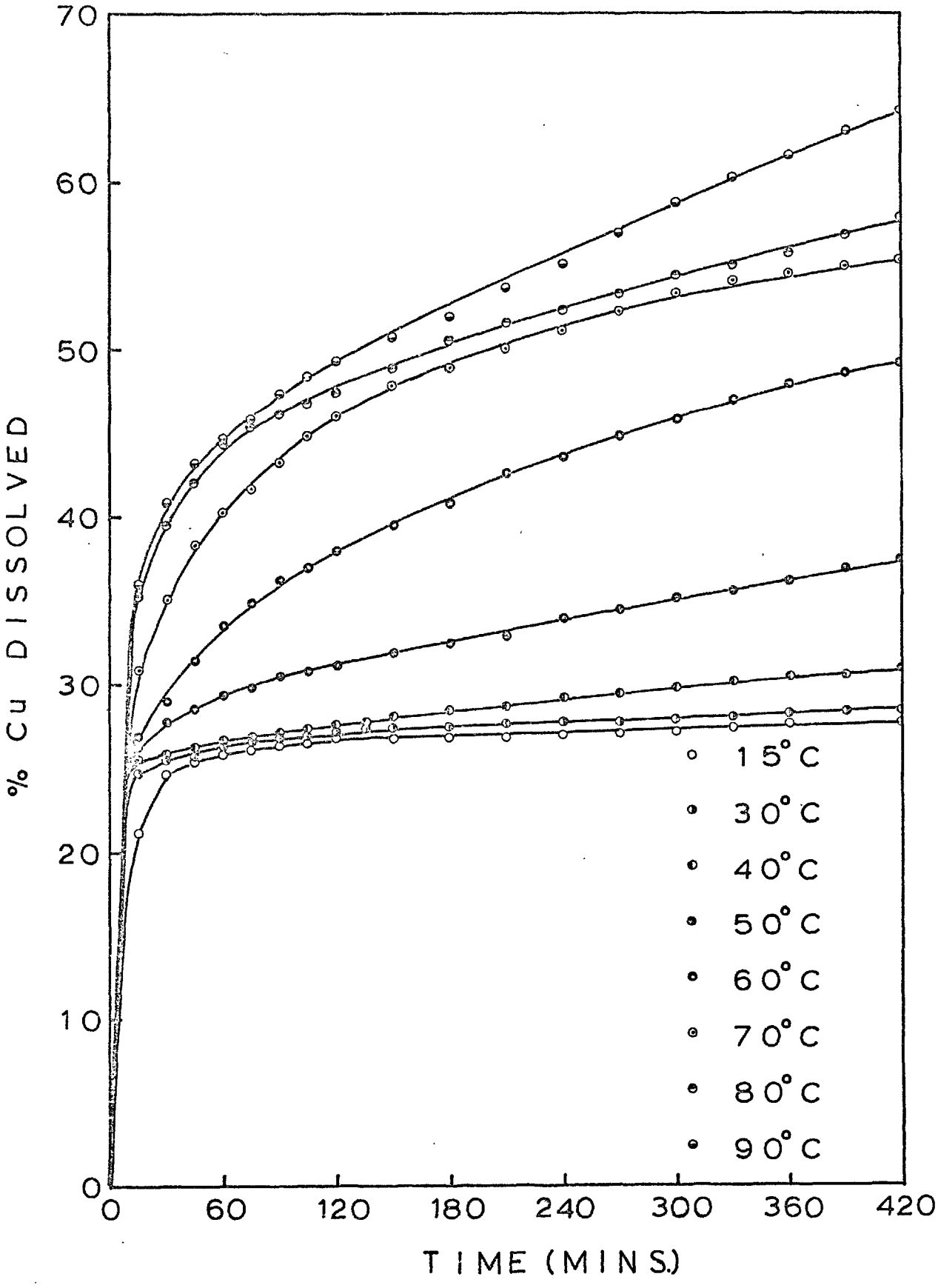

FIG. 29 Effect of temperature on the rate of leaching bornite

rate similar to that occurring in the first part of the reaction at higher temperatures); and a slower section from this point to a maximun of about 40 % of the copper dissolved.

The anomalies in the rate of dissolution, in the experiments made at high temperature, are belived to be caused by the flotation of the particles. This flotation proved impossible to eliminate.

During the first part of the reaction, at low or high temperatures, no iron was dissolved from the bornite and the appearance of sulphur was not detected.

Microscopic observations of the residues of leaching from the first part of the reaction (section 3.3) showed that the grains retain the original shape and the well defined edges of the original synthetic bornite.

These results can be explained by a mechanism consisting of a diffusion of copper ions in the lattice. X-ray powder photographs of the residues, of this part of the reaction (section 3.4), confirmed that the copper was removed by diffusion, until the bornite (Cu_5FeS_4) was transformed to a phase with a composition of Cu_3FeS_4 at the point when 40 % of the copper was dissolved. The composition

of this solid phase was determined by electron probe microanalysis (section 3.7).

Lattice parameter measurements (section 3.5) showed a marked contraction of the unit cell during the removal of the copper, until a point at which about 27 % of the copper was dissolved. From this point to that at which 40 % of the copper was dissolved, there was only a slight contraction of the unit cell.

The contraction of the unit cell was confirmed by density measurements (section 3.8) and by microscopic observation (section 3.3), which showed the formation of pores and cracks during the initial dissolution of copper.

From these results it is possible to explain the existence of the two sections which occur in the first part of the reaction, at temperatures below 40^{o} C, by the fact that to beggin with, copper is removed very easily by diffusion in the lattice until the contraction of the unit cell makes this process more difficult and the rate of dissolution falls. When the temperature is increased this drop in the rate is less noticeable because the temperature helps the diffusion process.

A final confirmation of a diffusion controlling step during the first part of the reaction was given

by the activation energy determination (section 3.2).

This determination was made from the percentage of copper dissolved in 2 minutes at 50,60,70,80 and 90° C. The Arrehnius plot gave a very good straight line. The slope of this line gave a value of 2.1 ± 0.1 kcal per mole for the activation energy of the first part of the reaction. This low value indicated that the diffusion of copper ions in the lattice was the rate-controlling step in the first part of the reaction.

The kinetic curves (figs.28 and 29), show a very much slower rate of dissolution during the second part of the reaction than that from the first.

The microscopic observations of the residues from leaching forming during the second part (section 3.3 , fig. 47) showed that grains of the phase with composition Cu_3FeS_4, (formed during the first part of the reaction), became increasingly attacked on their surface, and finally exhibited the presence of elemental sulphur in the zone in which the attack was most intense.

Electron probe microanalysis (section 3.7), of the residues from the second part of the reaction, showed that the composition of the solid phase remains Cu_3FeS_4 until its complete dissolution.

This composition, together with the reflectivity dispersion profile (section 3.6) allows the identification of this phase with the natural occuring mineral idaite (section 1.3).

The x-ray powder diffraction photographs (section 3.4) and the lattice parameter measurements (section 3.5) of the residues formed during the second part of the reaction, showed that the Cu_3FeS_4 phase remained structurally unaltered. The formation of sulphur during this part of the reaction was detected by, x-ray diffraction, electron probe microanalysis and a test using CCl_4 (section 3.3). The iron was dissolved, mantaining a Cu/Fe ratio in the residual solid equal to 3.

All these results indicate that during the second part of the reaction there is a direct transformation of the Cu_3FeS_4 phase to elemental sulphur.

The solid state transformations during the leaching can be explain structurally, using the hypothetical structure of bornite suggested by Manning (section 1.2.1). Thus, the layers of ionically bound copper ions present in the bornite structure are easily removed during the first part of the reaction, with a resulting contraction

of the unit cell.

When all the ionically bound copper is removed the structure that remains is a chalcopyrite-like structure with a formula unit Cu_3FeS_4. This chalcopyrite-like structure was confirmed by the x-ray diffraction powder photographs and the lattice parameter measurements.

The more difficult dissolution during the second part of the reaction is explained because the atoms are now covalently bound in a more ordered and compact structure. Thus, the dissolution, through a complete breakdown of this structure, results in the formation of elemental sulphur. The metals (copper and iron) go into solution.

It was not possible to determine the activation energy for the second part of the reaction because of the large amount of scatter of the experimental values. The main reason for this scatter was the flotation of the particles during the second part of the leaching (mentioned above), which caused uncontrolled variation in the rate of dissolution. The flotation of the particles was helped by, the formation of sulphur, the porosity originated during the first part of the reaction, and the decrease of density of the particles.

The charge neutrality of the bornite structure

during the removal of copper could be explained by the easy oxidation of the cuprous ions of the structure to cupric ions. In this way the charge neutrality is mantained.

The direct transformation from Cu_3FeS_4 or idaite to elemental sulphur is explained, because the arrangement of sulphur atoms in orthorhombic sulphur is completely different to the arrangement of sulphur atoms in the Cu_3FeS_4 lattice (section 1.2).

3.1.2 Particle Size.

Fig. 30 shows the effect of particle size on the dissolution of bornite. From this figure it is possible to see that grain size variation affected the first part of the reaction but not the second.

The increase in the rate of the first part of the reaction caused by a reduction in particle size occurs because the rate controlling-step is the diffusion of copper ions in the lattice. A reduction in particle size reduces the distances of the diffusion and thus increases the rate of dissolution.

The fact that the second part of the reaction was not affected by a reduction in particle size could be explained by a chemical attack in the

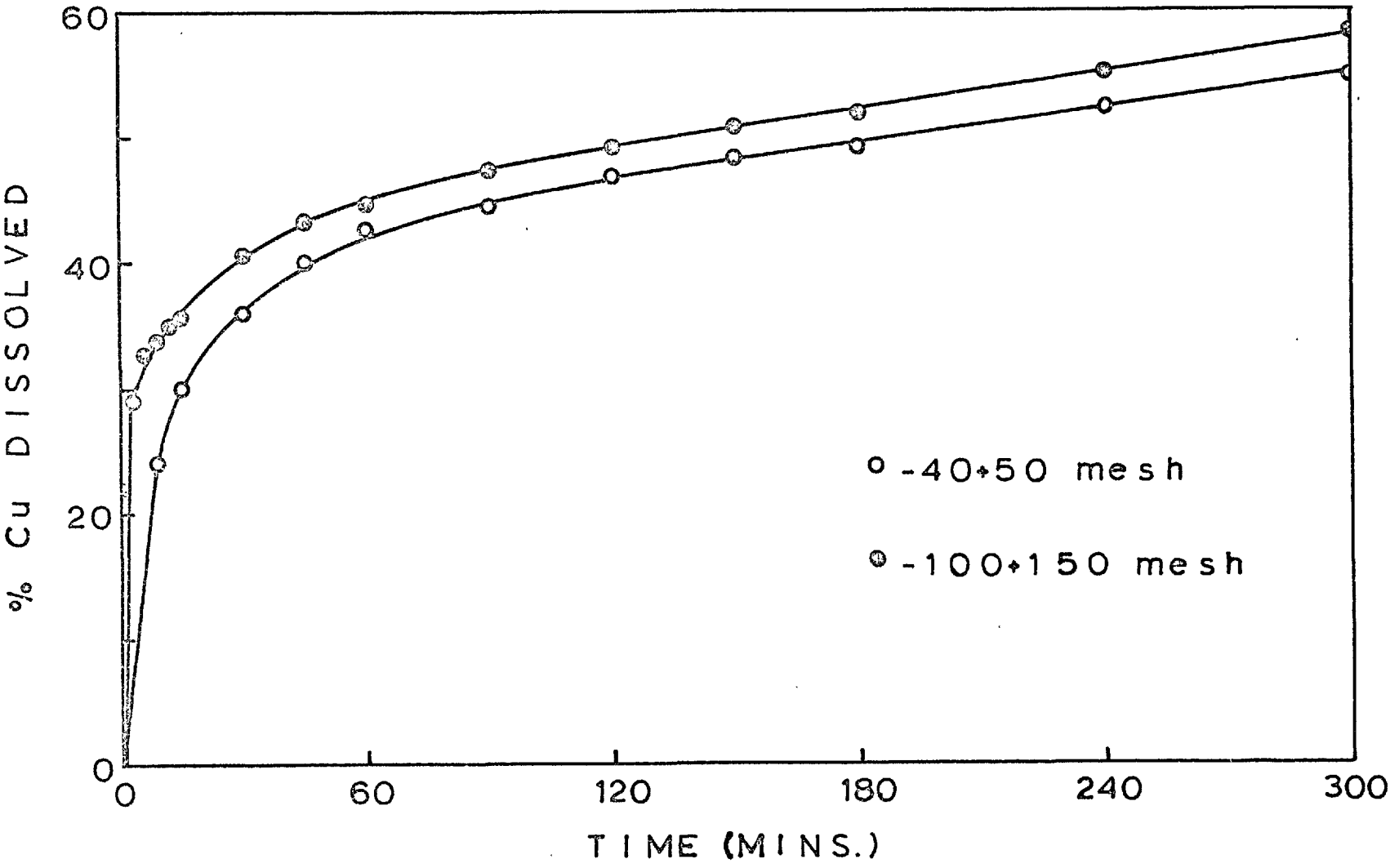

FIG. 30 Effect of particle size on the rate of leaching bornite

pores or by the fact that the rate-controlling step occurs in a homogenous phase either the solid or the solution.

However, because of the difficulties in the determination of the activation energy, for the second part of the reaction, and because there is no evidence of a chemical attack in the pores, it is not possible to conclude which of the posibilities mentioned above applies.

3.1.3 Stirring Speed.

Fig.31 shows the effect of stirring speed on the rate of dissolution of bornite.

The low rate produced at a stirring speed of 550 rpm is explained because this speed was insufficient to maintain all the particles in suspension and they tended to collect on the walls of the reaction vessel.

However, when a sufficient stirring speed was used, the rate of dissolution, in the first and in the second part of the reaction, was not affected by variation in the stirring speed. In section 3.1.4 it is shown that the ferric concentration did not affect the dissolution rate of the first part of the reaction and in section 3.1.2 that this rate was dependent on the particle size.

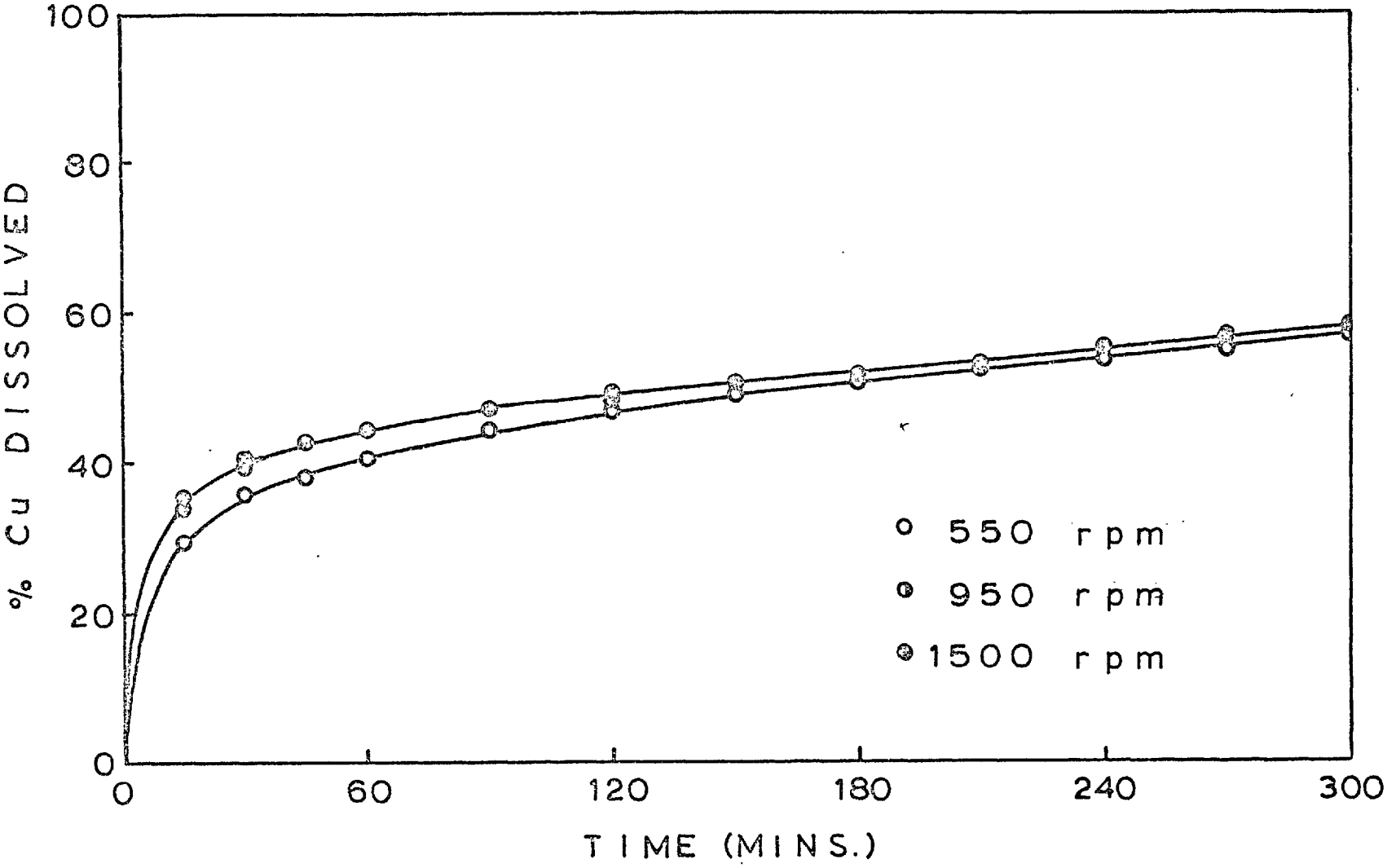

FIG. 31 Effect of stirring speed on the rate of leaching bornite

All these factors confirm that the rate-controlling step of this part of the reaction is the solid state diffusion of copper ions and not the diffusion of Fe^{+++} from the solution to the surface of the grains.

3.1.4 Ferric Ion Concentration.

The experiments to study the effects of Fe^{+++} concentration on the dissolution of bornite were carried out at 30 and 90° C using particle size of -100 +150 mesh.

The results are shown in figs. 32 and 33.

Fig.32 shows that acid alone does not dissolve bornite at all. The small dissolution effect produced is due to the presence of Fe^{+++} in the sulphuric acid used (section 2.10). The concentration was found to be 0.00009 M. The slope of this curve (fig. 32) results from the reoxidation of Fe^{++} to Fe^{+++} by the oxygen of the air.

The acid concentration used was 0.1 M H_2SO_4. This concentration allowed the retention of the ferric ions in solution, avoiding the hydrolysis and subsequent precipitation of iron.

In runs using higher concentration of Fe^{+++} (0.005 M and 0.01 M) there was more copper

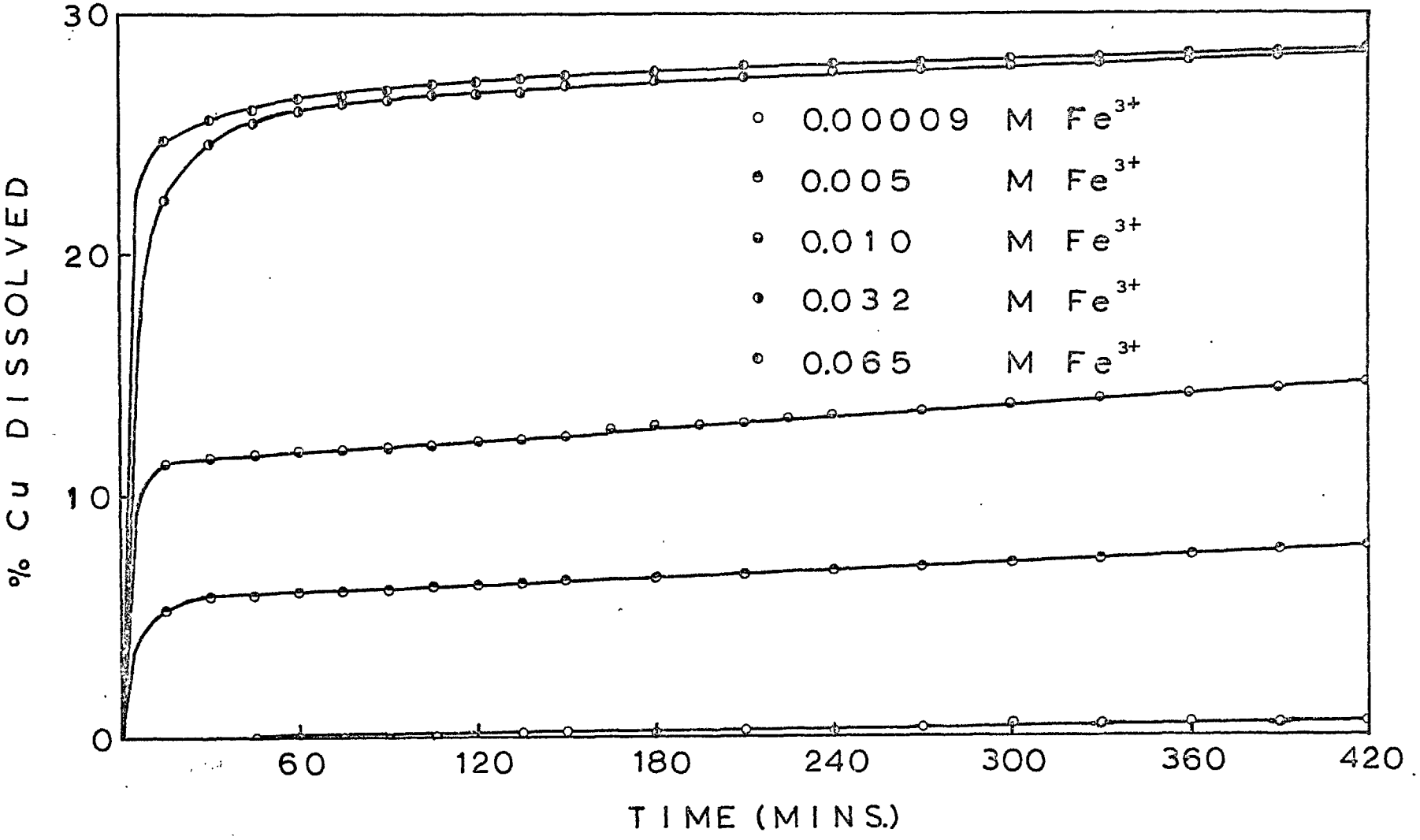

FIG. 32 Effect of ferric ion concentration on the rate of leaching bornite

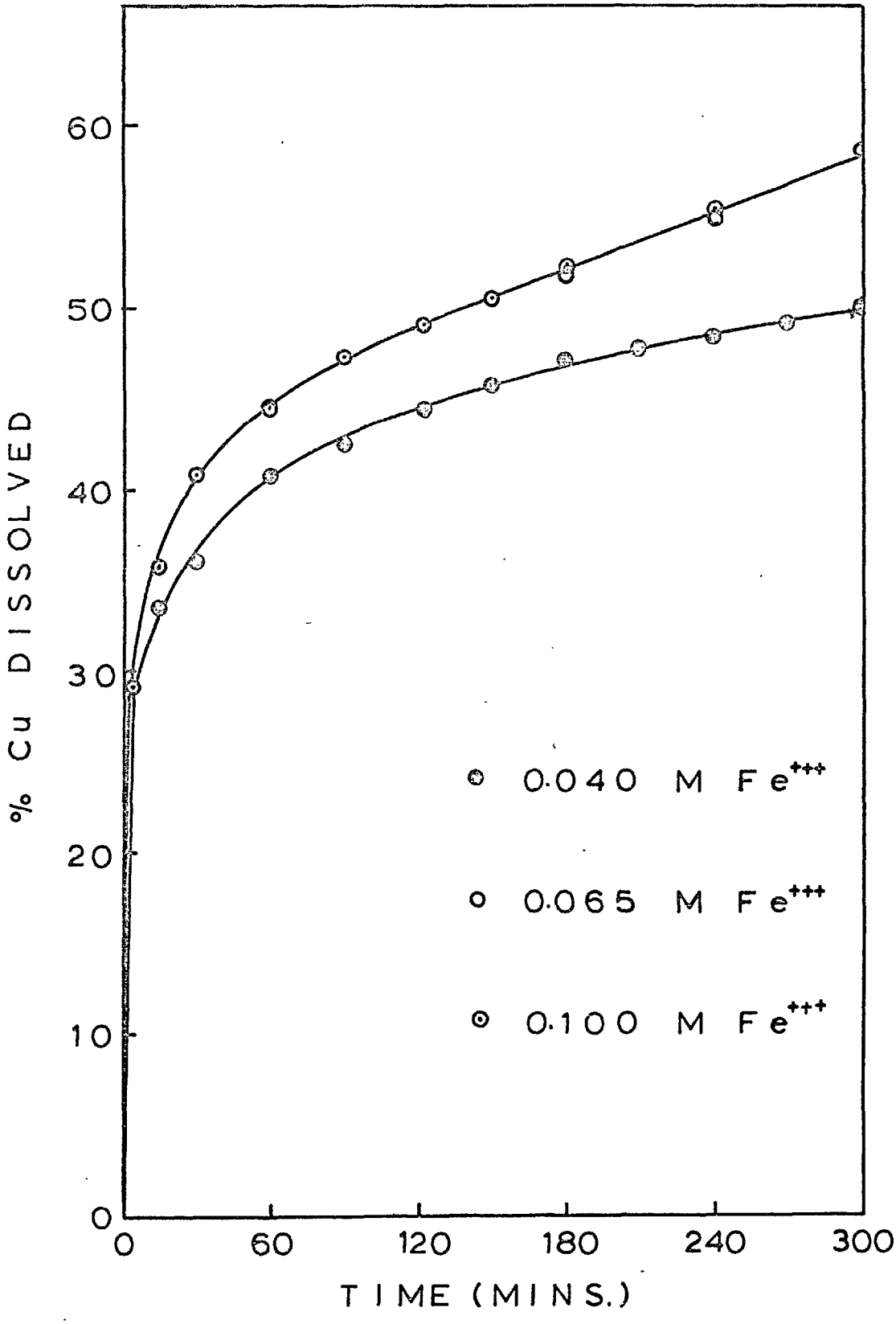

FIG. 33 Effect of ferric ion concentration on the rate of leaching bornite

dissolved but, as happened before, the reaction stopped when the Fe^{+++} was consumed. The small increase in the rate of dissolution after the reaction stopped, was caused by the reoxidation of Fe^{++} to Fe^{+++} by the air.

At 30^{o} C (fig. 32) concentrations of Fe^{+++} higher than 0.03 M did not increase the amount of copper dissolved, and the reaction stopped at the same point as the reaction using 0.03 M Fe^{+++}. In these these cases the termination of the reaction was controlled by the temperature.

During all the experiments the pH of the solution remained constant.

Fig. 33 shows the dissolution curves for the runs made at 90^{o} C with different Fe^{+++} concentrations.

From figs. 32 and 33 it is possible to see that, during the first part of the reaction, the rate of dissolution did not depend on the concentration of Fe^{+++} but in the second part the rate was dependent on Fe^{+++} concentration until a concentration of 0.065 M. At higher concentrations, the rate became independent of Fe^{+++}.

This, together with the fact that the rate of dissolution of the second part of the reaction

was independent of particle size (section 3.1.2) and stirring speed (section 3.1.3) suggest that the rate-controlling step is a chemical process. This is probably the chemical transformation of Cu_3FeS_4 to elemental sulphur through the oxidation of the sulphide ions.

3.1.5 Acid Concentration.

It was found (Appendix 1) that acid concentration had no effect on the rate of leaching.

However, its presence was necessary to maintain the ferric ions in solution, preventing their hydrolysis and precipitation.

Section 3.1.4 shows that acid alone did not attack the bornite unless an oxidant, in this case Fe^{+++}, was present.

3.1.6 Sample Weight.

Fig. 34 shows the influence of sample weight on the dissolution of bornite. From this figure it is possible to see that by doubling the weight there is no effect on the rate of dissolution per unit mass, of either the first or the second part of the reaction.

The slight difference observed is probably due to the flotation of the particles.

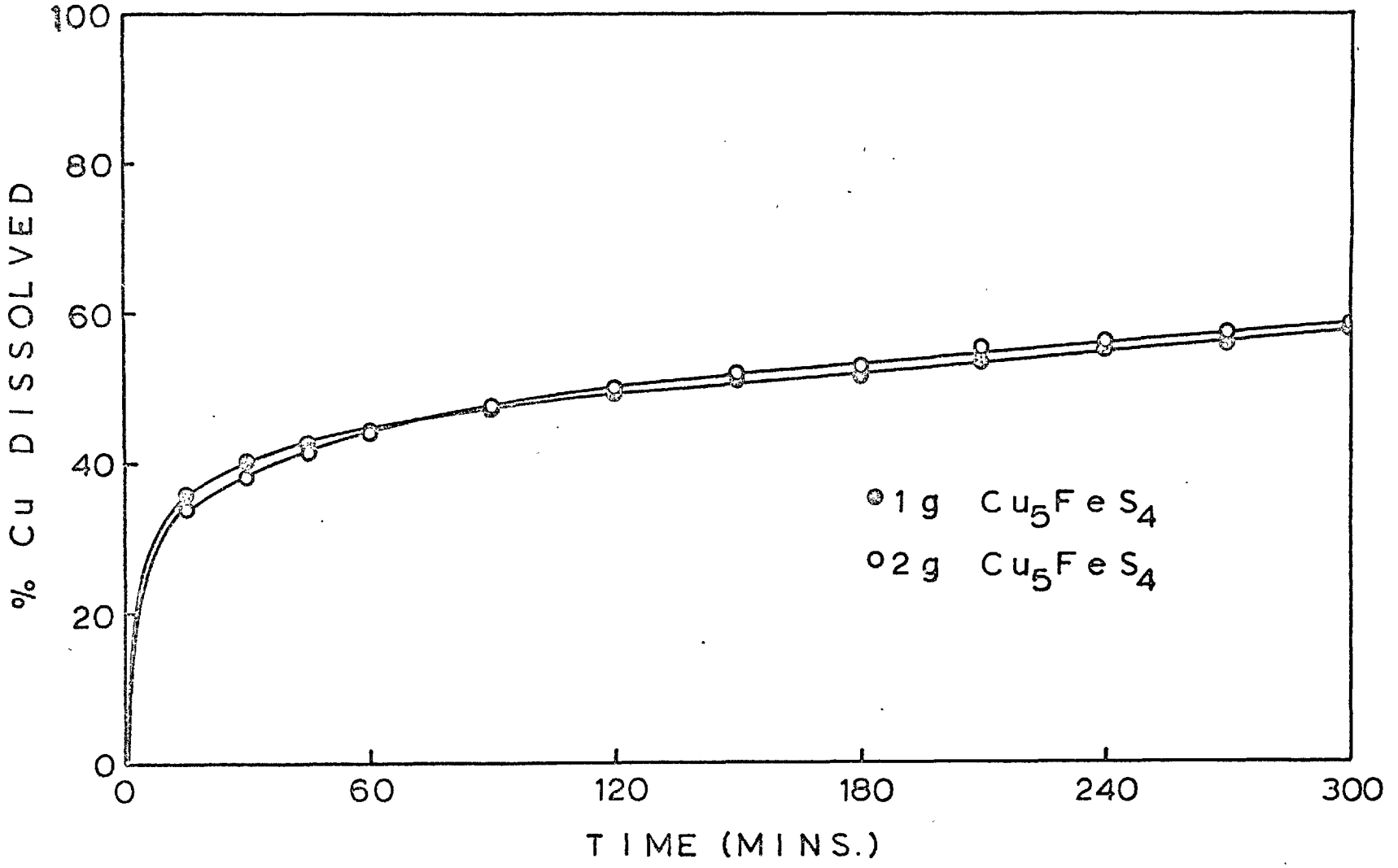

FIG. 34 Effect of sample weight on the rate of leaching bornite

3.2 Determination of the Activation Energy for the First Part of the Reaction.

In the determination of the activation energy for the first part of the reaction, leaching experiments at 50°, 60°, 70°, 80° and 90° C were performed under identical conditions.

The synthetic bornite was crushed and sieved very carefully. The same material was used in all the experiments mentioned above.

The basis for the calculation of the activation energy, for the first part of the reaction, was the amount of copper dissolved after two minutes of leaching.

Table 2 shows the values used and fig. 35 the Arrhenius plot in which the slope of the curve, $-\frac{E_A}{2.303\ R}$, was determined as $-4.5\ (\pm 0.2) \times 10^2$.

Using this value the activation energy was calculated to be $E_A = 2.1 \pm 0.1$ kcal per mole.

This activation energy for the first part of the reaction indicated a diffusion controlled process.

TABLE 2

Activation Energy Data

	50° C	60° C	70° C	80° C	90° C
Temperature °K	323	333	343	353	363
1/T °K x 10^3	3.096	3.003	2.915	2.833	2.755
% Cu dissolved	20.84	22.43	24.57	26.67	29.21
log % Cu dissolved	1.319	1.351	1.390	1.426	1.465

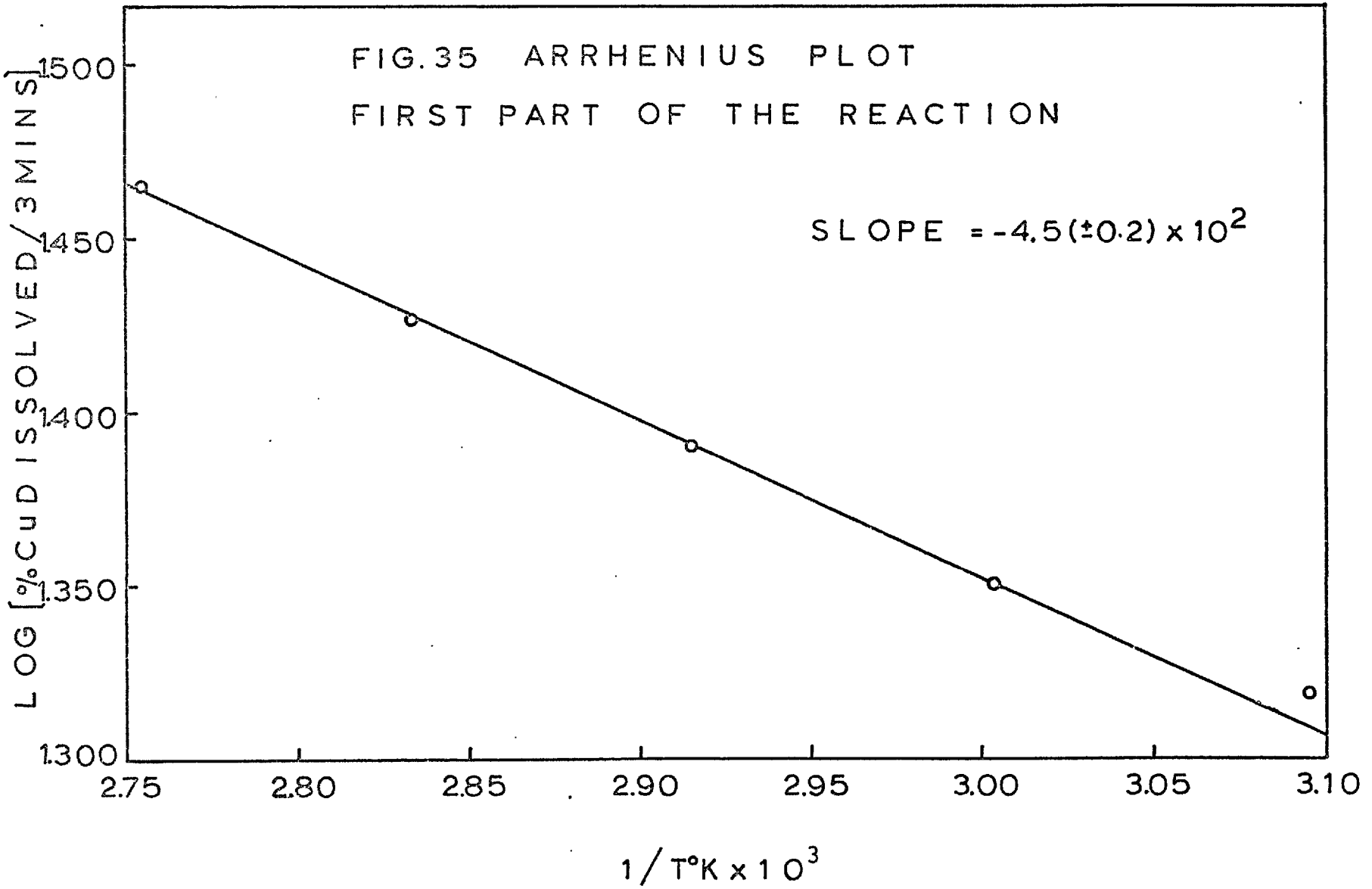
FIG. 35 ARRHENIUS PLOT
FIRST PART OF THE REACTION
SLOPE = -4.5 (±0.2) x 10²
LOG [% Cu DISSOLVED / 3 MINS]
1500
1450
1400
1350
1300
2.75
2.80
2.85
2.90
2.95
3.00
3.05
3.10
1 / T°K x 10³

3.3 Microscopic Observation.

The photomicrographs presented in this section show the effect of leaching on the grains of bornite.

All the photomicrographs were taken using high magnification (about 400 times).

Fig. 36 shows one of the small portions of the synthetic bornite presenting a minute intergrowth of chalcocite. This intergrowth was produced during the synthesis (section 2.1). This material was not used in the leaching experiments.

The crushed bornite used in the leaching experiments showed well defined edges similar to those ilustrated in fig. 36.

Fig. 37 shows a grain of bornite after a leaching using only 0.005 M Fe^{+++}. The low amount of Fe^{+++} caused the reaction to stop when 7.9 % of the copper was removed. It is possible to distinguish two different zones. In the centre of the grain there is a material which seems to be unreacted bornite. However, as will be seen in section 3.4 , the x-ray diffraction pattern is different from that of the original bornite and agrees very closely with that given by Yund and Kullerud [36] for x-bornite, which is a bornite

FIG. 36 Small portion of synthetic bornite showing minute intergrowths of chalcocite. (x 480)

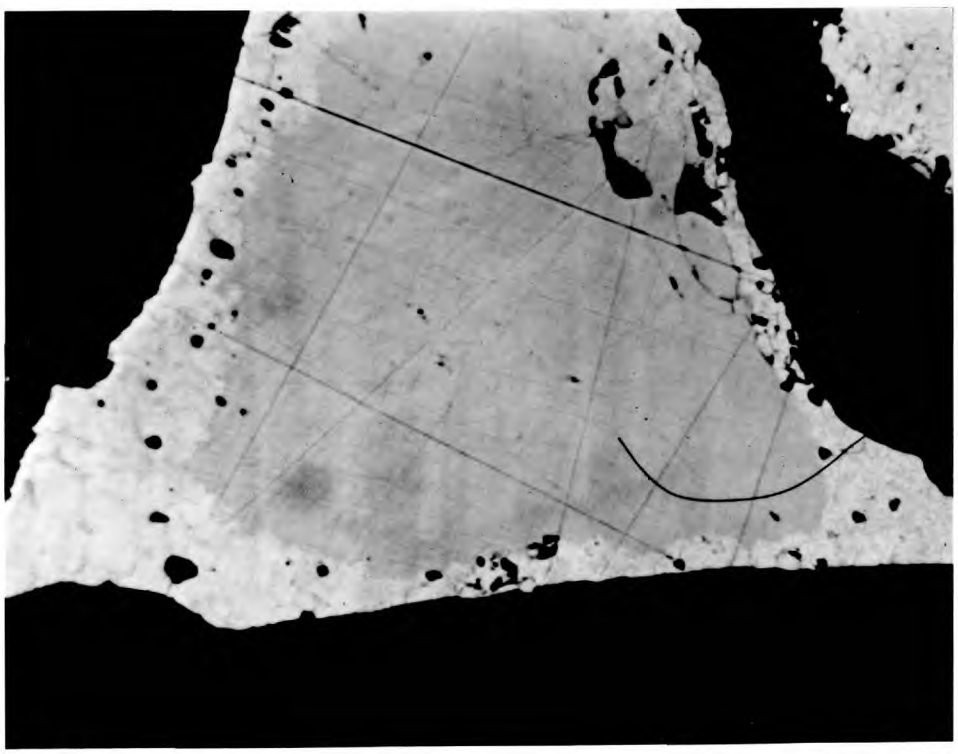

FIG. 37 Leaching residue (8% Cu dissolved) showing the nonstoichiometric bornite in which pores began to appear. (x512)

FIG. 38 Leaching residue (15 % Cu dissolved). The entire grain consists of nonstoichiometric bornite. (x480)

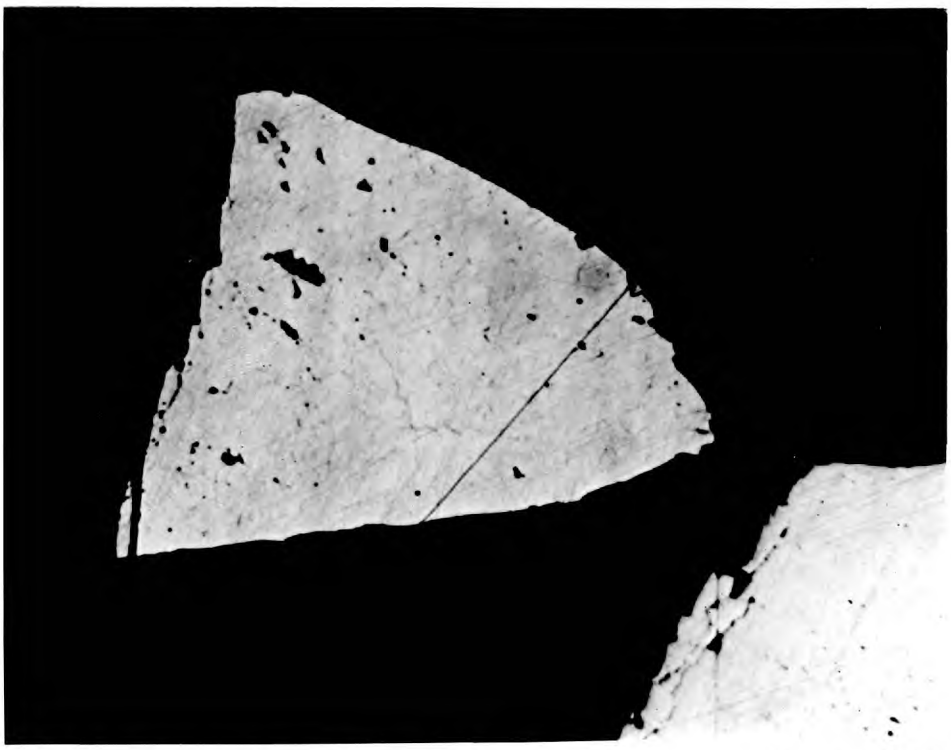

FIG. 39 Leaching residue (28 % Cu dissolved). The grains still show well defined edges. (x480)

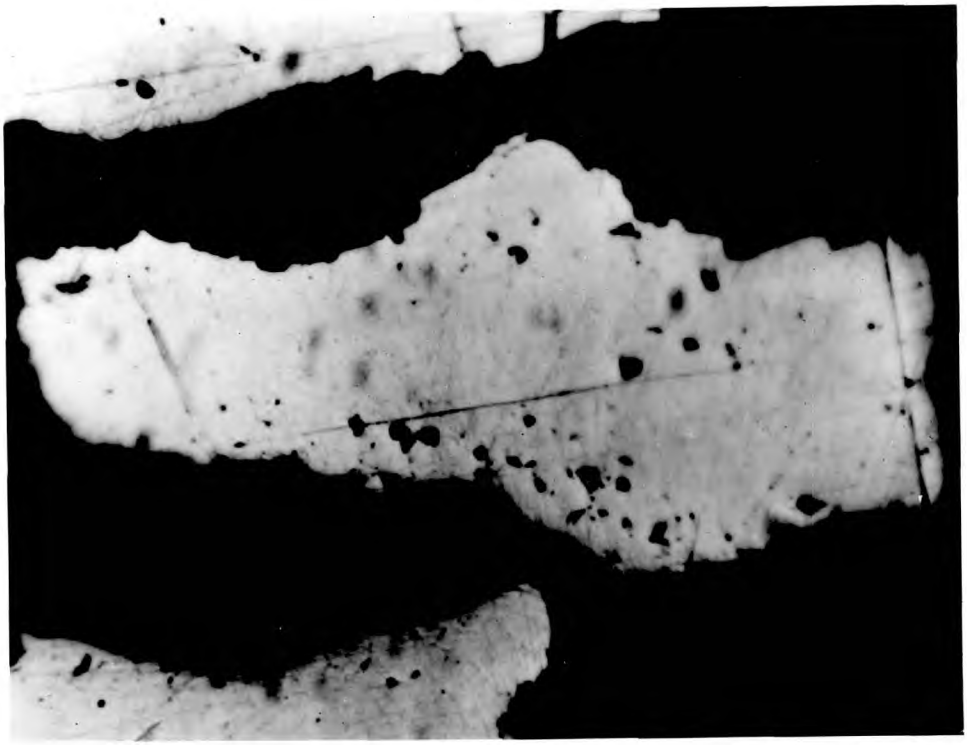

FIG. 40 Leaching residue (28 % Cu dissolved). (x 671)

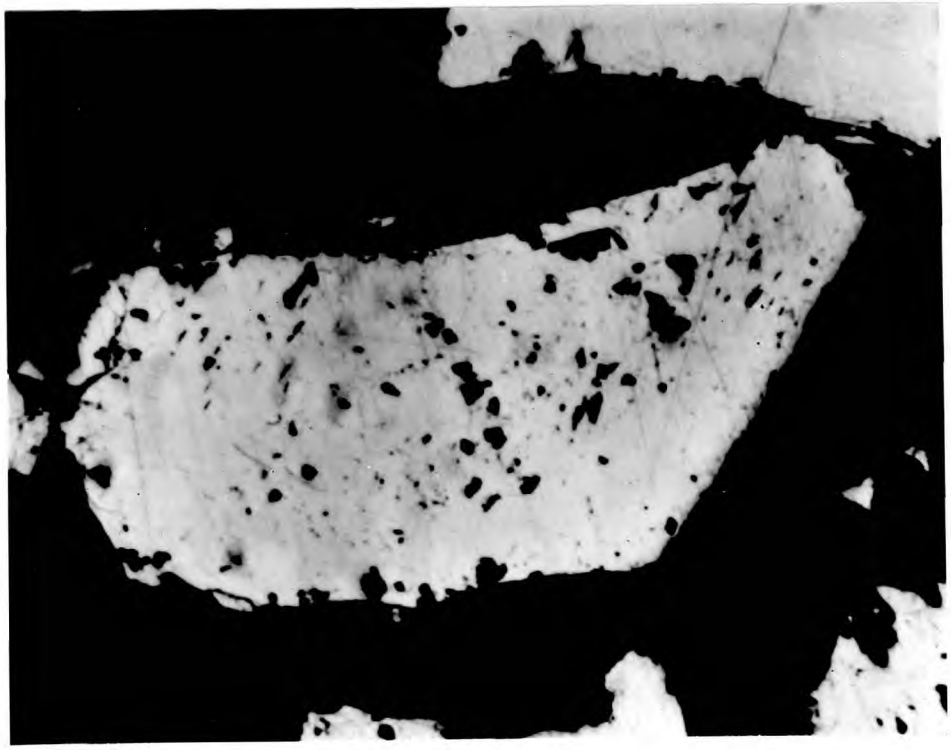

FIG. 41 Leaching residue (37 % Cu dissolved). The attack on the surface of the grains is starting. (x 704)

with slightly less copper than the stoichiometric form. Surrounding this zone there is a layer of nonstoichiometric bornite in which pores began to appear. The porosity and cracks developed in this phase can be explained by the contraction of the unit cell, produced during the removal of copper by diffusion.

Fig. 38 shows the residues from a leaching run in which 14.6 % of the copper had been dissolved. From this photomicrograph it is possible to see that the entire grain has been converted to nonstoichiometric bornite. The edges of the grain still remain very well defined suggesting that the removal of copper is only carried out by a diffusion in the solid state. This photomicrograph shows that the porosity extended throughout the whole grain.

Fig. 42 shows a residue in which about 49 % of the copper had been dissolved. It is possible to see the increasing attack on the surface of the grains. Fig. 45, showing a grain in which 64.1 % of the copper has been dissolved, is a good illustration of the intensity of the attack.

Figs. 46 and 47 show how impossible it is to polish the external part of the grains in which elemental sulphur is present.

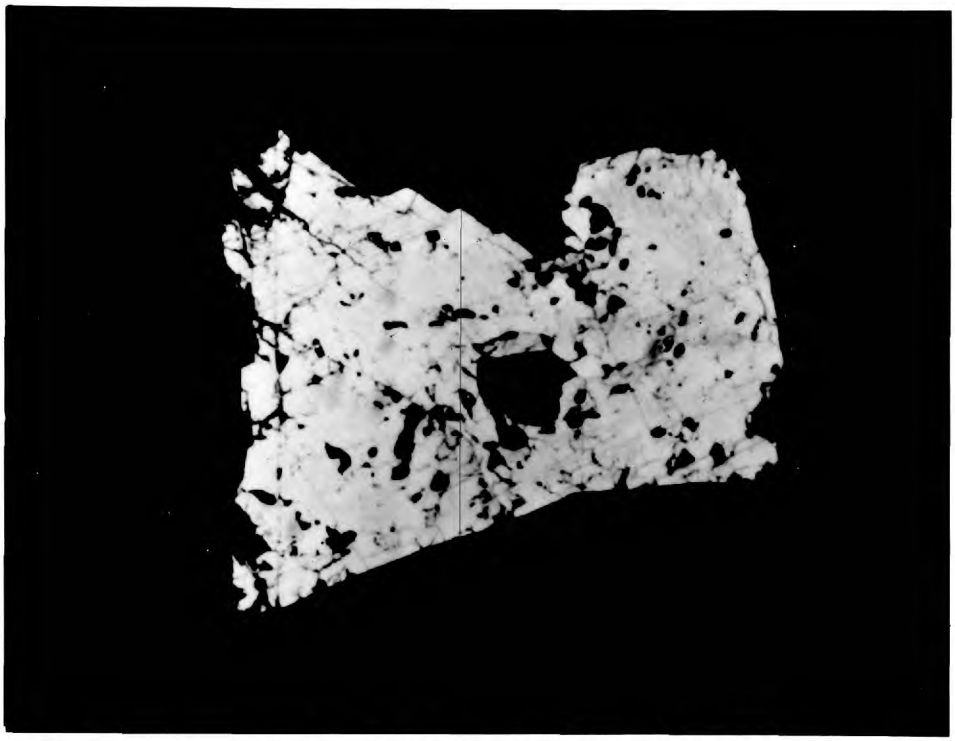

FIG. 42 Leaching residue (49 % Cu dissolved). (x496)

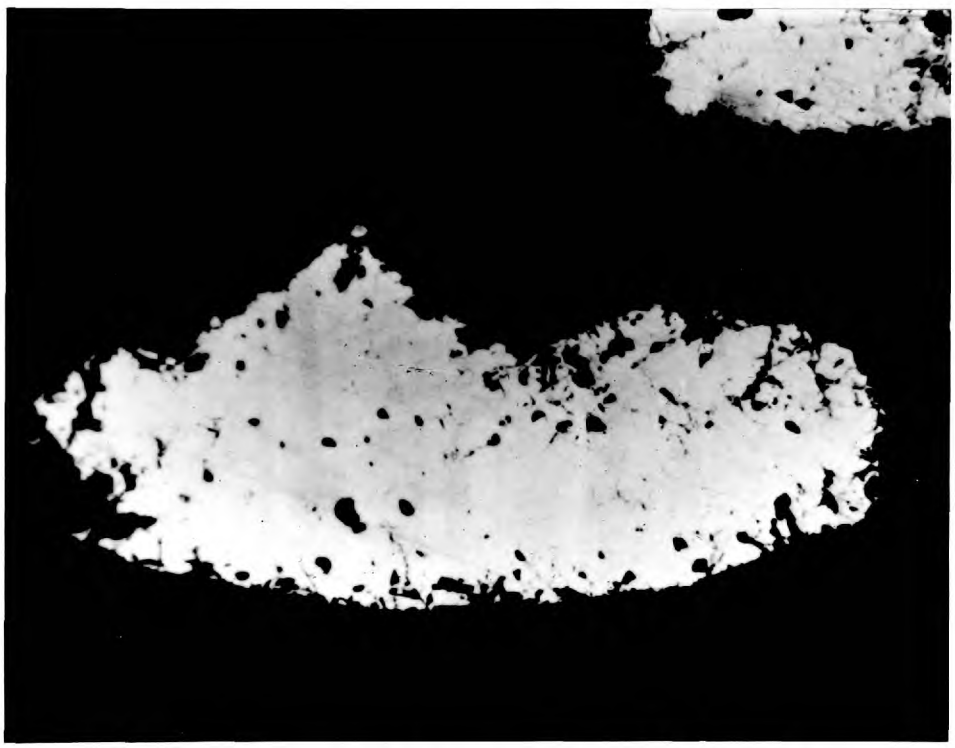

FIG. 43 Leaching residue (58 % Cu dissolved). (x480)

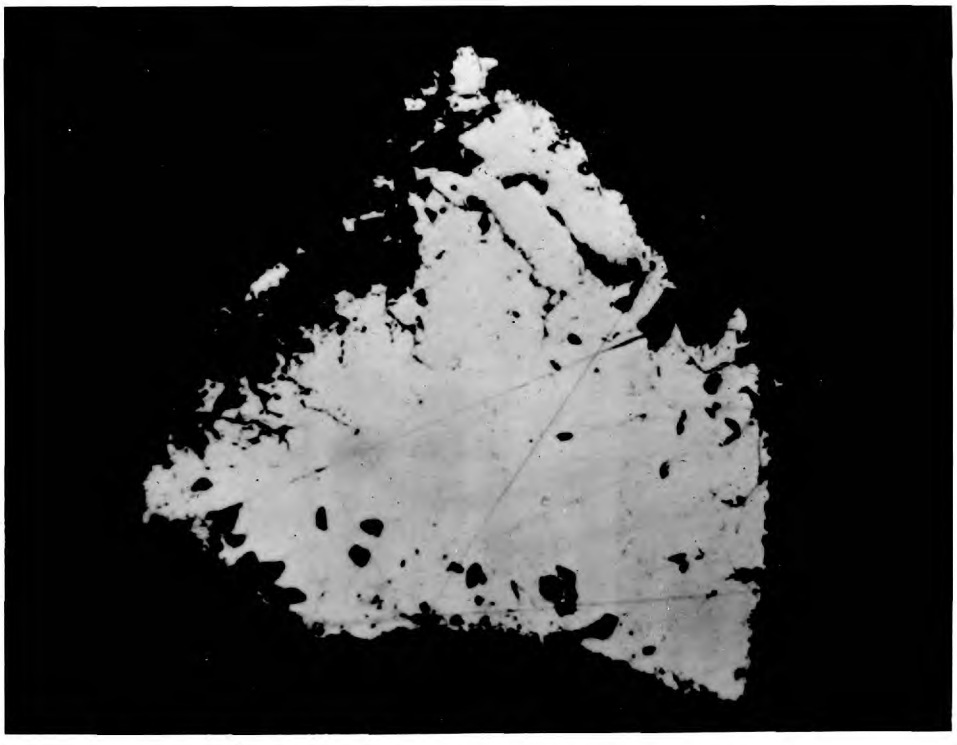

FIG. 44 Leaching residue (58 % Cu dissolved). (x480)

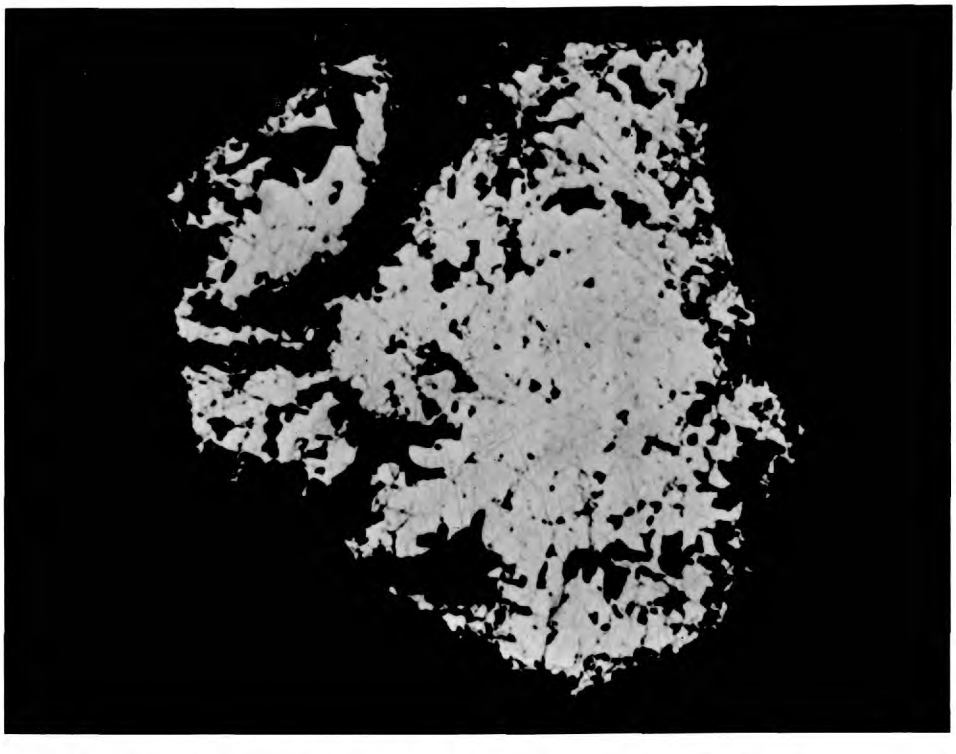

FIG. 45 Leaching residue (64 % Cu dissolved). (x480)

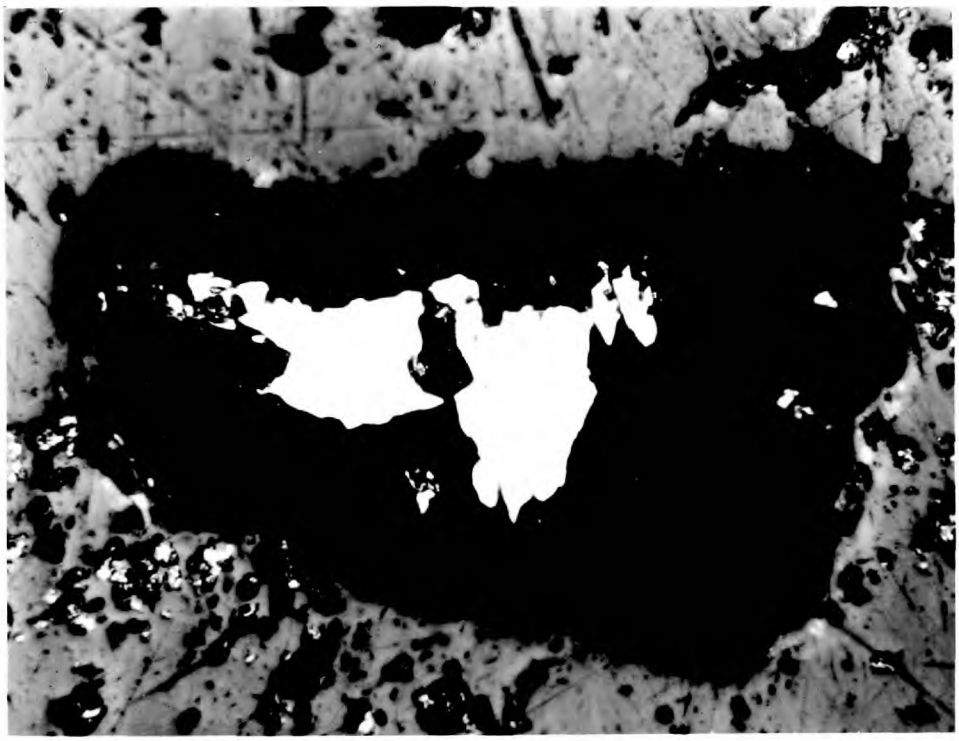

FIG. 46 Leaching residue (80 % Cu dissolved). The dark zone consisted of sulphur and sulphide removed during polishing. (x480)

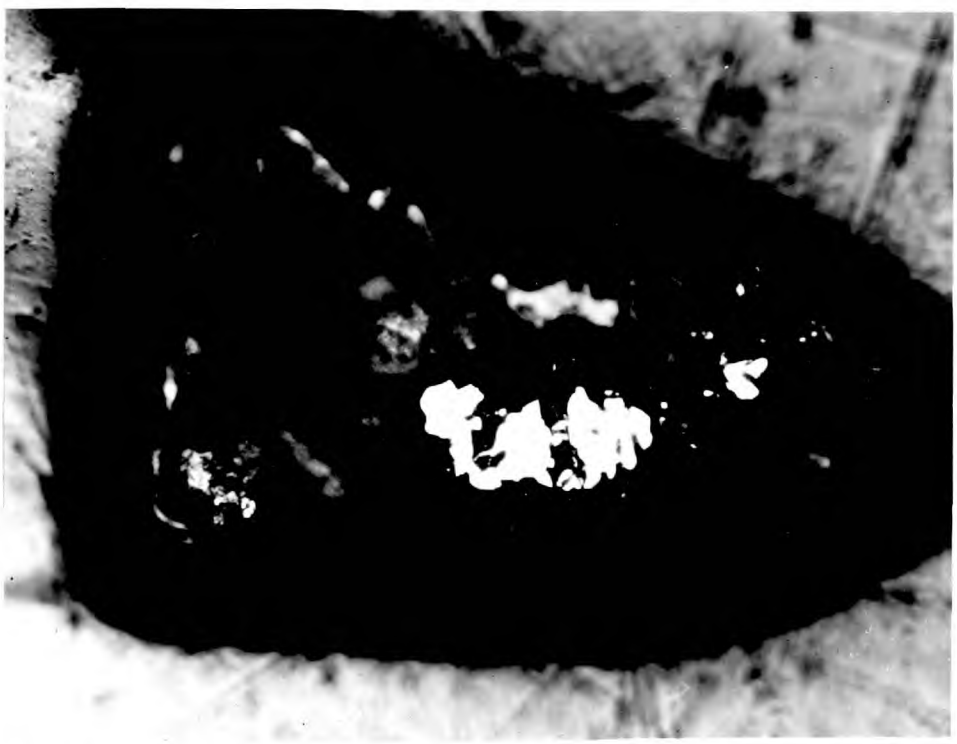

FIG. 47 Leaching residue (96 % Cu dissolved). (x480)

As a result of this, only the holes in the mounting resin sorrounding the remaining sulphide are shown in these photomicrographs.

The presence of sulphur was confirmed by x-ray diffraction (section 3.4), electron probe microanalysis (section 3.7) and by washing the grains with drops of CCl_4 over a glass cover. After the evaporation of the solvent the elemental sulphur recrystallized on the glass cover. These crystals are shown in figs. 48 and 49 .

In the central part of the grains showed in figs. 46 and 47 it is possible to see the remaining sulphide phase. Electron probe microanalysis performed in this area still gave a composition similar to that given by the electron probe microanalysis of residues with only about 40 % of the copper dissolved. (section 3.7).

With the exception of the residue shown in fig. 37 all the others are optically very homogeneous, and it is not possible to see any intergrowth of other secondary phases.

Reflectivity measurements were performed in a residue from leaching similar to that in fig. 41. The results of these measurements are given in section 3.6.

The strong attack on the surface of the grains

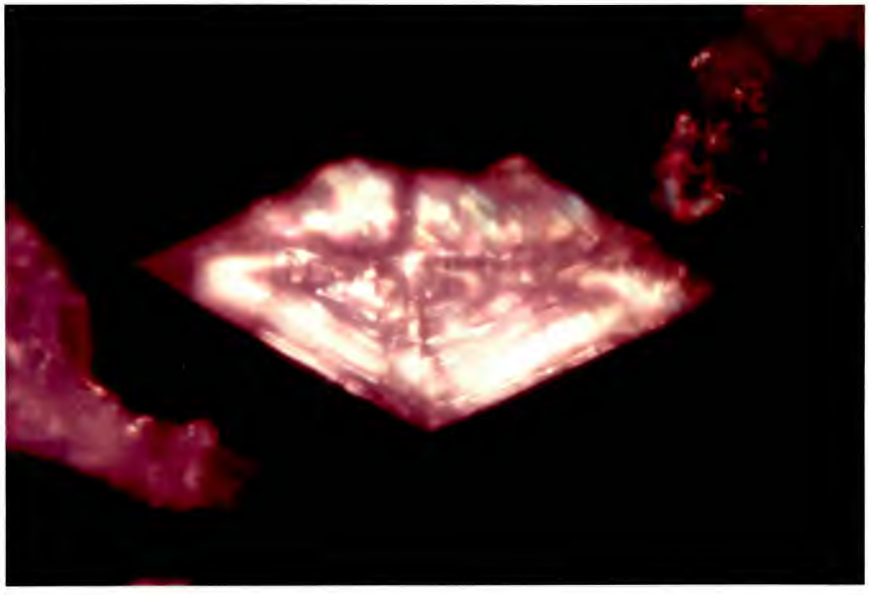

FIG. 48 Elemental sulphur recrystallized from the leach residue with 80 % of copper dissolved. (Polarized light, x620)

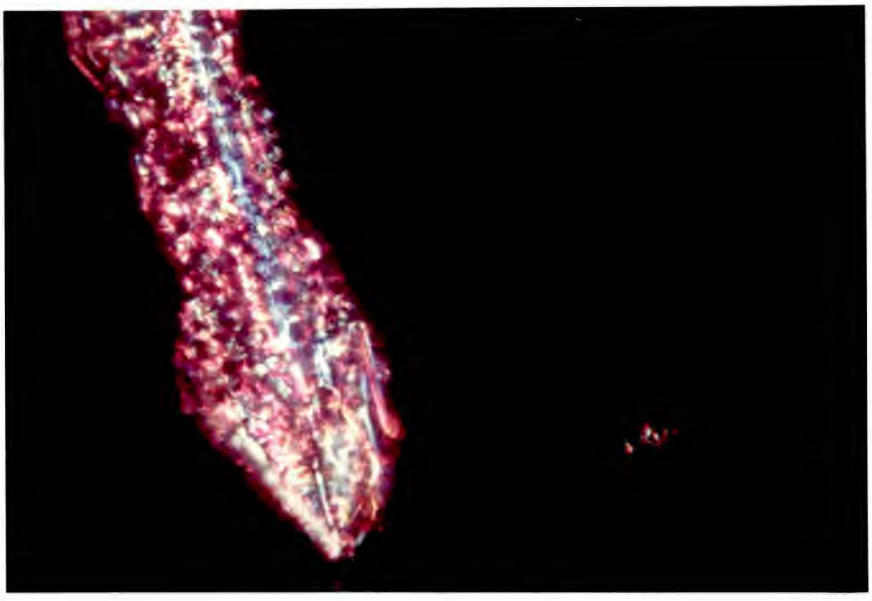

FIG. 49 Elemental sulphur recrystallized from the leach residue with 96 % of copper dissolved. (Polarized light, x620)

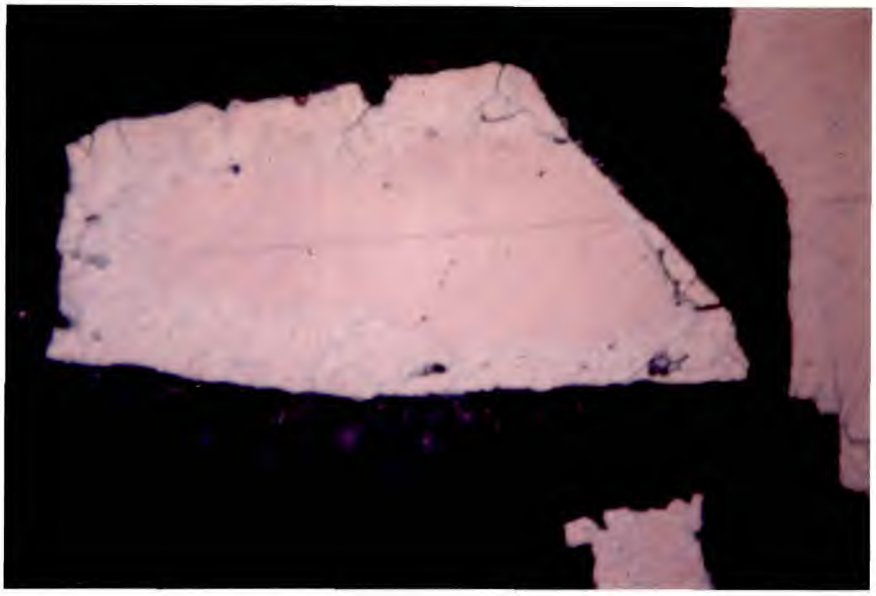

FIG. 50 A particle of a leach residue showing the formation of nonstoichiometric bornite (x550).

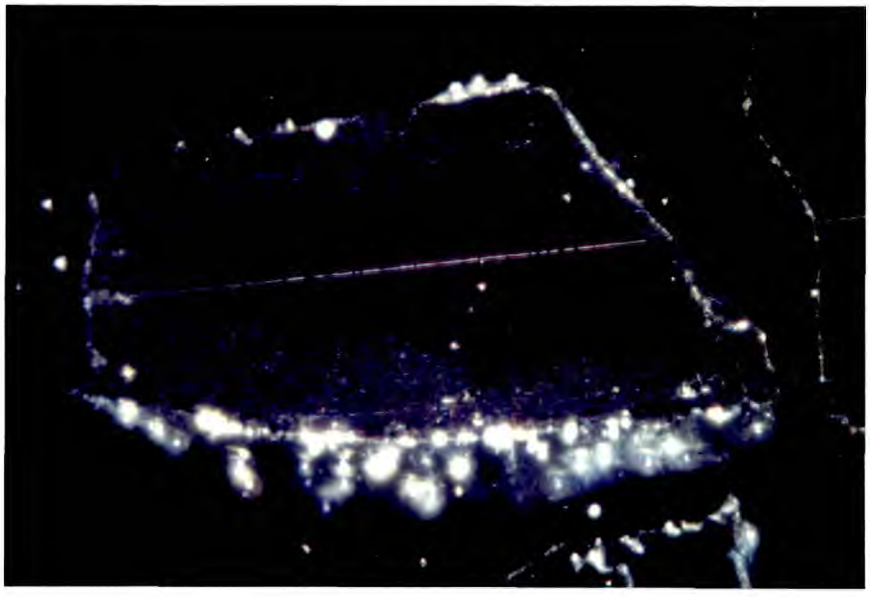

FIG. 51 Same particle as fig. 50 under polarized light (x550).

when more than 40 % of the copper has been dissolved, together with the appearance of elemental sulphur in the grains and the increase in total iron concentration in the solution (keeping the ratio Cu/Fe in the residues = 3) (Appendix 1) suggests that in the second part of the reaction a complete collapse occurred of the solid phase formed during the first part of the reaction.

Figs. 50 and 51 show photomicrographs of a residue from leaching, similar to that shown in fig. 37, under polarized light. The aspect of the nonstoichiometric bornite of the external part of the grain is similar to that reported [46] for natural anomalous (nonstoichiometric) bornite.

3.4 X-ray Diffraction Study of the Leach Residues.

Most of the residues from leaching were studied by x-ray diffraction. The results are given in Appendix 2. Some difficulties were found in the measurement of the angular positions of the lines, because some of the lines were very broad.

Fig. 52 a) shows the x-ray diffraction powder photograph of the synthetic bornite.

Fig. 52 b) shows the x-ray diffraction powder photograph of a residue with 7.9 % of the copper dissolved. There is a strong similarity between the resulting d-spacings and intensities of this material, and those of the x-bornite reported by Yund and Kullerud[36] (Appendix 3).

This residue is the same as that represented in fig. 37 in which some nonstoichiometric bornite appears surrounding the x-bornite-like material. This nonstoichiometric bornite has different optical properties to x-bornite (section 3.3), which has similar optical properties to normal bornite[36]. Some of the lines of this nonstoichiometric bornite appear in fig.52b) and in the corresponding table in Appendix 2.

Fig. 52 c) shows the x-ray diffraction powder photograph of a clearly nonstoichiometric bornite

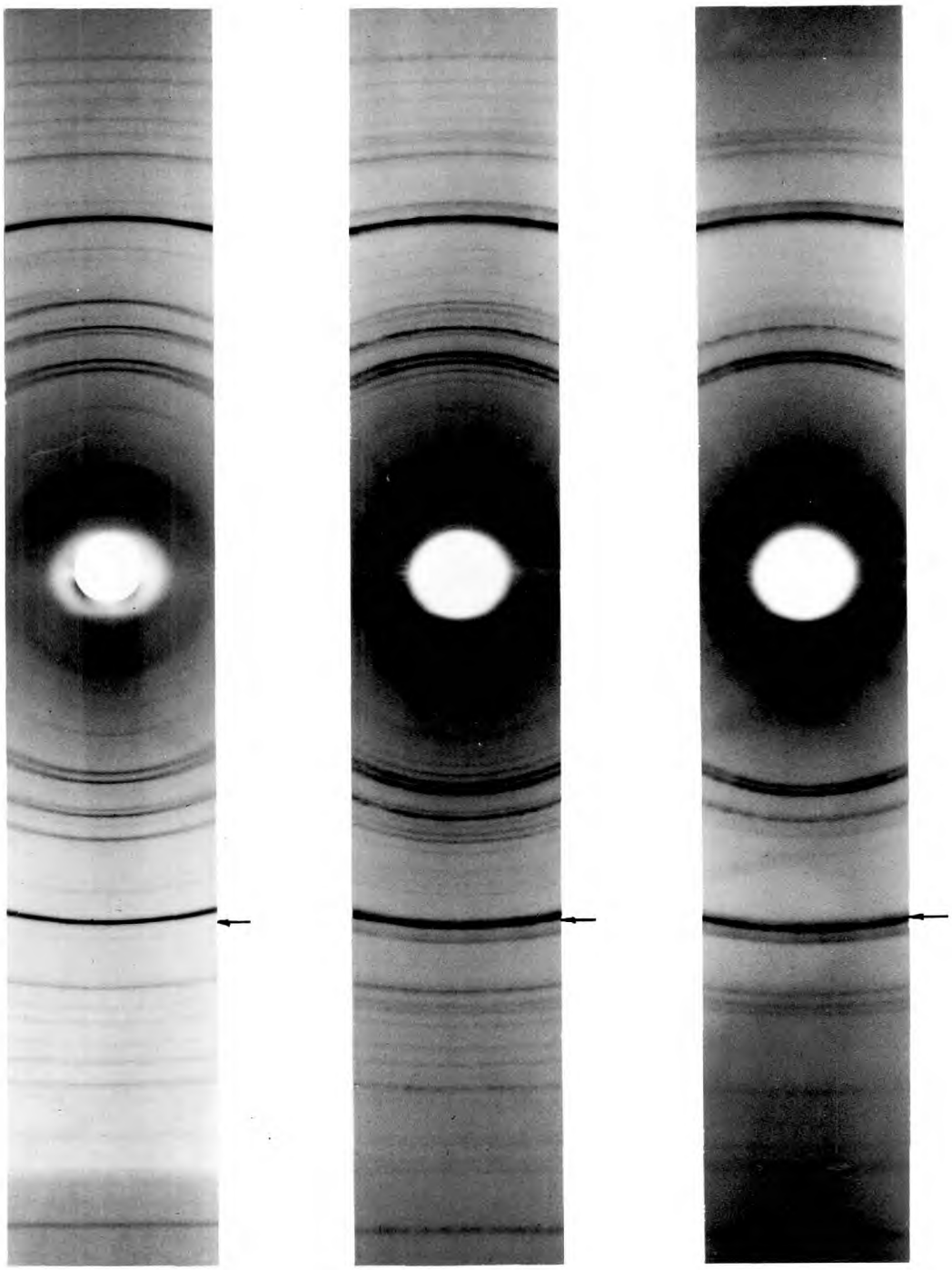

a b c

FIG. 52 X-ray Powder Photographs of the Residues.
a) BORNITE (Cu_5FeS_4). b) 7.9 % Cu dissolved. c) 14.6 % Cu dissolved.

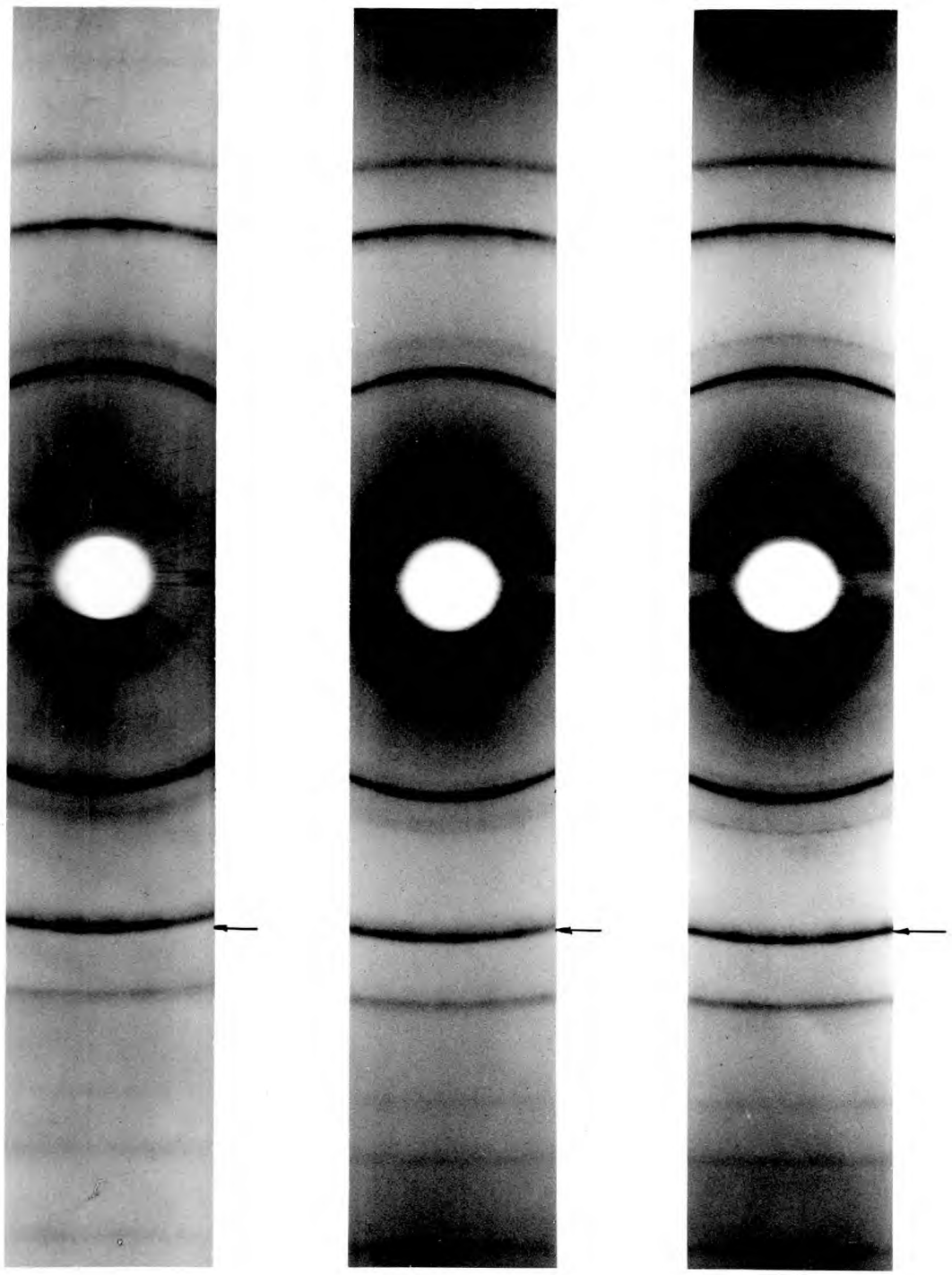

a b c

FIG. 53 X-ray Powder Photographs of the Residues.

a) 28.4 % Cu dissolved b) 30.8 % Cu dissolved c) 37.5 % Cu dissolved

in which 14.6 % of the copper had been dissolved.

A reference line was drawn in this and following figures to show the displacement of the lines with the increase in the percentage of copper dissolved.

Fig. 53 shows three x-ray diffraction powder photographs taken when 28.4, 30.8 and 37.5 % of the copper were dissolved. There is a small displacement of the lines. In Appendix 2 are given the d-spacings and intensities observed.

Fig. 54 shows that the lines did not move when more than 40 % of the copper was dissolved.

In fig. 54c) it is possible to see that the stronger lines of sulphur are beggining to appear.

Fig. 55 shows the decrease in intensity of the lines of the sulphide, with the corresponding increase in intensity of the lines of sulphur, when the amount of copper dissolved is increased.

In Appendix 3 the A.S.T.M. pattern of orthorhombic sulphur is given.

The d-spacings and intensities of the solid phase formed when more than 40 % of the copper was dissolved, are very similar to those of chalcopyrite (Appendix 3). The only difference being that a few more lines occur.

However, as shown in sections 3.7 and 3.6,

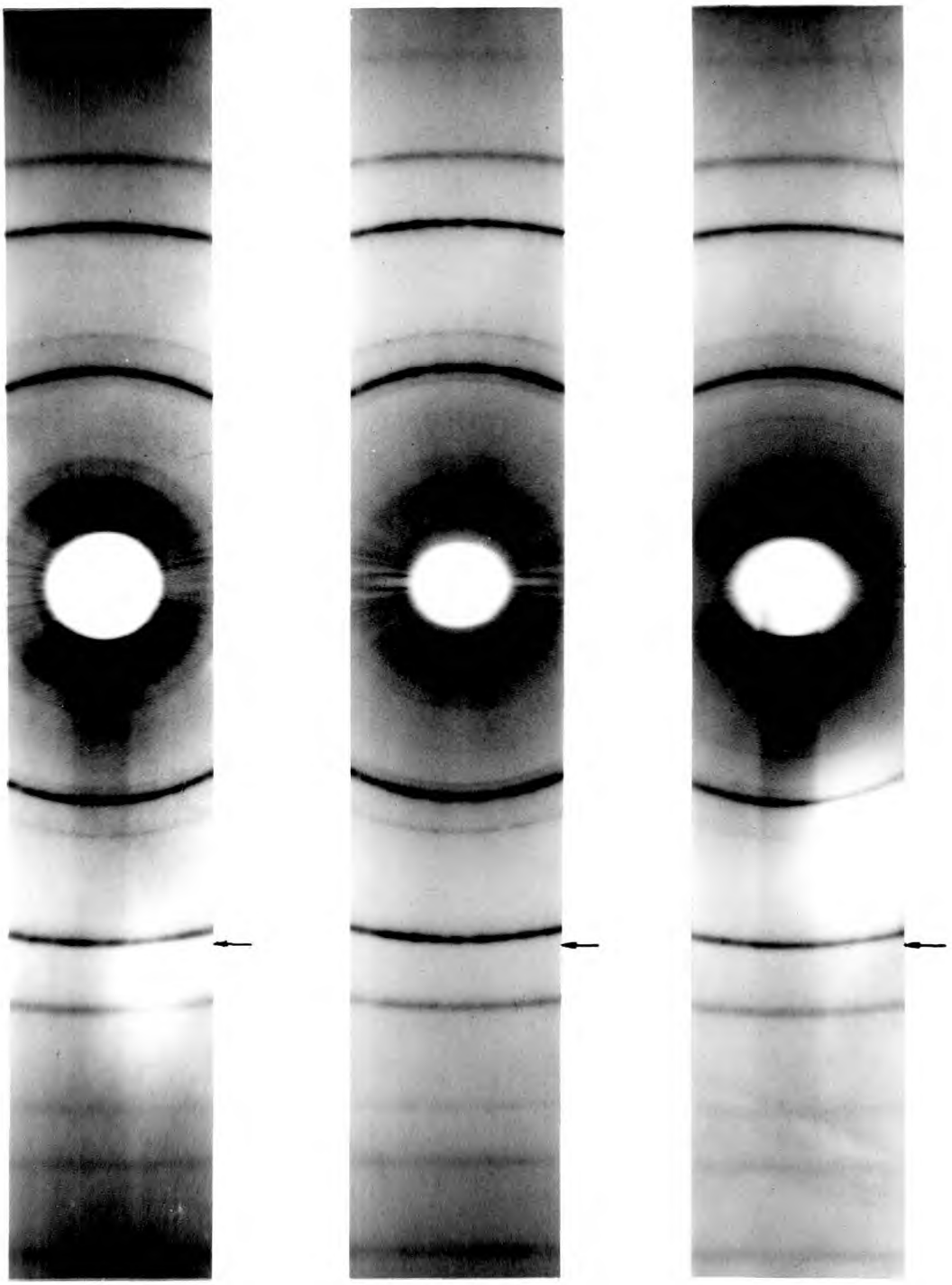

a b c

FIG. **54** X-ray Powder Photographs of the residues
a) 43.7 % Cu dissolved b) 49.1 % Cu dissolved c) 57.9 % Cu dissolved

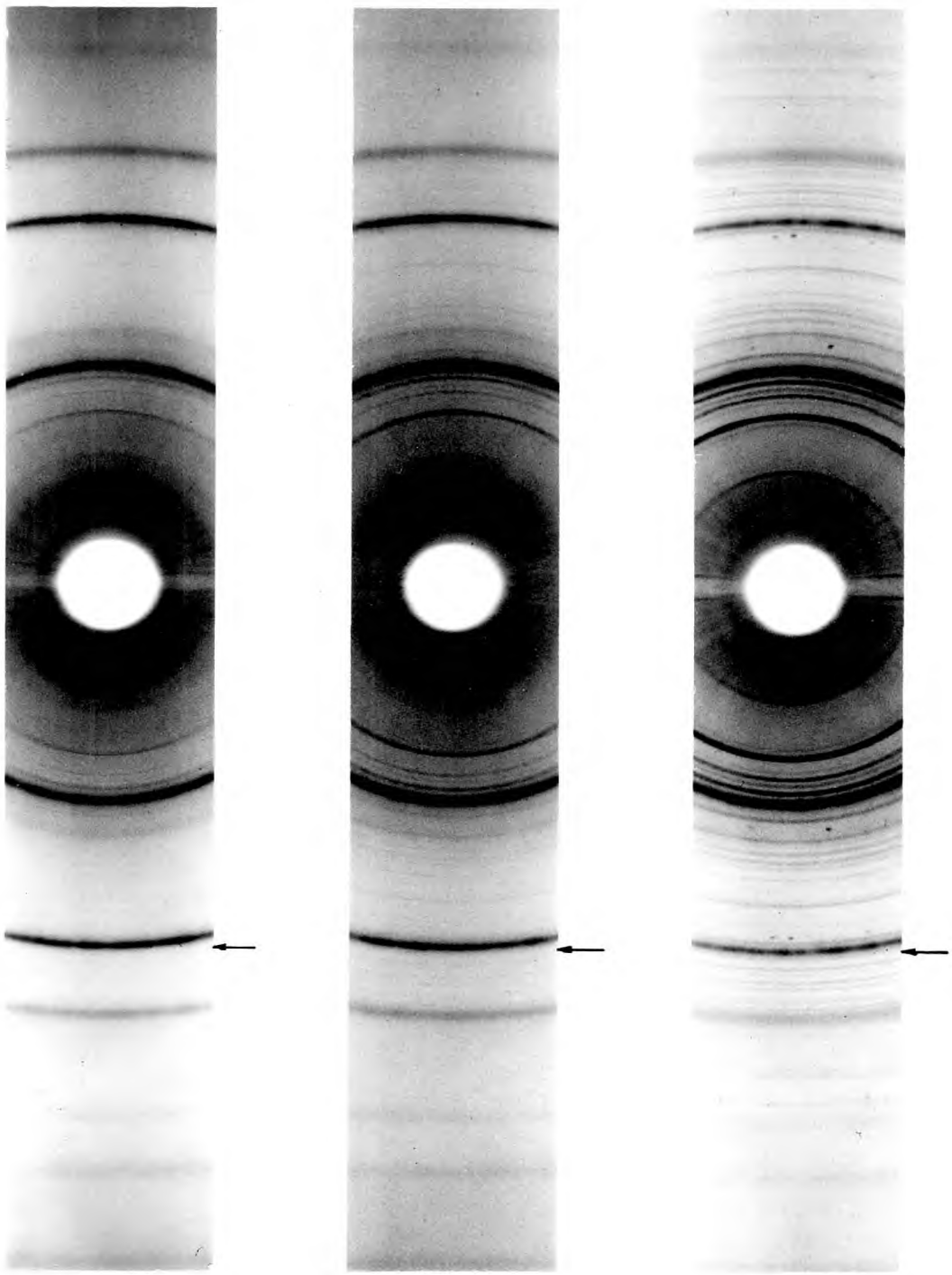

a b c

FIG. **55** X-ray Powder Photographs of the Residues

a) 64.1 % Cu dissolved b) 80.0 % Cu dissolved c) 96.0 % Cu dissolved

the composition determined by electron probe microanalysis and the reflectivity properties, are those of the mineral idaite with composition Cu_3FeS_4.

3.5 Variation in Lattice Parameters.

If we accept as valid the hypothetical structure of the low temperature form of bornite given by Manning, we can measure the variation in the lattice parameters as a function of the percentage of copper dissolved because by the action of the leaching the original bornite structure began to loose the layers of ionically bound copper. This results in the disappearance of the superstructural lines. Some of the reflections produced by the chalcopyrite-like skeleton (Cu_3FeS_4) retain the same indexing.

The reflections used in the calculation of the variation in lattice parameters are the (440) and the (44.16), because their intensities allow the measurements to be done on all the residues from leaching. They were also chosen because the same results are obtained from the indexing corresponding to the chalcopyrite-like structure, (220) and (228).

Special care was taken in the measurements of the angular positions of the (440) and (44.16) reflections, because of the generally poor appearance of the lines. An average of readings taken at both edges of the lines was used in the

calculations.

The formula used was the general one for the tetragonal system:

$$\frac{1}{d^2} = \frac{h^2 + k^2}{a^2} + \frac{l^2}{c^2}$$

Table 3 gives the values obtained for both a and c parameters. Figs. 56 and 57 show the variation in the dimensions of the unit cell versus the percentage of copper dissolved.

It is possible to see from these figures that there is a big contraction in the unit cell during the first part of the dissolution of bornite, specially when between 15 % and 28 % of the copper has been removed. This is supported by the optical evidence of the cracks and holes which appear during this part of the reaction. From 28 % to 40 % of copper dissolved, there is a further decrease in cell dimensions, but from this point until almost all the copper has been removed, the dimensions of the unit cell remain unaltered.

By taking a = 10.52 A and c = 20.93 A from table 3 and dividing them by 2, an idea of the dimensions of the unit cell of Cu_3FeS_4 can be obtained. These dimensions are very close to those of chalcopyrite as would be expected, with

TABLE 3

Variation in lattice parameters

Res.(% Cu diss.)	d_{440}	a A	$d_{44.16}$	c A
0.0	1.937	10.94	1.119	21.88
7.9	1.922	10.87	1.112	21.81
14.6	1.916	10.84	1.108	21.73
27.7	1.870	10.58	1.086	21.17
28.4	1.870	10.58	1.080	21.17
30.8	1.863	10.54	1.078	21.15
37.5	1.860	10.52	1.075	21.08
43.7	1.860	10.52	1.070	20.93
49.1	1.860	10.52	1.070	20.93
57.9	1.860	10.52	1.070	20.93
64.1	1.860	10.52	1.070	20.93
80.0	1.860	10.52	1.070	20.93
96.0	1.854	10.49	1.070	20.96

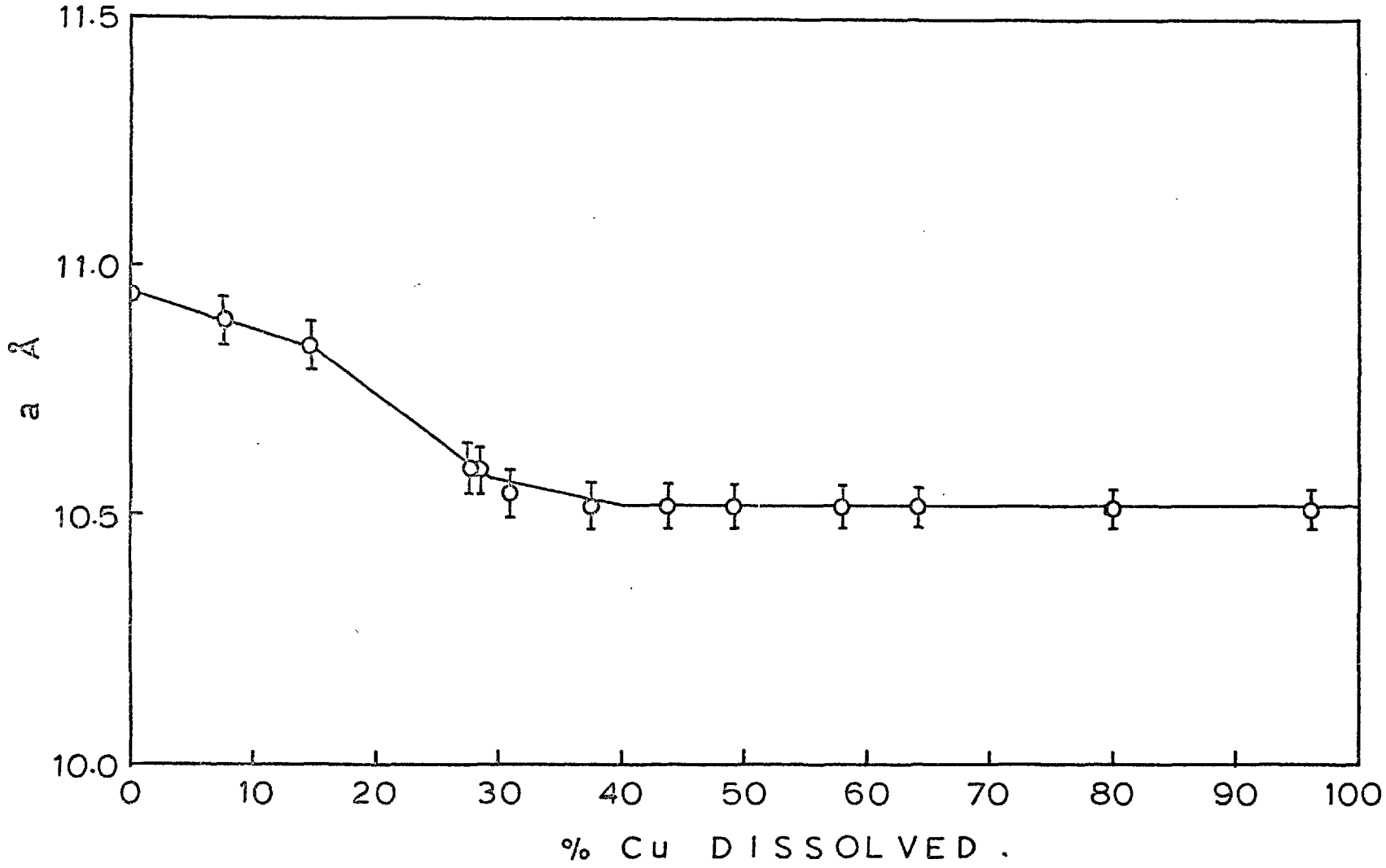

FIG. 56 Variation in lattice parameters

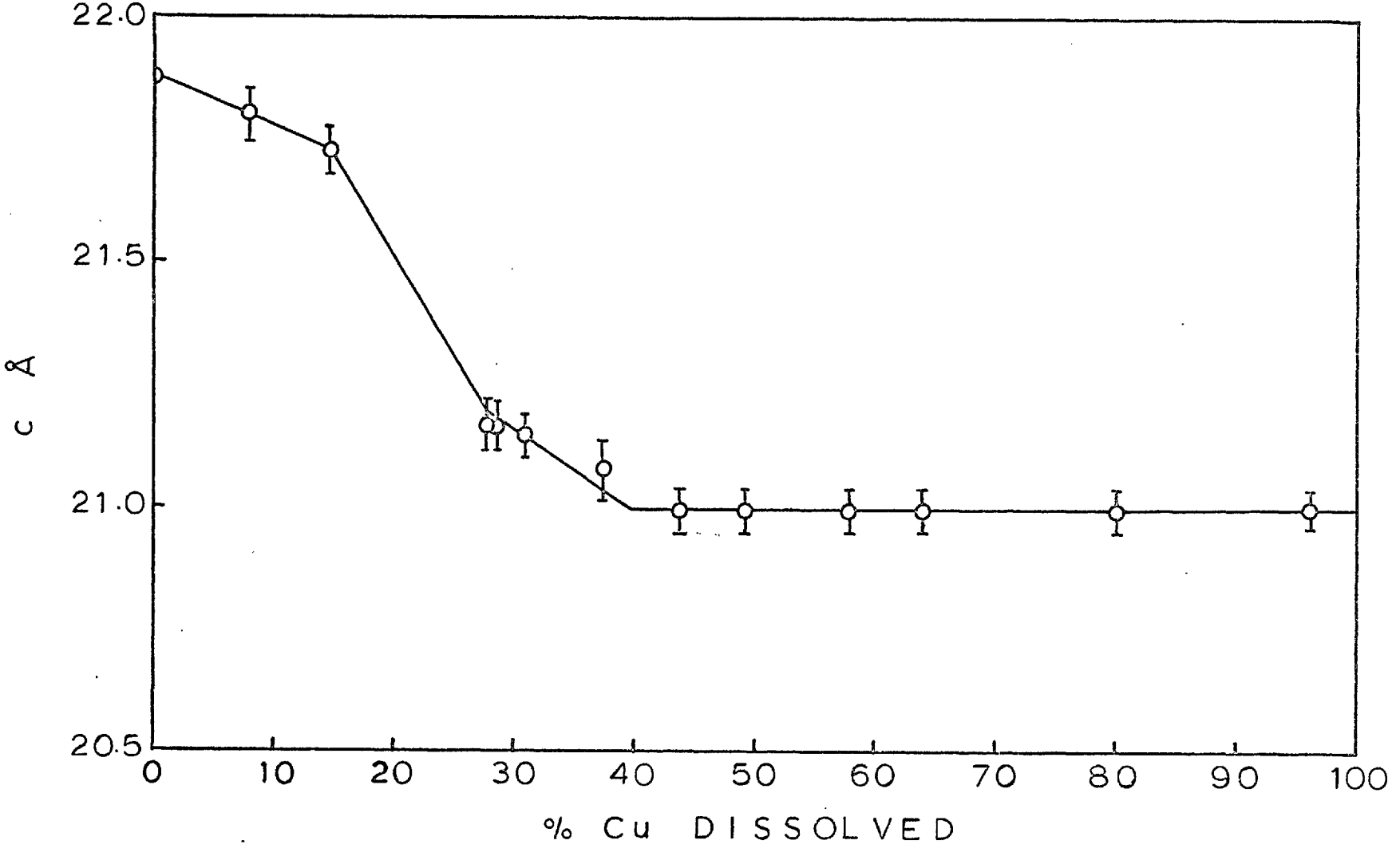

FIG. 57 Variation in lattice parameters

a = 5.26 A and c = 10.46 A.

Another conclusion that can be derived from figs. 56 and 57 is that because of the big contraction of the unit cell, before 28 % of the copper has been dissolved, the diffusion of the remaining ionically bound copper is more difficult. This is reflected in the rate of leaching, which drops noticeably after 28 % of the copper has been removed.

3.6 Reflectivity Measurements.

The reflectivity dispersion profile measurements of the residue from a leaching experiment, in which 37.5 % of the copper was removed, were taken using the apparatus and the technique described in section 2.

The sample used for this measurements was very homogeneous. It was checked both optically and by electron probe microanalysis. Photomicrograph 41 shows one grain of this product. Fig.53c) and table 32 (Appendix 2) give the x-ray diffraction data for this sample.

The composition given by electron probe microanalysis (section 3.7) was very close to stoichiometric Cu_3FeS_4.

Table 4 shows the values of reflectivity (R %) for different wavelengths. The values given in the readings (Rdg.) columns are the average values of several readings from different grains of the same sample.

The standard used was the R.S.M. pyrite standard calibrated by D. Vaugham in December 1967.

Fig. 58 shows the reflectivity dispersion profile for the residue with composition Cu_3FeS_4.

TABLE 4

Reflectivity Dispersion Profile (Cu_3FeS_4)

Wavelength (nm)	Py standard		Cu_3FeS_4	
	Rdg.	R %	Rdg.	R %
420	3.20	40.0	1.20	15.00
440	8.40	42.3	3.25	16.37
460	18.30	45.7	6.90	17.23
480	36.10	48.0	14.00	18.61
500	57.80	50.0	23.00	19.90
546	90.00	52.9	40.65	23.89
589	56.30	54.2	26.60	25.61
620	17.70	54.5	8.85	27.25
660	4.40	55.3	2.20	27.65

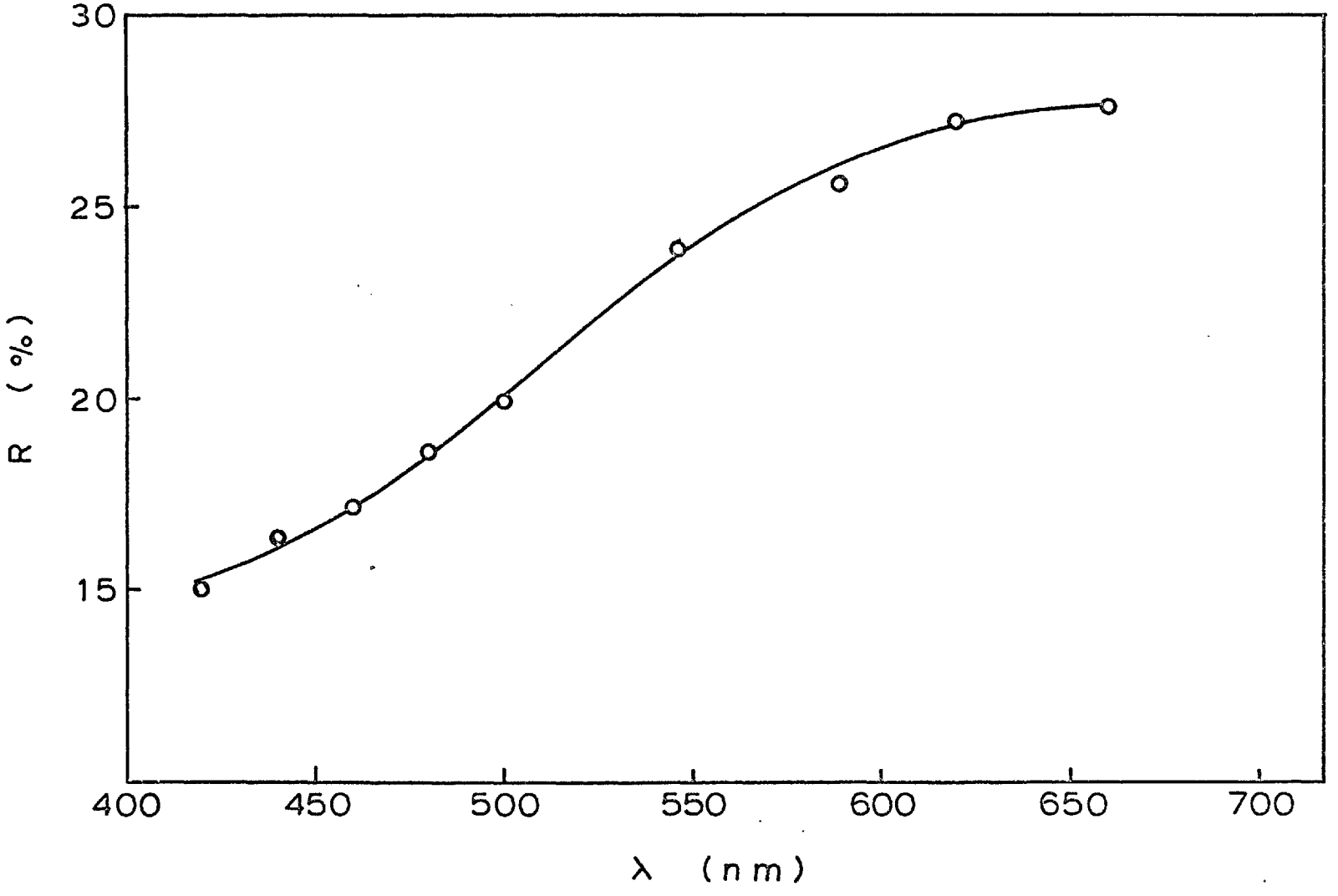

FIG. 58 Reflectivity dispersion profile of Cu_3FeS_4

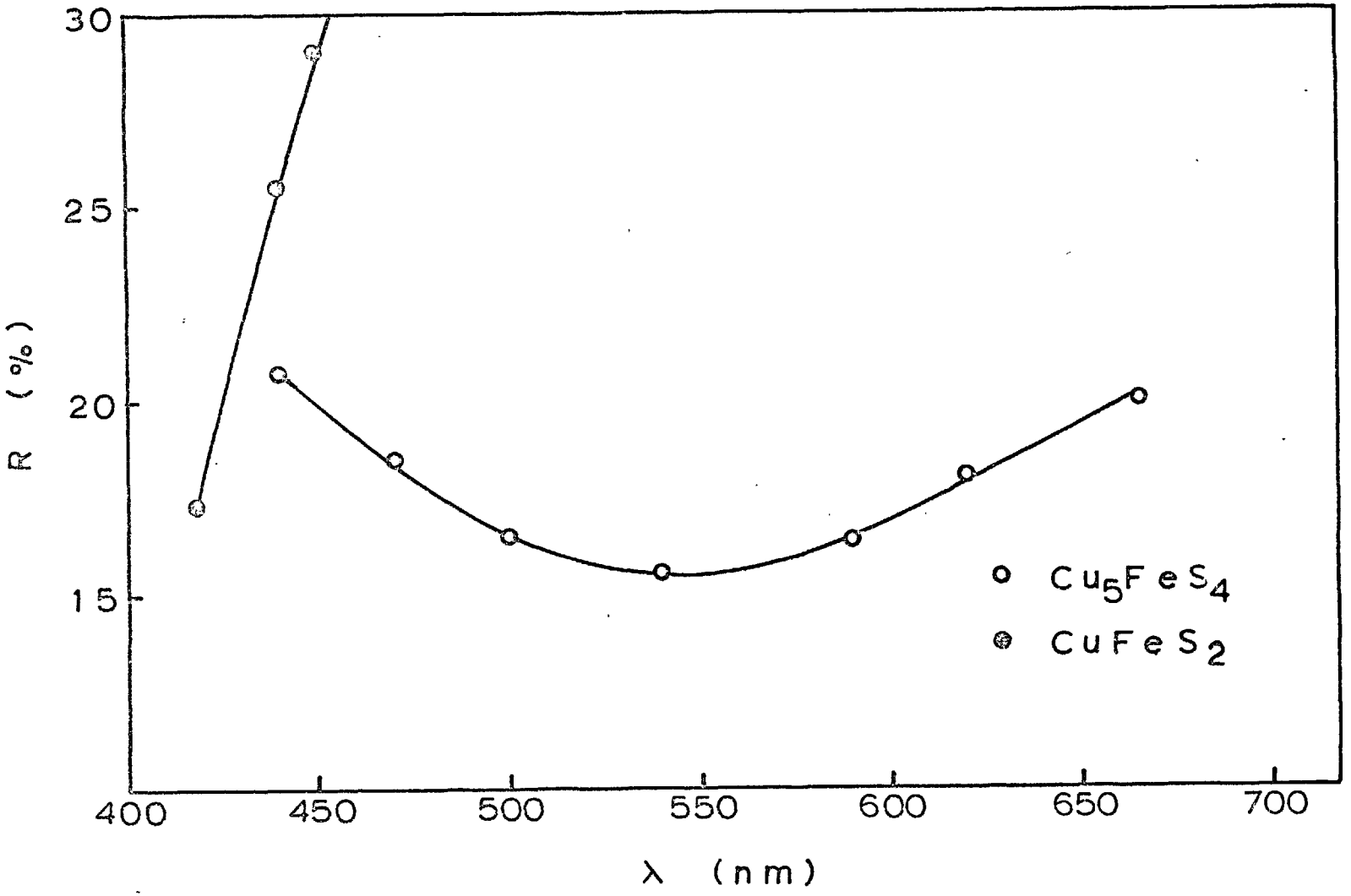

FIG. 59 Reflectivity dispersion profiles of bornite[46] and chalcopyrite[76]

This profile is very similar to that given by Levy[47](fig. 17) for the mineral idaite and very different to those of normal bornite and chalcopyrite (fig. 59), and the synthetic Cu_5FeS_6 (fig. 17) of Merwin and Lombard[34].

A very similar reflectivity dispersion profile was given by Sillitoe and Clark[46] for a supergene idaite from the Manto Esperanza Mine (Chile). They used the same Reichert microphotometer (R.S.M.) used in the present work.

3.7 Electron Probe Microanalysis.

Electron probe microanalysis was used to check the homogeneity of the synthetic bornite and to determine the composition of the solid residues from leaching under different stages of dissolution.

The apparatus and method of analysis are described in section 2.

The results of four differents analyses are presented in table 5 together with the theoretical compositions of Cu_5FeS_4 (bornite), $CuFeS_2$ (chalcopyrite), Cu_3FeS_4 (idaite), Cu_5FeS_6 and $Cu_{5.5}FeS_{6.5}$.

From table 5 it is possible to see that the residues from the leaching have a composition Cu_3FeS_4. This composition remained the same even when 80 % of the copper was dissolved.

These results agree those decribed previously in sections 3.3 and 3.4 and confirm that when the Cu_3FeS_4 phase was formed the only reaction was the dissolution of this product by a complete breakdown of the structure. This produced the release of iron to the solution together with copper and the formation of elemental sulphur which remained in the solid.

TABLE 5

Electron Probe Microanalyses

Res.(%Cu diss.)	Cu(wt.%)	Fe(wt.%)	S(wt.%)	Total %
37.5	51.5	13.8	33.0	98.3
64.1 (200 grain)	49.9	13.3	31.3	94.3
64.1 (50 grain)	50.5	14.4	33.7	98.6
80.0	48.6	16.7	35.1	100.4
Cu_5FeS_4	63.33	11.12	25.55	100.0
$CuFeS_2$	34.64	30.42	34.94	100.0
Cu_3FeS_4	50.87	14.90	34.23	100.0
Cu_5FeS_6	56.14	9.87	33.99	100.0
$Cu_{5.5}FeS_{6.5}$	56.94	9.11	33.95	100.0

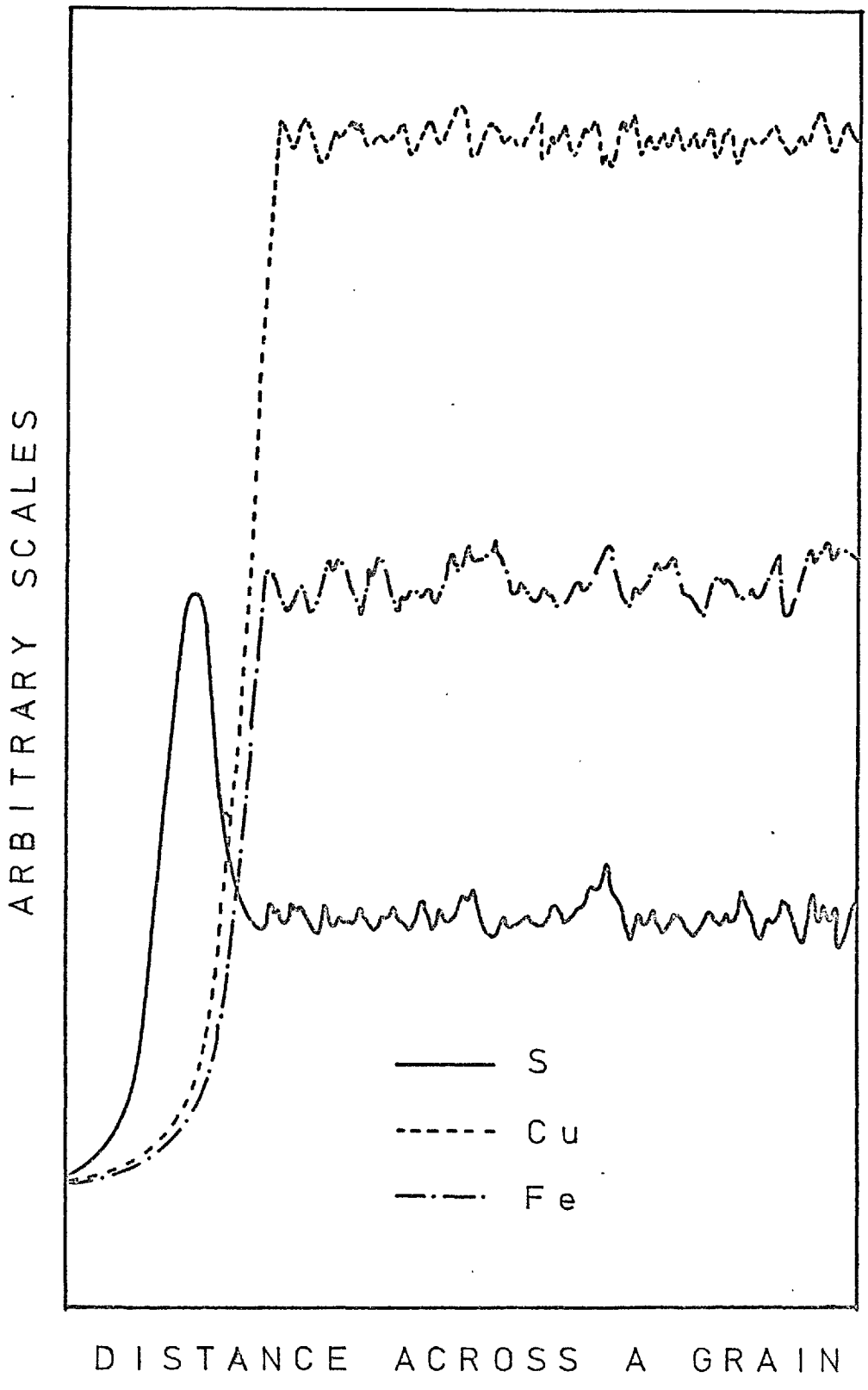

FIG. 60 Electron probe scan across the grain seen in FIG. 46

Electron probe microanalysis performed on the residue with 80 % of the copper dissolved, showed a high concentration of sulphur in the decomposed zone of the grains.

Fig. 60 shows a scan made across one side of a grain similar to that showed in fig. 46 The sulphur concentration was very high near the edge indicating that the dark zone of the photograph contained sulphur.

3.8 Density Measurements.

Attempts were made to measure the variation in density of the solid phases during the leaching of bornite.

Because the powder residues were unsuitable for a precise density measurement, only the relative decrease in density is given here. This minimises the errors in the measurements if identical experimental procedures are used in the determinations.

The density of Cu_5FeS_4 and Cu_3FeS_4 were calculated using the formula:

$$D = \frac{Z \times M}{N \times V}$$

where

$N = 6.02338 \times 10^{23}$

V = Volume of the unit cell.

Z = Number of formula units in a unit cell.

M = Molecular weight.

Calculated density for Cu_5FeS_4:

$$D = 5.09$$

Calculated density for Cu_3FeS_4:

$$D = 4.29$$

Calculated decrease in density:

$$\Delta D = 0.80$$

Using the technique described in section 2.9 the decrease in density of the solid phase during leaching was determined as:

$$\Delta D = 0.84$$

These results agree very well, indicating that, expressed in percentage, there is a decrease in density of about 18 % after the transformation of Cu_5FeS_4 to Cu_3FeS_4.

Also from the density measurements, an estimated value of the decrease in the unit cell volume of the solid phase equal to about 9 %, was obtained. This value is in agreement with the 10 % decrease in unit cell volume obtained from the lattice parameter measurements.

SECTION 4

CONCLUSIONS

4.1 Summary of Results.

At temperatures above 40° C the leaching of bornite, using acidified ferric sulphate solutions, proceeds in two stages, represented by the reactions:

$$Cu_5FeS_4 + 2\ Fe_2(SO_4)_3 = Cu_3FeS_4 + 2CuSO_4 + 4FeSO_4 \quad 9)$$

$$Cu_3FeS_4 + 4Fe_2(SO_4)_3 = 3CuSO_4 + 9FeSO_4 + 4S \quad 10)$$

Reaction 9) is faster than reaction 10).

At temperatures below 40° C, reaction 9) proceeds in two stages, shown by the reactions:

$$Cu_5FeS_4 + xFe_2(SO_4)_3 = Cu_{5-x}FeS_4 + xCuSO_4 + 2xFeSO_4 \quad 9')$$

$$Cu_{5-x}FeS_4 + (2-x)Fe_2(SO_4)_3 = Cu_3FeS_4 + (2-x)CuSO_4 + (4-2x)FeSO_4 \quad 9'')$$

Reaction 9') is very much faster than reaction 9"). In this range of temperature, reaction 10) is extremely slow and the leaching of bornite practically stops when reaction 9) has been completed.

In reaction 9') the maximun value for x is approximately 1.35.

In the first part of the reaction, bornite (Cu_5FeS_4) is rapidly transformed to idaite (Cu_3FeS_4), through the nonstoichiometric bornite ($Cu_{5-x}FeS_4$), by diffusion of copper ions in the solid state. Thus being the rate-controlling step. The activation energy for this part of the reaction is 2.1 ± 0.1 kcal per mole. Both, the nonstoichiometric bornite and the idaite formed are porous and maintain the original outline of the synthetic bornite.

During the second part of the reaction the surface of the idaite formed, is increasingly attacked, producing a direct transformation to elemental sulphur by a chemical reaction. Copper and iron ions are transferred to the solution.

4.2 Comparison of the Present Investigation with Previous Work.

The present work agrees very well with the following conclusions of Sullivan[3]:

a) The rate of dissolution of bornite is virtually independent of the strength of ferric sulphate if enough reagent is present.

b) The rate of dissolution is independent of the acid strength of solution if the ferric ion concentration remains constant.

c) The rate of dissolution is markedly affected by the temperature.

d) During the first part of the leaching of bornite only the copper is dissolved while the iron and sulphur are not removed.

Considering the experimental procedure of the time and the natural bornite used by Sullivan, the kinetic curves presented in his work agree very well with the present study.

Sullivan found that particle size did not affect the dissolution. This discrepancy can be explained by the fact that the experimental conditions used by Sullivan did not allow him to notice the effect in the faster first part of the reaction.

Sullivan found that sulphuric acid plus air,

attacked bornite more slowly than ferric sulphate solutions. The present work shows that acid alone does not attack bornite at all.

Sullivan found that the final product of the leaching of bornite was elemental sulphur. This is in agreement with the present work.

Sullivan's suggestion that bornite can be represented as $2Cu_2S.CuS.FeS$ is structurally invalid and, because of this, the mechanism of dissolution proposed by him is not discussed here.

However, the overall reaction (reaction 4) is in agreement with the present work.

The few results presented by Uchida et al. are in agreement with the present work. They did not suggest a mechanism of leaching.

The work of Kopylov and Orlov compares well with the present work. They found that an increase in the stirring speed from 200 to 1000 rpm increased only slightly the copper solubility. This agrees reasonably with the present work.

They also found that an increase of Fe^{+++} (as ferric sulphate) concentration from 9 to 35 g/l increased the rate of dissolution. This is in agreement with the present work.

From their work they concluded that the

factor, which most greatly affected the dissolution of bornite, was the temperature of the process. This is again in agreement with the present work.

Kopylov and Orlov found that a new solid phase formed after the first few minutes of dissolution. From the x-ray diffraction analysis they concluded that the new solid phase was chalcopyrite because the d-spacings coincided with the tabulated data for this mineral.

This discrepancy with the present work can be explained by the fact that the x-ray diffraction pattern of idaite as determined in the present work is almost identical to that of chalcopyrite. The formation of idaite was confirmed in the present work by electron probe microanalysis (section 3.7) and by reflectivity measurements (section 3.6).

Kopylov and Orlov determined the mean value for the activation energy as 5.5 ± 1.4 kcal per mole and they indicated that the dissolution of bornite is a process controlled by diffusion. This value agrees reasonably with the value of 2.1 ± 0.1 kcal per mole for the first part of the reaction presented in this work.

Finally Kopylov and Orlov discussed the dissolution mechanism writing the formula of

bornite as $2Cu_2S.CuFeS_2$. This representation is also structurally invalid.

Dutrizac et al.[7] found that in experiments below 25° C bornite was converted to nonstoichiometric bornite in which about 25 % of the copper is dissolved. When the synthetic pellet had been converted to this nonstoichiometric bornite the reaction virtually stopped. This process is similar to that described by reaction 9') in the present work. However, as was shown in section 3.1.1, (at temperatures below 40° C), the reaction continued slowly according to reaction 9'') until about 40 % of the copper was dissolved. The discrepancy between the two investigations can be explained by the fact that reaction 9'') is very slow below 25° C.

At temperatures above 40° C Dutrizac et al. proposed the mechanism represented by reactions 5), 6) and 7) (section 1.1).

They explained the fact that sulphur appeared only in tests made for long periods, by saying that reactions 5) and 6) are very much faster than 7). Reaction 6) requires that sulphur be produced in great quantity. However, this did not occur at this stage. They explained this by saying that the chalcopyrite formed was sulphur-rich and that some sulphur was oxidized to sulphate

which was not detected because of the high background of sulphate ions. Reaction 6) also predicts a Fe^{++}/Cu ratio of 2 but higher values were found. Because they had determined the existence of chalcopyrite only by x-ray diffraction the same discussion as given to Kopylov and Orlov's work, applies.

In the present work electron probe microanalysis and reflectivity measurements proved that the solid phase formed is Cu_3FeS_4.

Furthermore, chalcopyrite is very difficult to leach. The dissolution rate found in the second part of the leaching of bornite is very much higher than the dissolution rate of chalcopyrite under the same conditions[77]. Finally, it is very difficult to explain the formation of chalcopyrite from bornite by solid state reactions because there are only two posibilities : one is that the ferric ions present in the solution enter into the crystal lattice to replace the copper ions, and the other is a breakdown of the structure and a reorganization of the atoms to form chalcopyrite. The first posibility was proved invalid because the total iron concentration in solution remained constant during the first part of the reaction. The second posibility is very unlikely, and it also would produce

a great amount of sulphur which was not detected in the first part of the reaction.

In the other hand, the formation of Cu_3FeS_4 is easily explained by the structural model given in section 1.2.1.

Dutrizac et al. found that the dissolution rate depended directly on ferric ion concentration, for ferric ion strengths less than about 0.06 M, but it was insensitive to higher ferric concentrations. This is in agreement with the results of the present work.

Dutrizac et al. found that at different temperatures acid (0.1 M H_2SO_4) alone did not attack synthetic bornite. This is also in agreement with the present work.

They also found that, the effect of sulphuric acid concentration on the rate of bornite dissolution using Fe^{+++}, was negligible. This is in agreement with the present work.

Dutrizac et al. determined the average value of the activation energy for the dissolution of bornite as 5.7 $\pm$ 1.3 kcal per mole. This is in agreement with the value given by Kopylov and Orlov and agrees reasonable with the value determined in the present work.

Dutrizac et al. suggested that, in the temperature range 5^{o} to 35^{o} C, the diffusion rate-controlling step could be the diffusion of the "solution" through the constantly thickening layer of nonstoichiometric bornite (via pores or cracks) or by the diffusion of copper ions outward through the nonstoichiometric bornite. Because the nonstoichiometric bornite layer is porous and badly cracked they said that this suggests that the diffusion of "solution" is rate-controlling. In the present work it has been proved that the rate-controlling step in the first part of the reaction is the diffusion of copper ions through the lattice (section 3).

Dutrizac et al. suggested that at 70^{o} C the rate is controlled by the diffusion of ferric sulphate reactants through the liquid boundary layer as long as the ferric ion concentration is less than 0.06 M and that at higher ferric ion concentrations, the outward diffusion of ferrous sulphate controls the reaction. In section 3.1.3 it was shown that under the hydrodynamic conditions used in the present work the rate of dissolution was independent on the stirring speed. Although the activation energy for the second part of the reaction was not determined there are some indications

(section 3.1.4) that the rate-controlling step is a chemical reaction.

Finally, the present work is in agreement with the work of Levy[47] and of Sillitoe & Clark[46] in which idaite (Cu_3FeS_4) was found to be a product in the decomposition of natural bornite by oxidation. Sillitoe & Clark found that before the formation of idaite, the entire bornite was converted to anomalous bornite which corresponds to the nonstoichiometric bornite of the present work.

APPENDIX 1

Kinetic Results.

The experimental conditions for the determination of the general characteristics of the dissolution of bornite (fig. 28) were:

Temperature: 90^{o} C

H_2SO_4: 0.1 M

Fe^{+++}: 0.065 M

Stirring speed: 950 rpm

Sample weight: 1 g

Grain size: -100 +150 mesh

Volume of solution: 200 cc

The results are given in table 6.

1) Temperature.

The experimental conditions for the variation of temperature were:

H_2SO_4: 0.1 M

Fe^{+++}: 0.065 M

Stirring speed: 950 rpm

Sample weight: 1 g

Grain size: -100 +150 mesh

Volume of solution: 200 cc

The results are given in tables 7 to 14.

TABLE 6

Sample time (mins)	% Cu dissolved
15	35.93
120	49.20
180	51.79
270	56.90
330	60.14
420	64.05
810	80.00
1320	96.00

Sample time (mins)	% Fe dissolved
5	0.00
10	0.00
15	0.00
180	8.00
330	15.00
1320	91.50

TABLE 7

15^{o} C

Sample time (mins)	% Cu dissolved
5	13.62
10	18.31
15	21.04
30	24.66
45	25.43
60	25.79
75	26.08
90	26.31
105	26.43
120	26.51
150	26.60
180	26.68
210	26.77
240	26.88
270	26.99
300	27.13
330	27.27
360	27.38
420	27.66

TABLE 8

30° C

Sample time (mins)	% Cu dissolved
15	24.73
30	25.51
45	25.81
62	26.28
75	26.46
90	26.75
105	26.90
120	27.04
135	27.19
150	27.33
180	27.47
210	27.67
240	27.76
270	27.84
300	27.95
330	28.06
360	28.17
390	28.28
420	28.42
4320	37.00

TABLE 9

40° C

Sample time (mins)	% Cu dissolved
15	25.44
30	25.76
45	26.15
60	26.53
75	26.79
90	27.04
105	27.29
120	27.48
135	27.72
150	28.03
180	28.40
210	28.77
240	29.14
270	29.50
300	29.86
330	30.10
360	30.40
390	30.58
420	30.81

TABLE 10

50^{o} C

Sample time (mins)	% Cu dissolved
3	20.84
6	24.14
9	25.55
12	25.86
15	26.17
30	27.71
45	28.48
60	29.24
75	29.85
90	30.45
105	30.75
120	31.05
150	31.79
180	32.34
210	32.82
240	33.91
270	34.28
300	35.00
330	35.36
360	36.07
390	36.78
420	37.49

TABLE 11

60° C

Sample time (mins)	% Cu dissolved
3	22.43
6	24.86
9	25.58
12	26.10
15	26.82
30	28.91
45	31.42
60	33.47
75	34.83
90	36.19
105	36.94
120	37.98
150	39.50
180	40.98
210	42.65
240	43.62
270	44.84
300	45.71
330	47.00
360	47.92
390	48.63
420	49.14

TABLE 12

70° C

Sample time (mins)	% Cu dissolved
3	24.57
6	27.07
9	28.63
12	30.19
15	30.80
30	34.96
45	38.17
60	40.14
75	41.66
90	43.16
105	44.80
120	45.91
150	47.78
180	48.88
210	49.99
240	51.07
270	52.16
300	53.25
330	53.95
360	54.32
390	54.80
420	55.17

TABLE 13

80^{o} C

Sample time (mins)	% Cu dissolved
3	26.67
6	30.29
9	32.78
12	34.34
15	35.11
30	39.58
45	42.03
60	44.61
75	45.37
90	46.12
105	46.87
120	47.39
150	48.87
180	50.42
210	51.44
240	52.25
270	53.26
300	54.28
330	55.06
360	55.78
390	56.84
420	57.90

TABLE 14

90° C

Sample time (mins)	% Cu dissolved
3	29.21
6	32.67
9	33.76
12	35.00
15	35.93
30	40.86
45	43.16
60	44.68
75	45.82
90	47.33
105	48.45
120	49.20
150	50.68
180	51.79
210	53.62
240	55.09
270	56.90
300	58.70
330	60.14
360	61.57
390	62.99
420	64.05

2) Particle size.

The experimental conditions for the variation of particle size were:

Temperature: 90° C

H_2SO_4: 0.1 M

Fe^{+++}: 0.065 M

Stirring speed: 950 rpm

Sample weight: 1 g

Volume of solution: 200 cc

The results are given in tables 14 and 15.

3) Stirring speed.

The experimental conditions for the variation of stirring speed were:

Temperature: 90° C

H_2SO_4: 0.1 M

Fe^{+++}: 0.065 M

Sample weight: 1 g

Grain size: -100 +150 mesh

Volume of solution: 200 cc

The results are given in tables 14,16 and 17.

TABLE 15

-40 +50 mesh

Sample time (mins)	% Cu dissolved
15	30.11
30	36.03
45	40.01
60	42.64
90	44.50
120	47.00
150	48.07
180	49.15
240	52.01
300	54.49
360	55.90
420	58.71

TABLE 16

550 rpm

Sample time (mins)	%Cu dissolved
15	29.59
30	35.13
45	37.63
60	40.14
90	44.68
120	46.75
150	48.79
180	50.84
210	52.46
240	53.68
270	54.71
300	55.50

TABLE 17

1500 rpm

Sample time(mins)	% Cu dissolved
15	34.35
30	39.45
45	42.58
60	44.54
90	47.24
120	48.39
150	49.54
180	50.68
210	51.44
240	52.97
270	54.07
300	55.56

4) Ferric ion concentration.

The experimental conditions for the variation of ferric ion concentration were:

Temperature: 30^{o} and 90^{o} C

H_2SO_4: 0.1 M

Stirring speed: 950 rpm

Sample weight: 1 g

Grain size: -100 +150 mesh

Volume of solution: 200 cc

The results are given in tables 18 to 22 and tables 8 and 14.

5) Acid concentration.

The experimental conditions for the variation of acid concentration were:

Temperature: 90^{o} C

Fe^{+++}: 0.065 M

Stirring speed: 950 rpm

Sample weight: 1 g

Grain size: -100 +150 mesh

Volume of solution: 200 cc

The results are given in tables 14,23 and 24.

TABLE 18

Fe^{+++}: 0.00009 M - 30° C

Sample time (mins)	% Cu dissolved
15	0.08
30	0.15
45	0.15
60	0.20
75	0.22
90	0.25
105	0.31
120	0.31
135	0.31
150	0.31
180	0.31
210	0.37
240	0.41
270	0.45
300	0.45
330	0.48
360	0.54
420	0.60

TABLE 19

Fe^{+++}: 0.005 M - 30° C

Sample time (mins)	% Cu dissolved
15	5.22
30	5.77
45	5.83
60	5.99
75	6.02
90	6.08
105	6.14
120	6.25
135	6.31
150	6.43
180	6.58
210	6.72
240	6.87
270	7.01
300	7.15
330	7.29
360	7.45
390	7.69
420	7.86

TABLE 20

Fe^{+++}: 0.01 M - 30° C

Sample time (mins)	% Cu dissolved
15	11.28
30	11.59
45	11.66
60	11.89
75	11.89
90	11.97
105	12.04
120	12.12
135	12.26
150	12.48
175	12.78
180	12.93
195	12.93
210	13.07
225	13.21
240	13.36
270	13.50
300	13.72
330	13.98
360	14.14
390	14.34
420	14.63

TABLE 21

Fe^{+++}: 0.032 M - 30° C

Sample time (mins)	% Cu dissolved
15	22.13
30	24.52
45	25.46
60	25.80
75	26.16
90	26.32
105	26.47
120	26.53
135	26.65
150	26.95
180	27.10
210	27.25
240	27.40
270	27.55
300	27.70
330	27.84
360	27.99
390	27.28
420	28.42

TABLE 22

Fe^{+++}: 0.04 M - 90° C

Sample time (mins)	% Cu dissolved
15	33.62
30	36.08
45	39.31
60	40.93
90	42.53
120	44.52
150	45.85
180	46.92
210	47.85
240	48.49
270	49.26
300	50.03

TABLE 23

Fe^{+++}: 0.10 M - 90° C

Sample time (mins)	% Cu dissolved
3	29.25
15	35.95
30	40.88
45	43.20
60	44.82
75	45.83
90	47.36
105	48.48
120	49.25
150	50.73
180	52.05
210	53.81
240	55.35
270	56.94
300	58.61

TABLE 24

H_2SO_4: 0.01 M

Sample time (mins)	% Cu dissolved
15	35.89
30	40.81
45	43.12
60	44.64
75	45.79
90	47.31
105	48.43
120	49.17
150	50.65
180	51.76
210	53.60
240	55.07
270	56.88
300	58.68
330	60.12
360	61.53
390	62.97
420	64.12

TABLE 25

H_2SO_4: 1.00 M

Sample time (mins)	% Cu dissolved
15	35.98
30	40.90
45	43.21
60	44.72
75	45.85
90	47.36
105	48.49
120	49.23
150	50.71
180	51.80
210	53.65
240	55.11
270	56.93
300	58.72
330	60.16
360	61.60
390	63.02
420	64.10

6) Sample weight.

The experimental conditions for the variation of sample weight were:

Temperature: 90° C

H_2SO_4: 0.1 M

Fe^{+++}: 0.065 M - 0.130 M

Stirring speed: 950 rpm

Grain size: -100 +150 mesh

Volume of solution: 200 cc

The results are given in tables 14 and 26.

TABLE 26

Sample weight: 2 g - 0.130 M Fe^{+++}

Sample time (mins)	% Cu dissolved
15	33.74
30	38.06
45	41.58
60	44.30
90	47.79
120	50.28
150	52.20
180	53.34
210	55.43
240	56.56
270	57.63
300	58.80

APPENDIX 2

X-ray Diffraction Data of the Leach Residues.

The calculated d-values, and the intensities of the lines are given in this Appendix.

vst: very strong

st : strong

m : medium

w : weak

vw : very weak

TABLE 27

7.9 % Cu dissolved

2 θ	d	I
21.90	4.0583	w
22.40	3.9689	vw
24.40	3.6479	vw
25.70	3.4662	w
27.20	3.2784	m
28.40	3.1425	st
29.50	3.0278	st
32.00	2.7968	m
32.95	2.7183	st
34.10	2.6292	vw
35.00	2.5636	w

36.10	2.4880	w
37.50	2.3982	vw
39.90	2.2593	vw
40.60	2.2220	vw
41.60	2.1709	vw
43.10	2.0987	w
46.70	1.9450	w
47.30	1.9217	vst
48.60	1.8733	vw
49.40	1.8448	w
55.40	1.6584	vw
56.00	1.6420	m
57.80	1.5951	w
58.75	1.5716	w
60.40	1.5325	w
63.45	1.4660	w
65.70	1.4211	w
68.90	1.3627	m
75.30	1.2620	vw
76.20	1.2493	vw
78.50	1.2316	vw
79.80	1.2145	vw
87.80	1.1118	m
90.90	1.0817	vw
94.70	1.0481	vw
98.80	1.0153	vw

TABLE 28

14.6 % Cu dissolved

2 θ	d	I
25.95	3.4334	vw
27.40	3.2549	vw
28.60	3.1210	st
29.45	3.0328	st
33.05	2.7103	m
35.15	2.5530	w
37.65	2.3890	vw
40.25	2.2405	vw
46.80	1.9411	vw
47.45	1.9160	vst
49.25	1.8501	m
56.25	1.6353	m
57.75	1.5964	m
58.95	1.5667	m
69.15	1.3584	vw
76.55	1.2445	w
79.25	1.2087	w
88.15	1.1082	m
90.95	1.0813	w
95.05	1.0452	vw
98.85	1.0149	vw

TABLE 29

27.7 % Cu dissolved

2 θ	d	I
27.55	3.2375	w
29.45	3.0328	vst
32.85	2.7263	w
34.15	2.6254	w
47.15	1.9275	w
48.75	1.8674	st
57.65	1.5989	m
58.45	1.5789	w
70.85	1.3300	w
79.15	1.2100	w
91.05	1.0803	w
98.35	1.0187	vw

TABLE 30

28.4 % Cu dissolved

2-θ	d	I
27.35	3.2608	w
29.25	3.0531	vst
32.55	2.7507	vw
33.45	2.6788	vw
46.85	1.9391	w
48.65	1.8705	st
57.65	1.5989	m
70.95	1.3283	w
78.95	1.2126	w
90.65	1.0841	w
98.05	1.0211	vw

TABLE 31

30.8 % Cu dissolved

2 θ	d	I
27.60	3.2318	w
29.50	3.0278	vst
32.70	2.7385	vw
34.00	2.6367	vw
47.30	1.9217	w
48.90	1.8625	st
58.10	1.5876	m
71.30	1.3227	w
79.30	1.2081	w
91.30	1.0780	w
98.80	1.0153	w

TABLE 32

37.5 % Cu dissolved

2 θ	d	I
27.85	3.2033	w
29.50	3.0278	vst
34.15	2.6254	w
47.75	2.0251	vw
49.05	1.8572	st
58.10	1.5876	m
71.50	1.3195	w
79.35	1.2075	w
91.40	1.0771	w
98.80	1.0153	vw

TABLE 33

43.7 % Cu dissolved

2 θ	d	I
27.70	3.2203	w
29.60	3.0178	vst
34.20	2.6217	w
36.00	2.4947	vw
39.70	2.2703	vw
47.80	1.9028	w
49.00	1.8589	st
58.10	1.5876	m
71.70	1.3163	w
79.20	1.2094	w
91.30	1.0780	w
98.70	1.0161	vw

TABLE 34

49.1 % Cu dissolved

2 θ	d	I
27.75	3.2147	w
29.60	3.0178	vst
34.20	2.6217	w
49.10	1.8554	st
58.30	1.5826	m
71.80	1.3147	w
79.40	1.2068	w
91.50	1.0762	w
99.40	1.0108	vw

TABLE 35

57.9 % Cu dissolved

2 θ	d	I
23.30	3.8176	w
25.95	3.4334	w
27.95	3.1921	w
29.65	3.0128	vst
34.40	2.6069	vw
49.05	1.8572	st
58.35	1.5814	m
71.75	1.3155	w
79.55	1.2049	w
91.75	1.0739	w
98.95	1.0142	vw

TABLE 36

64.1 % Cu dissolved

2 θ	d	I
23.20	3.8338	m
25.20	3.5339	vw
26.00	3.4269	w
26.90	3.3143	w
27.90	3.1977	m
29.50	3.0278	vst
31.40	2.8488	vw
33.50	2.6749	vw
34.30	2.6143	w
42.90	2.1080	vw
48.10	1.8916	vw
49.15	1.8536	st
51.40	1.7776	vw
52.30	1.7491	vw
53.30	1.7187	vw
54.20	1.6922	vw
56.80	1.6208	vw
58.30	1.5826	m
71.80	1.3147	w
79.30	1.2081	w
91.80	1.0735	w
99.00	1.0138	vw

TABLE 37

80.0 % Cu dissolved

2 θ	d	I
21.90	4.0583	vw
23.25	3.8257	st
25.95	3.4334	m
26.80	3.3264	w
27.85	3.2033	m
29.55	3.0228	vst
31.50	2.8400	w
34.30	2.6143	w
36.05	2.4913	w
37.10	2.4232	w
38.00	2.3678	vw
39.45	2.2841	w
42.85	2.1104	w
48.05	1.8934	vw
49.10	1.8554	st
51.30	1.7809	w
52.05	1.7570	w
53.25	1.7202	w
54.15	1.6937	w
55.95	1.6434	vw
56.90	1.6182	vw
58.25	1.5839	m
69.45	1.3533	vw
71.90	1.3131	w
79.30	1.2210	w
91.80	1.0735	w
99.15	1.0127	vw

TABLE 38

96.0 % Cu dissolved

2 θ	d	I
11.40	7.7617	w
15.50	5.7166	m
22.00	4.0401	w
23.20	3.8338	vst
25.00	3.5617	w
25.95	3.4334	st
26.80	3.3264	w
27.85	3.2033	st
28.85	3.0945	w
29.55	3.0228	st
31.50	2.8400	m
33.50	2.6749	w
34.30	2.6143	vw
35.10	2.5565	w
36.15	2.4846	w
37.15	2.4200	m
38.10	2.3618	w
39.50	2.2813	w
40.75	2.2142	vw
42.25	2.1390	w
43.05	2.1010	m

45.55	1.9914	w
46.50	1.9529	vw
47.25	1.9236	vw
48.00	1.8953	w
49.15	1.8536	m
50.05	1.8224	vw
51.50	1.7744	m
52.20	1.7523	w
53.30	1.7187	w
54.20	1.6922	w
55.95	1.6434	w
56.90	1.6182	w
58.15	1.5863	w
60.45	1.5314	vw
61.70	1.5033	vw
63.15	1.4722	vw
64.95	1.4357	vw
66.00	1.4154	vw
67.50	1.3876	vw
69.50	1.3524	w
72.40	1.3053	vw
77.60	1.2303	vw
79.35	1.2204	vw
91.90	1.0726	vw
99.20	1.0123	vw

TABLE 39

Synthetic Bornite

2 θ	d	I
21.85	4.07	w
27.05	3.30	m
27.35	3.26	vw
28.25	3.16	st
29.80	3.00	vw
31.95	2.80	m
32.80	2.73	m
34.10	2.63	vw
35.95	2.50	m
42.45	2.13	w
43.10	2.10	vw
47.10	1.93	vst
49.25	1.85	w
57.70	1.65	m
58.40	1.58	vw
60.50	1.53	vw
63.25	1.47	vw
65.75	1.42	m
68.50	1.37	m
70.25	1.34	vw
75.45	1.26	m
87.00	1.12	st

APPENDIX 3

X-ray Diffraction Data

TABLE 40

Chalcopyrite ($CuFeS_2$) Burdick and Ellis[29]

d	I/I_1	hkl
3.03	100	112
2.63	5	020,004
1.865	40	220
1.854	80	024
1.591	60	132
1.573	20	116,033
1.518	5	224
1.323	10	040
1.303	5	008
1.214	10	332
1.205	30	136,143
1.077	60	244
1.069	30	228
1.018	20	152
1.014	10	336
1.005	5	1.1.10

TABLE 41

Bornite (Cu_5FeS_4)	Berry and Thompson[78],(F):Frenzel[33]	
d	I/I_1	hkl
4.08	10	105,213
3.64	5	214,006+
3.48	5	310,106+
3.31	40	116,312
3.18-3.15(F)	60	224
3.01	5	107,321
2.80-2.81(F)	20	305,323
2.74-2.73(F)	50	008,400
2.63	5	217,411+
2.50	40	413,325
2.13-2.12(F)	20	425,511
2.11	5	336,11.10
1.937	100	440,408
1.850(F)	10	21.11
1.652	30	624,22.12
1.584	10	448
1.534	10	712,11.14
1.47	5	705,723+
1.42	20	31.14,53.10
1.37	20	800,00.16
1.335(F)	5	44.12,804

1.300(F)	5	?
1.290(F)	5	660,22.16+
1.258(F)	50	62.12
1.225(F)	5	40.16,840+
1.198(F)	10	844
1.169(F)	5	64.12
1.145(F)	5	?
1.119(F)	50	44.16,848
1.097(F)	5	80.12
1.053	10	22.20,66.12
1.018(F)	5	64.16
0.9853(F)	10	

TABLE 42

Orthorhombic Sulphur	De Wolff[79]	
d	I/I_1	hkl
7.69	6	111
5.76	14	113
5.68	5	022
4.80	2	202
4.19	2	151
4.06	11	220
3.91	12	131
3.85	100	222
3.57	8	133
3.44	40	026
3.38	3	224
3.33	25	311
3.21	60	206
3.11	25	313
3.08	17	135
3.06	±	008
2.842	18	044
2.688	2	331
2.673	1	242
2.621	13	137
2.614	4	400
2.569	8	333

2.501	7	244
2.424	13	317
2.404	2	404
2.375	4	422
2.366	4	335
2.288	6	02.10
2.215	2	048,20.10
2.146	4	11.11
2.112	10B	319.062
2.098	2	22.10
2.057	1	511
2:041	1	00.12,248
2.003	2	353
1.988	4	408
1.957	2	262
1.926	1	444
1.900	7B	355,066,515
1.856	1	31.11
1.838	1	159
1.823	4	24.10
1.781	11	266,357
1.754	7	535
1.725	8	602
1.698	7	13.13
1.665	2	
1.658	2	
1.647	5	

1.622	6
1.607	6
1.601	2
1.595	3
1.563	2
1.542	1
1.531	1
1.515	1
1.504	1
1.490	1
1.475	2
1.461	1
1.439	3
1.424	3
1.419	1
1.391	1
1.362	1
1.354	3

TABLE 43

Chalcocite (Cu_2S), α (low) M.A. Peacock[80]

d	I/I_1	hkl
3.93	5	300
3.77	10	133,320,062
3.60	10	260
3,39	30	340,080
3.31	10	233,153
3.21	20	180
3.05	20	342,082
2.97	5	400
2.88	20	420
2.84	5	191
2.73	10	362,440,402
2.67	10	282
2.58	5	380
2.54	10	304
2.47	20	460
2.40	70	382,344,084
2.34	5	520,274
2.22	20	006
2.14	10	0.12.2
2.06	10	275
1.969	80	600

1.937	5	580,504
1.870	100	3122,0124 346,086
1.787	5	366,395,406
1.695	40	604,0160
1.645	20	682,644 0162
1.588	5	0126
1.514	20	684,3162 0164
1.471	5	3126
1.351	10	
1.278	30	
1.119	10	
1.074	10	
0.974	10	

ACKNOWLEDGEMENTS

The author is greatly indebted to his supervisor, Dr. A. R. Burkin for his constant kindness, continued advice and encouragement throughout the course of the present work.

The author wishes to thank the staff and members of the Nuffield Research Group, and in particular those of the Hydrometallurgy Group for their help. Thanks are due to Mr. G. M. Steed of the Geology Department for the electron probe microanalyses.

The author is indebted to the British Council and the University of Chile for making his studies at Imperial College possible.

F. J. G. Ugarte-Alvarez
Royal School of Mines,
London, S.W.7

REFERENCES

1) Monhemius A.J. : Chemical and Process Engng., 1970, Jan., p. 65.

2) Burkin A.R. : Minerals Sci. Engng., 1969, vol. 1, N° 1, p. 4.

3) Sullivan J.D. : U.S. Bureau of Mines, 1931, Tech. Paper 486.

4) Stender V.V., and Saltovskiy L.A. : Izv. A. Kaz. SSSR (News of the Academy of Sciences, Kazakh SSSR), 1951, vol. 101, N° 4.

5) Uchida T., Matsumoto H., Omori S.,and Murayama A. : Hakko Kyokaishi, 1967, vol. 25, p. 168.

6) Kopylov G.A., and Orlov A.I. : Izvest. Vysshikh Uchebn. Zavedenii Tsvetn. Met., 1963, vol. 6. p. 68.

7) Dutrizac J.E., Macdonald R.J.C., and Ingraham T.R. : Metallurgical Transactions, vol. 1, 1970, Jan., p. 225.

8) De Jong W. : Doctoral Thesis, Delft, 1928.

9) Lundqvist D., and Westgren A. : Ark. Kemi, Min. Geol. B,1936, vol. 12, N° 23, p. 1.

10) Tunell G., and Adams C.E. : Am. Mineral., 1949, vol. 34, p. 824.

11) Morimoto N., Greig J.W., and Tunell G. : Carnegie Inst. Wash., 1960, Year Book 59, p. 122.

12) Frueh A.J. : Am. Mineral., 1950, vol. 35, p. 185.

13) Kullerud G., and Roseboom E.H. : Bull. Geol. Soc. Am., 1958, vol. 69, p. 1602.

14) Kullerud G., Donnay G., and Donnay J.D.H. : Am. Mineral., 1960, vol. 45, p. 1062.

15) Morimoto N., and Kullerud G.: Am. Mineral., 1961, vol. 46, p. 1270.

16) Morimoto N. : Acta Crystallographica, 1964, vol. 17, part 4, p. 351.

17) Morimoto N. : Carnegie Inst. Wash., 1962, Year Book 61, p. 139.

18) Donnay G., Donnay J.D.H., and Kullerud G. : Am. Mineral., 1958, vol. 43, p. 230.

19) Manning P.G. : Can. Mineral., 1967, vol. 9, p. 85.

20) Craig D.P., and Magnusson E.A. : J. Chem. Soc., 1956, p. 4895.

21) Boshagovskii B.V., and Marfusim A.S. : Izv. Akad. Nauk SSSR, Ser. Khim., 1968, vol. 6, p. 1267.

22) Takeno S., Masumoto K., and Kamigaichi T. : J. Sci. Hiroshima Univ., Ser. C Geol., 1968, vol. 5, part 4, p. 321.

23) Allais G., and Curien H. : Radiation Effects, 1970, vol. 4, part 3-4, p. 271.

24) Manning P.G. : Can. Mineral., 1966, vol. 8, p. 567.

25) Manning P.G. : Can. Mineral., 1967, vol. 9, p. 57.

26) Wyckoff R.W.G. : Crystal Structures, 1948, Interscience Publishers, New York.

27) Donnay G., Corliss L.M., Donnay J.D.H., Elliott N., and Hastings J.M. : Phys. Rev., 1958, vol. 112, p. 1917.

28) Allais G. : Bull. Soc. franç. Min. Crist., 1968, vol. 91, p. 600.

29) Burdick C.L., and Ellis J.H. : Proc. Nat. Acad., 1917, vol. 3, p. 644.

30) Pauling L., and Brockway L.O. : Zeit. f. Krist., 1932, vol. 82, p. 188.

31) Donohue J., Caron A., and Goldish E. : Nature, vol. 182, p. 518.

32) Frenzel G. : Jahrb. Mineral. Monatsh, 1958, vol. 6, p. 142.

33) Frenzel G. : Neues Jahrb. Mineral. Abh., 1959, vol. 93, p. 87.

34) Merwin H.E., and Lombard R.H. : Econ. Geol., 1937, vol. 32, p. 203.

35) Roseboom E.H., and Kullerud G. : Carnegie Inst. Wash., 1958, Year Book 57, p. 222.

36) Yund R.A., and Kullerud G. : J. Petrology, 1966, vol. 7, p. 454.

37) Ramdohr P. : Die Erzmineralien und ihre Verwachsungen, 1960, Akad. Verlag, Berlin.

38) Kobe H.W. : Bol. Soc. Geol. Perú, 1961, vol. 36, p. 103.

39) Brodtkorb De M.K. : Rev. Ass. Geol. Argent., 1961, vol. 16, p. 109.

40) Takeuchi T., and Nambu M. : Tohoku Univ. Sci. Rept. 3rd. ser., 1961, vol. 7, part 2, p. 189.

41) Grafenauer S. : Rud. Met. Zb., 1963, vol. 3, p. 245.

42) Picot P., Sainfeld P., and Vernet J. : Bull. Soc. fr. Mineral. Cristallogr., 1963, vol. 86, p. 299.

43) Von Gehlen K. : Fortschr. Mineral., 1964, vol. 41, p. 163.

44) Krause H. : Norsk. Geol. Tidsskr., 1965, vol. 45, p. 416.

45) Tufar W. : Neues Jahrb. Mineral. Abh., 1967, vol. 106, p. 334.

46) Sillitoe R. H., and Clark N.H. : Am. Mineral., 1969, vol. 54, p. 1684.

47) Levy C. : Fr. Rep. Mem. Bur. Rech. Geol. Minieres Bull., 1967, vol. 54.

48) Yund R.A. : Am. Mineral., 1963, vol. 48, p. 672.

49) Frenzel G., and Ottemann J. : Miner. Deposita, 1967, vol. 1, p. 307.

50) Clark A.H. : Am. Mineral., 1970, vol. 55, p. 913.

51) Schlegel H., and Schüller A. : Freiberger Forschungsh, B, 1952, vol. 2.

52) Jensen E. : Am. J. Sci., 1942, vol. 240, p. 695.

53) Jensen E. : Avhandl. Norske Videnskap-Akad. Oslo, I. Mat.-Naturv. Kl., 1947, N° 6.

54) Greig J.W., Jensen E., and Merwin H.E. : Carnegie Inst. Wash., 1955, Year Book 54, p. 129.

55) Kullerud G. : Carnegie Inst. Wash., 1964, Year Book 63, p. 200.

56) Barton P.B., and Skinner B.J. : Geochemistry of Hydrothermal Ore Deposits, 1967, Ed. Barnes H. Ll., Holt, Rinehart and Winston, Inc., New York.

57) Kullerud G., Yund R.A., and Moh G.H. : Econ. Geol., 1969, Monograph 4, p. 323.

58) King J.A. : Ph. D. Thesis, Univ. of London, 1966.

59) Kullerud G., and Yoder H.S. : Econ. Geol., 1959, vol. 54, p. 533.

60) West A.W., and Menzies A.W.C. : Jour. Phys. Chem, 1929, vol. 33, p. 1880.

61) West J.R. : Ind. and Eng. Chem., 1950, vol. 42, p, 713.

62) Rassow H.: Zeitschr. anorg. u. allgem. Chemie, 1920, vol. 114, p. 117.

63) Baker E.H. : Inst. of Mining and Met. Trans., Section C, 1971, vol. 80, Bull. 775, p. 93.

64) Isakova R.A., Uranovich M.I. Potamina N.A., and Ugryumova L.E. : Izv. Akad. Nauk Kaz. SSSR, Ser. Khim., 1969, vol. 19, part 5, p. 78.

65) Schwartz G.M. : Econ. Geol., 1931, vol. 26, p. 739.

66) Schwartz G.M. : Econ. Geol., 1939, vol. 34, p. 399.

67) Edwards A.B. : Textures of the ore minerals, 1960, The Australasian Institute of Mining and Metallurgy, Melbourne.

68) Kullerud G. : Carnegie Inst. Wash., 1964, Year Book 63, p. 200.

69) Sandell E.B. : Colorimetric Determination of Traces of Metals, Third edition, 1959, Interscience.

70) PERKIN-ELMER : Analytical Methods for Atomic Absorption Spectrophotometry, 1966, The Perkin-Elmer Corp.

71) Wittkopp R.W. : Minerals Sci. Engng., 1971, vol. 3, N° 1, p. 17.

72) Kelly T.K. : Inst. of Mining and Met., Trans., Section B, 1966, vol. 75, Bull. 711, p. 59.

73) Kelly T.K. : Ph.D. Thesis, Univ. of London, in preparation.

74) Singh D.S. : Inst. Min. Met., Trans., Section B, 1965, vol. 74, p. 901.

75) Dana-Hurlbut : Dana's Manual of Mineralogy, 15 th. edition, John Wiley & Sons, Inc. New York.

76) Demirsoy S. : Neues Jahrb. Mineral. Monatsh, 1969, vol. 10, p. 477.

77) Ferreira R.C.H. : Ph.D. Thesis, Univ. of London, in preparation.

78) Berry and Thompson : Geol. Soc. Am. Mem., 1962, vol. 85, p. 44.

79) A.S.T.M. X-ray Index Files, N° 8-247.

80) A.S.T.M. X-ray Index Files, N° 9-328.